Body-Centric Radio Propagation Channels

characteristics and models

Wang, Yu

Publication date:
2009

Document Version
Publisher's PDF, also known as Version of record

Body-Centric Radio Propagation Channels: Characteristics and Models

Ph.D. Thesis

YU WANG

September, 2008

Yu Wang
Body-Centric Radio Propagation Channels: Characteristics and Models

ISBN
ISSN

Department of Electronic Systems
Aalborg University
Fredrik Bajers Vej 7
DK-9220 Aalborg east, Denmark
Phone: +45 9940 8650

This thesis was typeset using LaTeX.

Printed by Uniprint, Aalborg, Denmark.

I dedicate this work to my grandparents:

Zhenjiang Wang
&
Xiuru Zhu

Supervisors:

Prof. dr. Gert Frølund Pedersen, Aalborg University, Denmark

Dr. István Zsolt Kovács, Nokia Siemens Networks A/S, Denmark

Opponents:

Prof. Peter S. Hall, University of Birmingham, United Kingdom

Dr. Koichi Ogawa, Matsushita Electric Industrial Co. Ltd., Japan

Assoc. Prof. Patrick Claus F. Eggers, Aalborg University, Denmark

Committee Chairman:

Assoc. Prof. Patrick Claus F. Eggers, Aalborg University, Denmark

Moderator:

Assoc. Prof. Flemming Bjerge Frederiksen, Aalborg University, Denmark

The work described in this thesis has been carried out at the Antenna, Propagation and Network group Department of Electronic Systems at Aalborg University

Abstract

Body-centric wireless communication systems (BWCSs) which connect electronic devices placed at various parts of the human body are key components of future wireless systems. Recently a lot of research has been focused on the BWCS in the scope of a wireless personal area network (WPAN) and a wireless body area network (WBAN).

Comprehensive channel knowledge and accurate channel models are the basis of an optimized system design. The human body influences to the antennas and propagation channels have been deeply investigated in mobile communications since the start of the 1990's. However the body effects in the BWCS is different in several aspects. Firstly, the frequency band of the mobile communication systems is between 1 and 2 GHz while the BWCS may operate on higher frequencies above 5 GHz and on an ultra-wideband (UWB) frequency band between 3.1 and 10.6 GHz. Secondly, the radio links in the mobile communication are mainly outdoor-outdoor and indoor-outdoor channels. On the other hand most BWCSs target on indoor short range (< 10m in WPAN, < 2m in WBAN) radio communications. Furthermore, the devices in the BWCS can be much smaller than a handset and placed on a variety of body positions. Therefore, the BWCS channel requires further investigations.

This thesis focuses on the characterization and modeling of both WPAN and WBAN radio channels.

Body shadowing plays a key role in short range body-to-body communications since received signal is attenuated significantly due to body blockage. A correlation based stochastic model with correlated shadowing (CBSM-CS) for body-to-body multiple-input multiple-output (MIMO) radio channels is proposed based on channel characterizations derived from a series of channel experiments. The model introduces a shadowing matrix to represent unbalanced and correlated body shadowing effects. To the authors' knowledge, this is one of the first MIMO channel models including the body shadowing effects in open literature. It is disclosed that shadowing standard deviation is dominant to the ergodic capacity while shadowing correlations between the antennas significantly affect the outage capacity.

The UWB is a promising technology for the on-body BWCS. The UWB on-body

channel is characterized and modeled in indoor radio environments based on experiments performed with walking users and 15 different device on-body positions. The channel wideband power varied by up to 20 dB and the channel mean rms delay spread ranged from 5 to 20 ns at the various device positions. To separate the propagation around the human body from the propagation in the surrounding environment, the first cluster of the measured channel impulse response was detected, separated from remaining clusters and characterized. A UWB channel model for the on-body BWCS working in indoor environments is proposed. The model uses a joint approach to generate and combine the propagation around the human body and in the surrounding environment in the delay domain. The proposed model is one of a few existing UWB WBAN channel models taking the environment propagation into consideration. Since the model uses available UWB indoor channel models to generate multipaths from environments, it can be adapted to specific environments by applying different available models.

The spatial correlation properties of indoor WPAN UWB-MIMO channels are also presented and analyzed. The investigation was based on channel measurements of radio links between an access point like device and a walking user with a hand-held or a belt-mounted device. It was found that the channel shows spatial correlated wideband power, and spatial uncorrelated complex channel coefficients in both the time-frequency and time-delay domain. While the ergodic capacity was close to the independent identical distributed (IID) Rayleigh channel capacity, the 1% outage capacity dropped approximately 25% due to the signal shadowing introduced by the user bodies. It suggests that body shadowing plays an important role in the WPAN UWB-MIMO channels.

The channel characteristics and modeling parameters proposed in this work are specific to our measurement campaigns. However, the methodology can easily be reproduced and the models can be extended to different conditions. Therefore, more channel experiments in different environments, with different antenna types and in different end-user scenarios are highly encouraged and recommended to generalize the contributions of this thesis.

Preface

This thesis is submitted to the International Doctoral School of Technology and Science at Aalborg University as a partial fulfillment of the requirements for the degree of Doctor of Philosophy. The work was carried out during the period June 1st, 2005 - Sep. 30th, 2008 at the Department of Electronic Systems at Aalborg University. The project was funded by My personal Adaptive Global NET (MAGNET) project and Center for TeleInFrastruktur (CTIF) of Aalborg University.

First of all, I would like to thank my supervisors Gert Frølund Pedersen and István Zsolt Kovács. Their constant supports during the whole period of the project are invaluable to me. Their professional guidance and advice has always strengthened me when I explored new ideas, and their broad knowledge has been an important source of my learning and building my own competence.

I would also like to thank Jesper Ødum Nielsen, Kim Olesen and Ivan Bonev Bonev for their collaboration and guidance during the project. Many thanks to Persefoni Kyritsi, Patrick Claus F. Eggers, Jørgen Bach Andersen, Xin Zhou, Ondrej Franek, Tim Brown, Naizheng Zheng and Chunjian Li for their intellectual exchange and fruitful discussion. Thanks to Dorthe Sparre and all the secretaries who helped me to handle many formality and paper works. I appreciate all the staff members in the APNet group and Electronic Lab for their openness and helps. Special thanks to my officemate Hung Tuan Nguyen for the great time we shared and to Chenguang Lu who has been greatly supportive and helpful for years since our days in Sweden as MSc students.

Finally I would like to thank all my friends in Denmark as well as in other places around the world. Without them I can not be where I am now. Special thanks to my girlfriend Xiangyun Du who accompanies me during the last stage of my PhD with her great helps and supports. I am grateful to my parents, aunts, uncle and other relatives who have helped and watched my progress despite the physical distance.

Most importantly I dedicate this work to my dearest grandparents.

Yu Wang
Aalborg, August 2008

Acronyms

AP	Access Point
BAN	Body Area Network
BM	Belt-Mounted
BW	Body-Worn
BWCS	Body-centric Wireless Communication System
BS	Base Station
BPI	Branch Power Imbalance
CAN	Conference room
CBSM-CS	Correlation Based Stochastic Model with Correlated Shadowing
CDF	Cumulative Density Function
CIR	Channel Impulse Response
CMD	Correlation Matrix Distance
COR	Corridor
DFT	Discrete Fourier Transform
DSP	Directional Stacked Patch antenna
DSSS	Direct-Sequence Spread Spectrum
EIRP	Effective Isotropic Radiated Power
ETSI	European Telecommunications Standards Institute
FC	First Cluster
FCC	Federal Communications Commission
FDTD	Frequency Domain Time Difference
FM-UWB	Frequency Modulation-UWB
HAA	Hallway
HDR	High Data Rate
HH	Hand-Held
IID	Independent Identical Distributed
H-S/MIMO	Hybrid antenna Selection/MIMO
K-S	Kolmogorov-Smirnov
LAB	Laboratory

LDR	Low Data Rate
LOS	Line-Of-Sight
MAGNET	My personal Adaptive Global NET
MIMO	Multiple-Input Multiple-Output
NLOS	Non-LOS
OFDM	Orthogonal Frequency-Division Multiplexing
PAN	Personal Area Network
PDA	Personal Digital Assistant
PDF	Probability Density Function
PDP	Power Delay Profile
PHY	PHYsical layer
PIFA	Planar Inverted F-Antennas
PN	Pseudo Noise
RC	Remaining Cluster
RLN	Rayleigh-Lognormal
RMS	Root Mean Square
RV	Random Variable
Rx	Receiver
SISO	Single-Input Single-Output
SNR	Signal to Noise Ratio
SP	Simplified Parameter
ToA	Time-of-Arrival
Tx	Transmitter
UD	User Device
UWB	Ultra-WideBand
WBAN	Wireless Body Area Network
WPAN	Wireless Personal Area Network
WSS	Wide Sense Stationary

Contents

Abstract i

Preface iii

Acronyms v

I Introduction 1

1 Background: body-centric wireless communication systems 3
2 Objective 5
3 Outline 6
4 Body-to-body WPAN channels 8
4.1 Body shadowing in the body-to-body channel 8
4.2 Joint modeling of the fading and body shadowing 9
4.3 Body shadowing investigation approaches 9
4.4 Body-to-body channel with multiple antennas 10
5 On-body UWB WBAN channels 12
5.1 UWB in WBAN 12
5.2 Antennas in WBAN channels 12
5.3 Propagation in WBAN channels 14
5.4 A summary of UWB WBAN channel investigations 14
6 UWB-MIMO WPAN Channels 16
6.1 UWB in WPAN 16
6.2 Potential benefits of UWB-MIMO systems 16
6.3 UWB-MIMO channels in WPAN 17
7 Conclusions 19
Reference 22

II Papers **29**

Paper A: Characterization of the Indoor Multi-Antenna Body-to-Body Radio Channel **A1**

1 Introduction . . . A3
2 Measurement Campaign . . . A4
3 Antenna Characterization . . . A6
4 Channel Characterization . . . A10
4.1 Channel representation and normalization . . . A10
4.2 Losses in received power due to body blockage . . . A10
4.3 Path-loss . . . A11
4.4 Body shadowing statistics . . . A12
4.5 Coherence bandwidth . . . A14
4.6 Fading statistics . . . A15
5 Distributed Antenna Diversity for the body-to-body communication . . . A16
5.1 Distributed antenna selection diversity of the spot measurements A16
5.2 Distributed antenna selection diversity of the route measurements A17
6 Conclusion . . . A18
References . . . A19

Paper B: MIMO Channel Modeling for Body-to-Body Communications **B1**

1 Introduction . . . B3
2 Body-to-Body MIMO Channel Model . . . B4
2.1 Normalized CBSM-CS . . . B5
2.2 Structure of $\mathbf{R}_{\mathrm{X,dB}}$ . . . B6
3 Numerical Analysis of Modeling Parameters and Channel Capacity . . . B6
3.1 Effects of $\mathbf{\Sigma}_{\mathrm{X,dB}}$ on Channel Capacity . . . B7
3.2 Effects of $\mathbf{R}_{\mathrm{X,dB}}$ on Channel Capacity . . . B7
3.3 Effects of BPI on Channel Capacity . . . B9
3.4 MIMO Size and Channel Capacity . . . B9
3.5 Body-to-Body MIMO Systems with Antenna Selection . . . B10
4 Measurement Setup and Data Processing . . . B10
4.1 Measurement Devices, Environments and Scenarios . . . B11
4.2 Measured Channel Representation and Data Processing . . . B12
5 Measured Channel Capacity and Model Verification . . . B13
5.1 Measured Channel Statistics . . . B13
5.2 Measured Channel Capacity . . . B13
5.3 Model verification . . . B16
6 Conclusion . . . B18
References . . . B19

Paper C: Characterization and Modeling of UWB WBAN Channel in Indoor Environments **C1**
1 Introduction . . . C3
2 Measurement Setup . . . C4
2.1 Measurement Devices, Environments and Scenarios . . . C5
2.2 Data Processing . . . C6
3 Channel Characterization . . . C8
3.1 Channel Wideband Power . . . C8
3.2 Channel Delay Spread . . . C9
3.3 First Cluster Characterization . . . C10
3.4 Body Propagation and Environment Propagation . . . C13
4 Channel Model and Verification . . . C14
5 Conclusion . . . C16
References . . . C17

Paper D: Spatial Correlation of PAN UWB-MIMO Channel Including User Dynamicsl **D1**
1 Introduction . . . D3
2 Measurement Setup And Environment . . . D4
3 Data Analysis and Processing . . . D5
3.1 Stationarity of the measured channel . . . D5
3.2 Spatial Correlation . . . D7
4 Results Analysis . . . D7
4.1 Spatial correlation of wideband power (ρ_{pow}) . . . D7
4.2 Spatial correlation of complex channel coefficients at different delays (ρ_{delay}) . . . D8
4.3 Spatial correlation of complex channel coefficients at different frequency (ρ_{freq}) . . . D8
4.4 Spatial correlation at transmitter and receiver . . . D9
4.5 Spatial correlation with different Rx antenna spacing . . . D10
4.6 Spatial structure of the measured channel . . . D11
4.7 Capacity . . . D12
5 Conclusion . . . D14
References . . . D15

Part I

Introduction

Introduction

1 Background: body-centric wireless communication systems

Convergence and personalization are two essential concepts of future wireless communications. Emerging body-centric wireless communication systems (BWCS) are key components to make them happen [1].

A wireless personal area network (WPAN) and a wireless body area network (WBAN) are often used to refer to the BWCS. The concept of the BWCS is shown in Figure 1. Three BWCS application scenarios, health monitoring [2–4], wearable computers [5] and motion detection [6, 7], are illustrated. For all the applications a common scenario is that a number of sensors, e.g. health monitors, computer components and motion detectors, are distributed to a variety of on-body positions, and connects with a central device such as a personal digital assistant (PDA) for further processing and communications with other systems. When the central device is placed on the same person wearing the sensors they form a WBAN. The central device connects to another person or other fixed devices with which a WPAN is established. In some cases the sensors may connect to the other person or the fixed devices directly, e.g. when a gym instructor monitors physical condition information sent by the body sensors mounted on an exerciser.

According to the locations of the devices, the BWCS can be classified into three categories: off-body, on-body and in-body communication systems [8]. This thesis focuses on the channel characterization and modeling of the off-body and on-body systems. The scopes and interconnection of the WPAN/WBAN and off/on/in body BWCS are summarized in Fig. 2.

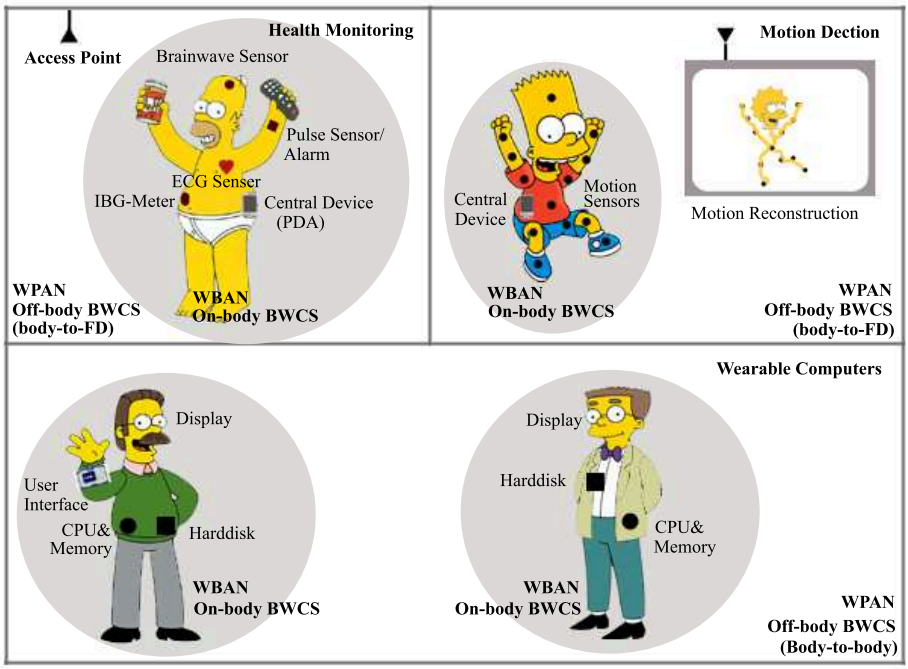

Figure 1: Illustrations of WPAN/WBAN applications (ECG: Electrocardiogram, IBG-Meter: Intelligent Blood Glucose Meter)

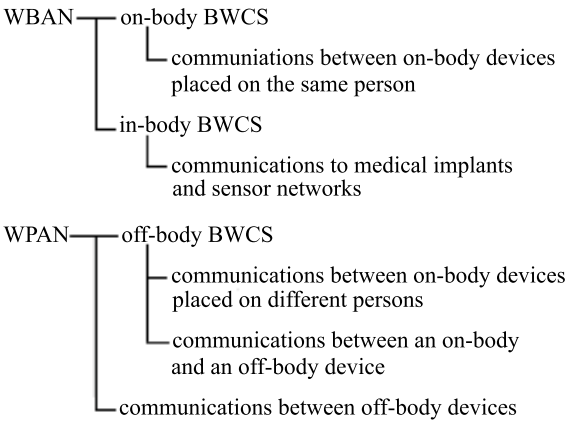

Figure 2: The scopes and interconnection of the WPAN/WBAN and off/on/in body BWCS

2 Objective

The development and optimization of any wireless system requires comprehensive radio channel knowledge and accurate channel models. Although the human body influence to the antennas and propagation channels has been deeply investigated in mobile communications, the BWCS is different from the mobile communication systems in operating frequency bands, communication ranges and environments and device size and on-body positions. All these differences may change the channel characteristics and require new investigations of the BWCS channel.

In this thesis we contribute to the following issues:

- How to characterize and model body-to-body radio channels in the presence of body shadowing
- What is the potential gain of implementing multiple antennas in the body-to-body communication
- How to model ultra-wideband (UWB) WBAN channels in indoor environments
- How much UWB WPAN systems can benefit from multiple-input and multiple-output (MIMO) transmission systems

3 Outline

Section 4 to Section 6 in Part I are summaries and discussions based on a number of reported/submitted papers. In each section, the problem definition, motivation and obtained results are related to one or two papers listed in Part II.

Section 4 reviews the characterization and modeling of the body-to-body radio channel. The body shadowing is identified as a key phenomenon in the off-body communication. The potential gain of using multiple antennas to mitigate the body shadowing is analyzed. One of the first MIMO channel models including the body shadowing effects is proposed. Detailed results of the body-to-body channel studies were reported in the following two papers

[Paper A] Y. Wang, B. B. Ivan, J. Ø. Nielsen, I. Z. Kovacs and G. F. Pedersen, "Characterization of the Indoor Multi-Antenna Body-to-Body Radio Channel", *IEEE Transactions on Antennas and Propagation Special Issue on Body-Centric Wireless Communications*. (submitted, Jan 2008)

[Paper B] Y. Wang, J. Ø. Nielsen, I. Z. Kovacs and G. F. Pedersen, "MIMO Channel Modeling for Body-to-Body Communications", *IEEE Transactions on Wireless Communications*. (to be submitted, Aug 2008)

Section 5 focuses on the investigation of the UWB WBAN channel. The effects of body proximity on antennas and propagation channels are summarized in this section. Based on the state of the art a summary of the current UWB WBAN channel investigation results is provided. The methodology and advantages of modeling the propagation around the human body and the propagation in the surrounding environment separately are presented. Details of the proposed UWB WBAN channel model can be found in the paper

[Paper C] Y. Wang, I. Z. Kovacs and G. F. Pedersen, "Characterization and Modeling of UWB WBAN Channel in Indoor Environments", *IEEE Transactions on Antennas and Propagation*. (to be submitted, Aug 2008)

Section 6 is devoted to the channel investigation of UWB-MIMO systems which have obtained increasing research interests recently. Motivations and potential gains of combining the UWB and MIMO for WPAN applications are presented. Current research results on spatial correlation and channel capacity are summarized. This section is related to the paper

[Paper D] Y. Wang, I. Z. Kovacs, G. F. Pedersen, and K. Olesen, "Spatial Correlation of PAN UWB-MIMO Channel Including User Dynamics", *in EURO-COST 2100*, Duisburg, Sep 2007

Section 7 is for conclusions. Major results and findings of the thesis are summarized in this part. Some discussions and directions for future work are also introduced.

4 Body-to-body WPAN channels

In the context of the WPAN the body-to-body communication considered in this study is a short-range (<10m) radio connection between small or medium size devices mounted/worn on different persons. It is a special form of the off-body BWCS. Applications of the body-to-body radio communications can be found in Section 1.

4.1 Body shadowing in the body-to-body channel

For the off-body radio communication working in the microwave frequency band, it is well known that the human body causes a deep null in the antenna pattern since the electromagnetic wave at this frequency can not penetrate through the body. When the dominant propagation path, e.g. line-of-sight (LOS), is aligned with the direction of the null, the average received signal power will be significantly reduced. This attenuation is referred to as the body shadowing.

In the mobile communication the changes of the antenna pattern due to the body proximity and body shadowing have been investigated for years [9–12]. In the BWCS the body induced pattern variation was also measured in recent years at 5.2 GHz [13] and at a UWB frequency band [14]. The two systems are differed in the operating frequency bands and the communication ranges. Also in the BWCS the LOS often exists which is not the case in the mobile communication. These make the body shadowing in the BWCS requiring further investigations.

It should be noticed that in literature the term of the body shadowing is also used to represent the signal attenuation when a human body moves into the LOS of a communication channel [15–17]. The difference between the two scenarios are illustrated in Figure 3. To distinguish between the two scenarios, in this study the signal blockage due to the human body which moves into the LOS path between a transmitter (Tx) and a receiver (Rx) is called body obstruction, and the body shadowing is dedicated to the body blockage in the off-body communication in particular.

Compared with the body obstruction, the body shadowing is almost inevitable in the BWCS with moving users. Furthermore since the distance between the antennas and the bodies is much closer the body shadowing will block signals in a region with a wider angular spread. In addition the effects of the body obstruction are only significant when the body block the LOS path, while the body shadowing also causes considerable signal variations in non-LOS (NLOS) channels as shown in [Paper A] and [18].

Therefore the body shadowing is a key phenomenon in the off-body communication. It is even more critical for the body-to-body channel since the body shadowing of the body-to-body channel can be much larger than the shadowing in the channel between a body and an access point (AP) [18, 19].

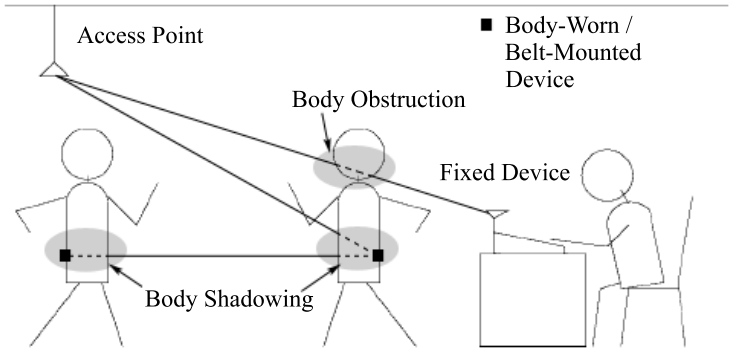

Figure 3: An illustration of the difference between the body shadowing and body obstruction

4.2 Joint modeling of the fading and body shadowing

Conventionally the shadowing is considered as a large-scale channel phenomenon which is constant in a local area, and usually modeled as a power variation around the local mean of the channel gain. In this case the evaluations of baseband and antenna systems are based on small-scale fading characteristics, and the shadowing is considered in link budgets. The shadowed fading channel studies are only necessary for the systems with stationary transmitters and receivers which do not experience more small-scale fading states than the shadowing states [20] and for large scale investigations in cellular systems [21].

In the off-body, especially the body-to-body channel, the body shadowing usually changes during a fraction of a second or several seconds [18]. Consequently the changes in channel power due to the body shadowing and small-scale fading are difficult to be separated especially when people change their relative orientations frequently. Therefore joint modeling of the shadowing and fading becomes a necessity in the body-to-body communications.

4.3 Body shadowing investigation approaches

As stated in the previous section, the body shadowing and the small-scale fading vary simultaneously in the body-to-body channel and it is difficult to separate them. A number of approaches for the body shadowing investigation are summarized as follows,

- Antenna pattern based approaches

  Since the body shadowing is induced by the variation of antenna patterns, the investigation of the antenna on-body radiation patterns is a straightforward method

to study the body shadowing. The on-body patterns can be obtained by simulations [Paper A] [13] or measurements [12]. The advantage of this approach is the accurate quantization of the body effects in all the directions. However to model the body shadowing in indoor environments the simulated or measured patterns need to be combined with indoor channel models such as ray tracing, geometrically-based or parametric-based channel models.

- Channel measurements with separated fading and shadowing

  Instead of investigating the variation of the antenna patterns, the body shadowing can be obtained by channel measurements in indoor environments. The measurements need to be carefully elaborated in order to separate the fading and the body shadowing. Similar approaches were used in [Paper A] and [18]. In this two studies a number of channels were measured within a small area and with the same test person orientations. Several orientations were measured in the same manner at each measurement location. For each orientation the small-scale fading was removed from the measured channels by averaging in the spatial and/or frequency domain. During this process the variation of the channel gain among the different orientations was preserved. Since it is the body shadowing that changes the channel gain the statistics the body shadowing can be derived by analyzing the channel gain variation.

- Channel measurements with joint fading and shadowing

  The method presented above is able to separate the fading and the body shadowing during the channel measurements. However the test persons have to behave in an artificial manner which is very different from real life scenarios. Given the assumption that the compound shadowed fading channel follows a predefined statistics, it is possible to derive the body shadowing statistics based on the measured shadowed fading channel by post processing. In this way the measurements can be performed in a more free manner. In [Paper B] the channel measured with test persons changing their relative orientations continuous was assumed to be Rayleigh-Lognormal distributed according to the channel characteristics presented in [Paper A]. And the body shadowing statistics were calculated based on a series of relations between the statistics of a normalized Rayleigh-Lognormal random variable (RV) and a Lognormal RV.

4.4 Body-to-body channel with multiple antennas

Multiple antennas are widely used in wireless communications to improve signal quality, enhance throughput and suppress interference by the use of antenna diversity, spatial multiplexing and/or beamforming techniques. In the body-to-body communications, we are interested in mitigating the body shadowing by using multiple antennas.

The development of "smart clothes" [22] using E-textiles and wearable antennas which can be easily embedded into clothes, e.g. [23, 24], provide a unique opportunity to mitigate the body shadowing by distributing antennas to various body positions. Studies in [25–27] and [Paper A] have shown the distributed on-body antennas can decrease the effects of the body shadowing effectively.

To investigate the performance of such multi-antenna systems a MIMO channel model which takes the body shadowing into consideration is required. In [Paper B] we propose a novel correlation based stochastic model with correlated shadowing (CBSM-CS). The proposed model can be used to simulate both the body-to-body and body-to-AP channels. To the authors' knowledge, this is one of the first MIMO channel models including the body shadowing effects in open literature.

5 On-body UWB WBAN channels

An on-body communication system connects various wearable electronic devices, such as body sensors, body monitors and motion detectors, placed on the same body. Applications of the on-body BWCS can be found in Section 1.

5.1 UWB in WBAN

The UWB signals are defined as signals with either a large relative bandwidth ($> 20\%$), or a large absolute bandwidth (> 500 MHz). In 2002 Federal Communications Commission (FCC) in US granted unlicenced frequency band between 3.1 and 10.6 GHz for indoor communications with a power mask of 41.3 dBm/MHz [28]. UWB spectral regulations have also been finalized in Europe by European Telecommunications Standards Institute (ETSI) in 2007 and in Japan in 2006.

The UWB is a promising technology for short range radio communications. Most possibly the transmission data rate will be less than 1 Mbps for the WBAN applications between the on-body sensors and the central devices as shown in Fig. 1 [29]. The low power consumption and low complexity of the low data rate (LDR) UWB system make it a competent candidate for the WBAN applications. IEEE working group $802.15.4a$ has presented a number of physical layer (PHY) specifications based on the UWB technology for the WPAN and WBAN applications [29]. The ZigBee, which is widely used in the WBAN, has adopted some of the proposed specifications [7, 30].

In an European project 'My personal Adaptive Global NET' (MAGNET) which aims at developing solutions for the WPAN and WBAN applications, an alternative air interface for the WBAN systems based on frequency modulation-UWB (FM-UWB) has been developed, evaluated and implemented [31].

To achieve the full potential advantages provided by the UWB comprehensive channel knowledge is required.

5.2 Antennas in WBAN channels

There are additional requirements for the antennas used in the BWCS compared with the ones in other systems mainly due to two reasons: user proximity and size limitation. These two factors are more stringent to body-worn (BW) devices than hand-held (HH) and belt-mounted (BM) devices due to their smaller physical size and shorter distance to the body surface. The knowledge obtained from the investigations of the body proximity in mobile communications can be partly reused in the BWCS [11, 32–35]. An overview of antenna design challenges in the BWCS can be found in [36]. Almost all the antenna parameters need a second thought in the BWCS:

- Impedance matching

The changes in impedance matching due to the body proximity for both narrowband [9, 37–39] and UWB [23] antennas have been addressed in literature. It is critical to limit the shift of resonant frequency for the narrowband antennas and the increase of return loss (S11) for the UWB antennas in an acceptable range.

- Radiation efficiency

  The radiation efficiency of the antennas working close to the human body may decrease significantly compared with the free-space efficiency since part of radiation energy is absorbed by the human body. Preliminary researches of the body proximity effects on the radiation efficiency were performed for the mobile communication since the last century [9, 40–43]. Since the amount of the efficiency loss depends on the distance between the antenna and the body surface [Paper A], the loss may be more severe in the BWCS than in the mobile communication due to the smaller size and accordingly the shorter antenna to body distance [44] [Paper A].

  The on-body radiation efficiency of three types of antennas were simulated by a frequency domain time difference (FDTD) method in [Paper A]. The simulations were performed with three antenna types, four device on-body positions and two antenna body distances. The larger efficiency loss with the omni-directional antenna and the smaller distance to the body is evident.

  Besides the body proximity the size of the WBAN devices may force antenna designers to sacrifice some efficiency to realize electronically small antennas [45].

- Radiation pattern

  The influence of the BWCS to the antenna radiation pattern is two fold.

  Firstly, most antennas have more directional far-field patterns when mounted on the human body due to the absorption and reflection of the energy radiating into the body as shown in [Paper A] and [13, 46–48]. This suggests that using directional antennas in the BWCS can increase antenna efficiency.

  Secondly, experiments performed in anechoic chambers have shown that for the on-body BWCS the body diffraction is the primary propagation mechanism when there is no LOS between the Tx and the Rx [48, 49]. In this condition aligning the maximum radiation intensity direction of the antenna with the tangent of the body surface will enhance the diffraction component. As a consequence it will increase the channel gain and reduce the delay spread [50]. It should be noticed that the conclusion above was drawn based on an assumption of no multipaths from environments. In the indoor environments with rich scatterers the conclusion may be vulnerable. The UWB WBAN channels were in two indoor environments measured in [Paper C]. The power ratio between the body diffraction and the

multipaths from the environments is as low as -10 dB when the Tx and Rx are placed on the different sides of the human body. In other words most channel power is contributed by the reflections from the environments. Although this result is specific to the antennas used in the measurements, such a low power ratio indicates that the channel gain may be increased by radiating more energy into the environment. Therefore the operating environment needs to be considered when selecting the antenna radiation patterns for the UWB WBAN applications.

5.3 Propagation in WBAN channels

Compared with other radio channels the WBAN channel is featured by the short range direct link, body diffraction and body reflection. The penetration through the body is usually negligible in the microwave frequency band [48]. The term of the 'around body' propagation is used in this study to represent the radio propagation close to human bodies. An extensive summary of narrowband on-body channel propagation was given in [1].

5.4 A summary of UWB WBAN channel investigations

FDTD was usually used as a channel simulation method for the UWB WBAN channel investigations [48, 51, 52] [Paper A]. A simpler ray theory based approach also provided reliable solutions [51]. Most experimental investigations for the WBAN channel were performed in anechoic chambers and focused on the around body propagation. Body diffraction was found as the dominant propagation mechanism between the ears of the human head [48]. Path-loss models along torsos were derived in [49, 53, 54]. Distance dependent exponential power decay with decay factors between 2.7 and 4.4 was reported. The distribution of the body diffraction components was summarized in [55, 56] and Lognormal was found as a good fit for the small-scale fading statistics. Some WBAN channel parameters, e.g. delay spread, were proved sensitive to the antenna positions, body gestures and antenna types [49].

When the on-body BWCS system works in indoor environments the reflection, diffraction and scattering from the environments will also be parts of the radio channel. However few experimental studies have been conducted for the UWB WBAN channel in realistic end-user scenarios. The measurement results on channel path loss [57], wideband power variation [46], path arrival times [58] and delay spread [46, 57] have been presented. In reference [53] the body diffraction and surrounding environments are modeled separately based on experiments with the antennas placed on the torso.

In [Paper C] we propose a UWB WBAN channel model which uses a joint approach to take both the around body and the environment propagation into consideration.

It is well known that the indoor UWB channel usually consists of a number of

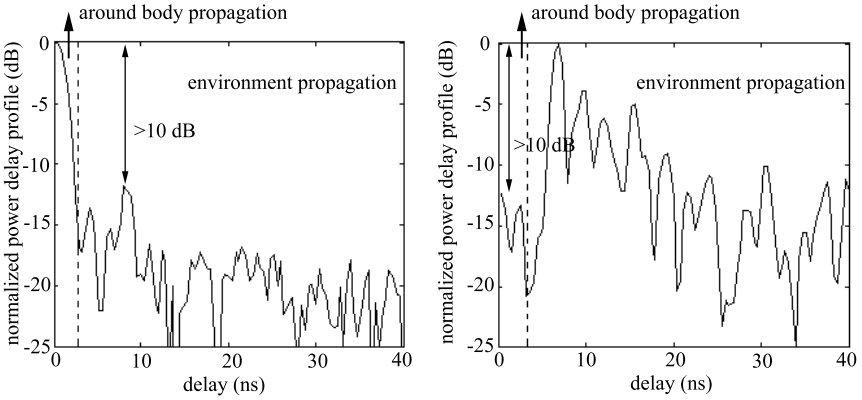

Figure 4: Normalized measured channel power delay profiles (left: right-wrist to right-waist, right: left-wrist to right-waist)

clusters [53, 55, 59, 60]. Given sufficient distance between the body and scatterers in the environments, the first cluster in the UWB WBAN channel is only composed of signals from the around body propagation. Due to the fine delay resolution of the UWB system, it is possible to separate the around body propagation and the environment propagation in the delay domain. Figure 4 shows two examples of measured power delay profiles (PDPs). The peak of the PDP is normalized to one. The one to the left is taken form the measurement between a Tx placed on the right-wrist and a Rx mounted on the right-waist, and the right plot shows a PDP of the channel between the left-wrist and the right-waist. As shown in the figure the propagation around the human body and from the environment can be well separated. In addition the around body propagation is dominant compared with the environment propagation in the right-wrist to right-waist channel and the left-wrist to right-waist channel shows the opposite. It implies that different characterization and modeling parameters need to be proposed for the channels with the different relative Tx-Rx positions.

The channel model proposed in [Paper C] reuses previous developed indoor UWB channel models to generate multipaths from environments, it can be adapted to specific environments by applying different available models. Several popular indoor UWB channel models are listed as follows: an IEEE 802.15.3a Model [61], an IEEE 802.15.4a Model [62] and a Mobile-to-mobile model [63]. More indoor UWB channel models can be found in [59].

6 UWB-MIMO WPAN Channels

The UWB-MIMO systems have captured increasing research interests in recent years. In this section the potential of the UWB-MIMO system in the WPAN applications is analyzed and summarized with emphasis on the channel characteristics.

6.1 UWB in WPAN

The UWB systems for the WPAN applications can be categorized into high data rate (HDR) and low data rate (LDR) systems. The LDR UWB system has been summarized in Section 5.1. Since the UWB-MIMO system is most possibly designed for the HDR transmission, a summary of the HDR UWB system is given below.

The transmission rate of the HDR UWB system is usually higher than 100 Mbps. IEEE 802.15.3a working group was established in 2002 for the standardization of the HDR UWB systems. System specifications including achieving a data rate of 110 Mbps at a 10 meter distance and 480 Mbps at 4 meter distance have been presented. In 2006 the working group is divided into two parts: WiMedia Alliance and UWB Forum. They use Orthogonal Frequency Division Multiplexing (OFDM) and Direct Sequence Spread Spectrum (DSSS) as PHY layer solutions respectively. Up to now a number of prototype systems have been developed based on each of the two solutions.

6.2 Potential benefits of UWB-MIMO systems

The motivations of combining the UWB and MIMO techniques are listed below:

- Higher data rate by spatial multiplexing

  The linearly increasing of the UWB-MIMO channel ergodic capacity with the minimum number of transmitter and receiver antennas under Nakagami fading channels has been shown in [64]. The UWB-MIMO system holds the large bandwidth and high spectral efficiency at the same time, and have an tremendous potential in achieving very high data rate transmission. The WPAN applications which demand high data rate, e.g. video transmission and mass data transfer, may benefit from the high capacity of the UWB-MIMO system.

- Larger coverage by array gains

  Due to the spectral masks regulated by FCC, ETSI and other regulation bodies, the coverage range of the UWB system is limited. Since multiple receive antennas provide antenna array gain, they can be used to improve the coverage of the UWB systems [65]. It should be noticed that beamforming at transmitters may violate the effective isotropic radiated power (EIRP) requirements defined by the regulation bodies.

- Reduced number of RAKE fingers by diversity gain

  The UWB channel has already provided a sufficient frequency diversity gain with the large bandwidth. However a great number of RAKE fingers may be required to achieve the diversity gain [59]. The spatial diversity provided by the multiple antennas can reduce the required number of fingers in the RAKE receiver [65, 66].

An overview of recent research advances in the study of the UWB-MIMO system can be found in [67].

6.3 UWB-MIMO channels in WPAN

MIMO wireless systems, characterized by multiple antenna elements at both the transmitter and receiver, have demonstrated the potential for increased capacity in rich multipath environments given low correlation between antenna links [68–71].

Handset MIMO systems have been investigated for years in the mobile communication systems. It has been proved that low antenna link correlation and high channel capacity can be achieved with two to four antennas placed in one handset [72–75]. For the off-body BWCS experimental works proved low correlation between two dual-polarized antenna elements placed in handset-like devices for both wideband [18, 76] and UWB [Paper D] systems. For multi-antenna body-worn devices low fading correlation between antenna elements was reported in [77] and [Paper A]. Therefore the feasibility of implementing MIMO systems with typical WPAN devices has bee proved.

The spatial correlation of the UWB-MIMO channel between two fixed devices has been characterized at different delays [66, 78], different frequency bins [78–81] and for the whole frequency transfer functions [82]. Low correlation coefficients (< 0.5) were disclosed in different environments and with different antenna arrays. One exception is in [66] the correlation of the first delay bin was 0.7. A correlation-based double-directional stochastic channel model for indoor UWB-MIMO channels is proposed in [83]. The model extends the IEEE 802.15.3a standard model to spatially correlated MIMO channels. A review of existing stochastic UWB-MIMO channel model is also given in [83]. A deterministic UWB-MIMO channel model is presented in [84].

Few UWB-MIMO channel studies have been performed for the off-body BWCS. In [77] short range (1m) body-to-fixed device MIMO channels were measured in the LOS condition in an empty room. High spatial correlation and high MIMO capacity were observed at the same time which was explained with the spherical nature of the wave front in the short distance range. In [Paper D] UWB-MIMO channels in HH-to-AP and BM-to-AP scenarios were investigated based on measurements with walking users in three typical indoor environments. Low spatial correlation in both the delay and frequency domain was disclosed. The channel wideband power is correlated since

the antennas at both the AP and the user side are likely to experience similar body shadowing.

7 Conclusions

This thesis work focuses on the investigations of radio channel propagation in body-centric wireless communication systems (BWCSs). The emphasis was put on experimental based characterization and modeling of both off-body and on-body channels in wireless personal area networks (WPANs) and wireless body area networks (WBANs), respectively. The thesis consists of three parts.

In the first part we characterized and modeled the indoor body-to-body radio channel with multiple antennas at both the transmit and receive side in [Paper A] and [Paper B]. The study was based on two sets of measurement campaigns performed at 5.5 GHz frequency band. In the first campaign body shadowing and small-scale fading were deliberately separated in the measurements while in the second one the test persons were moving in a more random manner. Based on the first campaign the path-loss exponent was less than 2.0 and the standard deviation of the log-normal distributed shadowing was 4.8 dB. This indicates that the body shadowing plays a key role in the short range body-to-body communication. Due to the low shadowing correlation between antennas placed at different parts of the human body, a distributed antenna selection diversity scheme was presented to mitigate the body shadowing. The mean selection diversity gain was 5 dB when two antennas were mounted on each of the transmit and receive sides of the channel. A correlation based stochastic model with correlated shadowing (CBSM-CS) for body-to-body multiple-input multiple-output (MIMO) radio channels was proposed based on the first measurement campaign. The modeling accuracy in terms of channel capacity was verified by the second measurement campaign. The relative model error is always less than 5% for different MIMO configuraitons. The model introduces a shadowing matrix to represent unbalanced and correlated body shadowing effects. A Rayleigh-Lognormal distributed CBSM-CS channel model was derived and analyzed. To the authors' knowledge, this is one of the first MIMO channel models including the body shadowing effects in open literature. It is disclosed that shadowing standard deviation is dominant to the ergodic capacity while shadowing correlation between the antennas significantly affects the outage capacity. For larger size MIMO arrays, keeping shadowing correlation low becomes more essential to avoid small capacity at the outage level.

The second part of the thesis focuses on the characterization and modeling of the UWB WBAN channel in indoor environments in [Paper C]. The study was based on experiments performed with realistic end-user scenarios at a frequency band between 3.5 and 5.5 GHz. The receiver was placed on the right-waist and a total of 15 different transmitter on-body positions were evaluated. The channel wideband power varied by up to 20 dB and the channel mean rms delay spread ranged from 5 to 20 ns at the various device positions. To separate the propagation around the human body from the propagation in the surrounding environment, the first cluster of the measured channel impulse

response was detected, separated from remaining clusters and characterized. Power ratio and arrival time interval between the first cluster and the remaining clusters were investigated. The decay factor of the remaining cluster was found linearly dependent on the power ratio in dB. Based on the channel knowledge above a channel model for the UWB WBAN system working in indoor environments was proposed. The model uses a joint approach to generate and combine the propagation around the human body and in the surrounding environment in the delay domain. A modeling procedure was presented in order to implement the channel for system evaluations. The proposed model is one of a few existing ones including the environment propagation. Since the model uses available UWB indoor channel models to generate multipaths from environments, it can be adapted to specific environments by applying different available models.

In the third part of the thesis we presented an analysis of the spatial correlation properties of indoor UWB-MIMO channels in the off-body BWCS [Paper D]. The investigation was based on channel measurements of radio links between an access point like device and a walking user with a hand-held or a belt-mounted device. The measurements were performed at a frequency band between 3.5 and 5.5 GHz. It was found that the channel shows spatial correlated wideband power, and spatial uncorrelated complex channel coefficients in both the time-frequency and time-delay domain. The channel was found to be quasi spatially white since all link pairs showed similar correlation properties. The Kronecker model was proved unsuitable for these WPAN scenarios where the receiver and transmitter are located in the same cluster of main radio scatterers. The ergodic and 1% outage wideband capacity of the measured 2×2 channel were determined to be 5.4 bit/s/Hz and 4 bit/s/Hz at 10 dB SNR. While the ergodic capacity was close to the independent identical distributed (IID) Rayleigh channel capacity the 1% outage capacity dropped approximately 0.8 bit/s/Hz due to the signal shadowing introduced by the user bodies during their movement. Adding two more antennas at the receiver (access point) side increased the ergodic and outage capacity to 6.1 and 5.6 bit/s/Hz respectively.

The channel characteristics and modeling parameters proposed in this thesis are specific to our measurement campaigns. However, the methodology can easily be reproduced and the models can be extended to other conditions. Therefore, more experiments at other frequency bands, in different environments, with different antennas and in different user scenarios are highly encouraged and recommended to generalize the contributions of this thesis. For the body-to-body channel, the distribution of the body shadowing depends on both the antenna on-body radiation pattern and the surrounding environment. Therefore the Lognormal distributed body shadowing needs to be verified in more environments and with more types of antennas. For the UWB WBAN channel if the distance between the human body and scatterers are very short the propagation around the human body and in the surrounding environment may be overlapped in the delay domain. In this condition the proposed model needs to be adjusted and verified

by simulations or measurements. In addition, the correlation between the multiple antennas at central devices is subject to further research in the UWB WBAN channel to investigate the potential diversity gain of using the multiple antennas. Concerning the WPAN UWB-MIMO channel while low correlation has been disclosed the studies on the distribution and variation of channel eigenmodes are important for practical system design.

Reference

[1] P. S. Hall and Y. Hao, *Antennas and propagation for body-centric wireless communications*. Artech House, INC., 2006.

[2] R. S. H. Istepanian, E. Jovanov, and Y. T. Zhang, "Introduction to the special section on m-health: Beyond seamless mobility and global wireless health-care connectivity," *IEEE Transactions on Information Technology in Biomedicine*, vol. 8, no. 4, pp. 405–414, Dec 2004.

[3] J. Edimison, D. Lehn, M. Jones, and T. Martin, "E-textile based automatic activity diary for medical annotation and analysis," in *Wearable and Implantable Body Sensor Networks, 2006.BSN 2006.International Workshop on*, Apr 2006, pp. 4–7.

[4] E. Monton, J. F. Hernandez, J. M. Blasco, T. Herve, J. Micallef, I. Grech, A. Brincat, and V. Traver, "Body area network for wireless patient monitoring," *Iet Communications*, vol. 2, no. 2, pp. 215–222, Feb 2008.

[5] C. L. Lisetti and F. Nasoz, "Using noninvasive wearable computers to recognize human emotions from physiological signals," *Eurasip Journal on Applied Signal Processing*, vol. 2004, no. 11, pp. 1672–1687, Sep 2004.

[6] F. Lorussi, W. Rocchia, E. P. Scilingo, A. Tognetti, and D. De Rossi, "Wearable, redundant fabric-based sensor arrays for reconstruction of body segment posture," *IEEE Sensors Journal*, vol. 4, no. 6, pp. 807–818, Dec 2004.

[7] E. Jovanov, A. Milenkovic, C. Otto, and P. De Doncker, "A wireless body area network of intelligent motion sensors for computer assisted physical rehabilitation," *Journal of NeuroEngineering and Rehabilitation*, vol. 2, Mar 2005.

[8] P. S. Hall and Y. Hao, "Antennas and propagation for body centric communications," in *European Space Agency, (Special Publication) ESA SP*, vol. 626 SP, Oct 2006.

[9] J. Toftgard, S. N. Hornsleth, and J. B. Andersen, "Effects on portable antennas of the presence of a person," *IEEE Transactions on Antennas and Propagation*, vol. 41, no. 6, pp. 739–746, Jun 1993.

[10] G. F. Pedersen, J. Ø. Nielsen, K. Olesen, and I. Z. Kovacs, "Measured variation in performance of handheld antennas for a large number of test persons," in *Vehicular Technology Conference, 1998.VTC 98.48th IEEE*, vol. 1, May 1998, pp. 505–509.

[11] K. Ogawa, T. Matsuyoshi, and K. Monma, "An analysis of the performance of a handset diversity antenna influenced by head, hand, and shoulder effects at 900 MHz: Part I - effective gain characteristics," *IEEE Transactions on Vehicular Technology*, vol. 50, no. 3, pp. 830–844, May 2001.

[12] J. O. Nielsen and G. F. Pedersen, "Mobile handset performance evaluation using radiation pattern measurements," *IEEE Transactions on Antennas and Propagation*, vol. 54, no. 7, pp. 2154–2165, Jul 2006.

[13] K. I. Ziri-Castro, W. G. Scanlon, and N. E. Evans, "Indoor radio channel characterization and modeling for a 5.2-GHz body worn receiver," *IEEE Antennas and Wireless Propagation Letters*, vol. 3, no. 1, pp. 219–222, 2004.

[14] T. B. Welch, R. L. Musselman, B. A. Emessiene, P. D. Gift, D. K. Choudhury, D. N. Cassadine, and S. M. Yano, "The effects of the human body on UWB signal propagation in an indoor environment," *IEEE Journal on Selected Areas in Communications*, vol. 20, no. 9, pp. 1778–1782, Dec 2002.

[15] S. Obayashi and J. Zander, "A body-shadowing model for indoor radio communication environments," *IEEE Transactions on Antennas and Propagation*, vol. 46, no. 6, pp. 920–927, Jun 1998.

[16] M. Ghaddar, L. Talbi, T. A. Denidni, and A. Sebak, "A conducting cylinder for modeling human body presence in indoor propagation channel," *IEEE Transactions on Antennas and Propagation*, vol. 55, no. 11, pp. 3099–3103, Nov 2007.

[17] A. Pradabphon, N. Kaewboonruean, M. Chamchoy, P. Supanakoon, and S. Promwong, "Experimental evaluation scheme of UWB radio propagation channel with human body," in *ISCIT 2005 - International Symposium on Communications and Information Technologies , Proceedings*, vol. 11, 2005/// 2005, pp. 638–641.

[18] J. Karedal, A. J. Johansson, F. Tufvesson, and A. F. Molisch, "Characterization of MIMO channels for handheld devices in personal area networks at 5 GHz," in *14th European Signal Processing Conference (EUSIPCO 2006)*, Sep 2006.

[19] P. Kyritsi, P. C. Eggers, and J. M. Lourenco, "Measurement based investigation of cooperative relaying," in *Proceedings of VTC 2006 Fall*, 2006, pp. 178–182.

[20] G. L. Steuber, *Principles of mobile communication*. Springer, 2004, vol. 2nd.

[21] J. C. Lin, W. C. Kao, Y. T. Su, and T. H. Lee, "Outage and coverage considerations for microcellular mobile radio systems in a shadowed-rician/shadowed-nakagami environment," *IEEE Transactions on Vehicular Technology*, vol. 48, no. 1, pp. 66–75, Jan 1999.

[22] Z. W. Tang and A. S. Mohan, "An investigation of MIMO performance in the indoor ricean environment," *Wireless Personal Communications*, vol. 39, no. 1, pp. 99–113, Oct 2006.

[23] M. Klemm, I. Z. Kovacs, G. F. Pedersen, and G. Troster, "Novel small-size directional antenna for UWB wban/wPAN applications," *IEEE Transactions on Antennas and Propagation*, vol. 53, no. 12, pp. 3884–3896, Dec 2005.

[24] P. Salonen, Y. Rahmat-Samii, and M. Kivikoski, "Wearable antennas in the vicinity of human body," in *Antennas and Propagation Society International Symposium, 2004.IEEE*, vol. 1, 2004, pp. 467–470.

[25] S. L. Cotton and W. G. Scanlon, "Spatial diversity and correlation for off-body communications in indoor environments at 868 MHz," in *Vehicular Technology Conference, 2007.VTC2007-Spring.IEEE 65th*, 2007, pp. 372–376.

[26] Y. Ouyang and W. Chappell, "Distributed body-worn transceiver system with the use of electro-textile antennas," in *Microwave Symposium, 2007.IEEE/MTT-S International*, Jun 2007, pp. 1229–1232.

[27] E. C. Kohls, A. Abler, P. Siemsen, J. Hughes, R. Perez, and D. Widdoes, "A multi-band body-worn antenna vest," in *Antennas and Propagation Society International Symposium, 2004.IEEE*, vol. 1, 2004, pp. 447–450.

[28] FCC, “Revision of part 15 of the commission’s rules regarding ultra-wideband transmission systems,” Tech. Rep., Apr 2002.

[29] I. C. Society, “IEEE standard 802.15.4a-2007,” Tech. Rep., Aug 2007.

[30] A. Wheeler, “Commercial applications of wireless sensor networks using zigbee,” *IEEE Communications Magazine*, vol. 45, no. 4, pp. 70–77, Apr 2007.

[31] IST-2004-507102, “My personal Adaptive Global Net (MAGNET) deliverable d3.2.2a candidate air interfaces and enhancements,” Tech. Rep., Oct 2004. [Online]. Available: http://www.ist-magnet.org/public+deliverables/phase1wp3

[32] G. F. Pedersen, J. B. Andersen, and S. Skjaerris, “Integrated handset antenna with low absorption and handset antenna diversity,” in *IEE Colloquium (Digest)*, 1997, pp. 4/1–4/7.

[33] K. Ogawa, T. Matsuyoshi, and K. Monma, “An analysis of the performance of a handset diversity antenna influenced by head, hand, and shoulder effects at 900 MHz: Part Ii - correlation characteristics,” *IEEE Transactions on Vehicular Technology*, vol. 50, no. 3, pp. 845–853, May 2001.

[34] G. F. Pedersen and J. O. Nielsen, “Radiation pattern measurements of mobile phones next to different head phantoms,” in *Proceedings.VTC 2002-Fall.2002 IEEE 56th*, vol. 56, 2002, pp. 2465–2469.

[35] K. Ogawa, A. Yamamoto, and J. Takada, “Multipath performance of handset adaptive array antennas in the vicinity of a human operator,” *IEEE Transactions on Antennas and Propagation*, vol. 53, no. 8, pp. 2422–2436, Aug 2005.

[36] P. S. Hall, “Antennas challenges for body centric communications,” in *Antenna Technology: Small and Smart Antennas Metamaterials and Applications, 2007.IWAT ’07.International Workshop on*, Mar 2007, pp. 41–44.

[37] G. F. Pedersen, K. Olesen, and S. L. Larsen, “Bodyloss for handheld phones,” in *Vehicular Technology Conference, 1999 IEEE 49th*, vol. 2, Jun 1999, pp. 1580–1584.

[38] K. Ogawa, T. Uwano, and M. Takahashi, “Shoulder-mounted planar antenna for mobile radio applications,” *IEEE Transactions on Vehicular Technology*, vol. 49, no. 3, pp. 1041–1044, May 2000.

[39] K. Ogawa, M. Takahashi, Y. Koyanagi, and K. Ito, “Automatic impedance matching of an active helical antenna near a human operator,” in *33rd European MicrowaveConference 2003 Intl.Symp.Digest*, Oct 2003, pp. 1271–1274.

[40] G. F. Pedersen, K. Olesen, and S. L. Larsen, “Antenna efficiency of handheld phones,” in *Electromagnetic Assessment and Antenna Design Relating To Health Implications of Mobile Phones (Ref.No.1999/043), IEE Seminar on*, vol. 6, 1999, pp. 1–5.

[41] G. F. Pedersen, M. Tartiere, and M. B. Knudsen, “Radiation efficiency of handheld phones,” in *Vehicular Technology Conference Proceedings, 2000.VTC 2000-Spring Tokyo.2000 IEEE 51st*, vol. 2, 2000, pp. 1381–1385.

[42] G. F. Pedersen, “Phantoms for radiation measurements of mobile phones,” in *IEEE International Symposium on Personal, Indoor and Mobile Radio Communications, PIMRC*, vol. 1, 2001, pp. C95–C99.

[43] K. Ogawa, T. Matsuyoshi, and K. Monma, "A study of the effects of the shoulder on the effective gain characteristics in the multiple radio wave environment of a dipole antenna close to a human head," *Electronics and Communications in Japan Part I-Communications*, vol. 84, no. 1, pp. 21–30, 2001.

[44] T. Salim and P. S. Hall, "Efficiency measurement of antennas for on-body communications," *Microwave and Optical Technology Letters*, vol. 48, no. 11, pp. 2256–2259, Nov 2006.

[45] J. S. Mclean, "A re-examination of the fundamental limits on the radiation q of electrically small antennas," *IEEE Transactions on Antennas and Propagation*, vol. 44, no. 5, pp. 672–676, May 1996.

[46] I. Z. Kovacs, G. F. Pedersen, P. C. Eggers, and K. Olesen, "Ultra wideband radio propagation in body area network scenarios," in *Proc.IEEE Eighth International Symposium on Spread Spectrum Techniques and Applications*, Sep 2004, pp. 102–106.

[47] K. Y. Yazdandoost and R. Kohno, "UWB antenna for wireless body area network," in *Microwave Conference, 2006.APMC 2006.Asia-Pacific*, 2006, pp. 1647–1652.

[48] T. Zasowski, G. Meyer, F. Althaus, and A. Wittneben, "UWB signal propagation at the human head," *IEEE Transactions on Microwave Theory and Techniques*, vol. 54, no. 4, pp. 1836–1845, Apr 2006.

[49] A. Alomainy, Y. Hao, X. Hu, C. G. Parini, and P. S. Hall, "UWB on-body radio propagation and system modelling for wireless body-centric networks," *IEE Proceedings-Communications*, vol. 153, no. 1, pp. 107–114, Feb 2006.

[50] A. Alomainy, Y. Hao, C. G. Parini, and P. S. Hall, "Comparison between two different antennas for UWB on-body propagation measurements," *IEEE Antennas and Wireless Propagation Letters*, vol. 4, pp. 31–34, 2005.

[51] Y. Zhao, Y. Hao, A. Alomainy, and C. Parini, "UWB on-body radio channel modeling using ray theory and subband fdtd method," *IEEE Transactions on Microwave Theory and Techniques*, vol. 54, no. 4, pp. 1827–1835, Apr 2006.

[52] T. Wuren, T. Takai, M. Fujii, and I. Sakagami, "Effective 2-debye-pole fdtd model of electromagnetic interaction between whole human body and UWB radiation," *IEEE Microwave and Wireless Components Letters*, vol. 17, no. 7, pp. 483–485, Jul 2007.

[53] A. Fort, J. Ryckaert, C. Desset, P. De Doncker, P. Wambacq, and L. Van Biesen, "Ultra-wideband channel model for communication around the human body," *IEEE Journal on Selected Areas in Communications*, vol. 24, no. 4, pp. 927–933, Apr 2006.

[54] H. Ghannoum, C. Roblin, and X. Begaud, "Investigation and modeling of the UWB on-body propagation channel," *Wireless Personal Communications (Article in Press)*, pp. 1–12, 2008.

[55] A. Fort, C. Desset, P. De Doncker, P. Wambacq, and L. Van Biesen, "An ultra-wideband body area propagation channel model - from statistics to implementation," *IEEE Transactions on Microwave Theory and Techniques*, vol. 54, no. 4, pp. 1820–1826, Apr 2006.

[56] K. T. Pak, H. C. Yong, C. O. Ling, M. K. Haldar, and L. Bin, "Small-scale transmission statistics of UWB signals for body area communications," in *Proceedings of VTC 2006 Fall*, Sep 2006, pp. 1–5.

[57] Y. P. Zhang, L. Bin, and C. Qi, "Characterization of on-human-body UWB radio propagation channel," *Microwave and Optical Technology Letters*, vol. 49, no. 6, pp. 1365–1371, Jun 2007.

[58] A. A. Goulianos and S. Stavrou, "UWB path arrival times in body area networks," *IEEE Antennas and Wireless Propagation Letters*, vol. 6, pp. 223–226, 2007.

[59] A. F. Molisch, "Ultrawideband propagation channels - theory, measurement, and modeling," *IEEE Transactions on Vehicular Technology*, vol. 54, no. 5, pp. 1528–1545, Sep 2005.

[60] I. Z. Kovacs, H. T. Nguyen, P. C. Eggers, and K. Olesen, "Enhanced UWB radio channel model for short-range communication scenarios including user dynamics," in *IST Mobile & Wireless Communications Summit*, ser. IST Mobile & Wireless Communications Summit, 2005.

[61] J. R. Foerster and e. al, "IEEE p802.15 wireless personal area networks channel modeling sub-committee report final," Tech. Rep., Feb 2003.

[62] A. F. Molisch and e. al, "IEEE p802.15.4a channel model-final report," Tech. Rep., 2005.

[63] I. Z. Kovacs, Y. Wang, P. C. Eggers, and K. Olesen, "UWB radio channel model for short-range mobile-to-mobile communication scenarios," in *Wireless Personal Multimedia Communications (WPMC) Symposia 2005*, Sep 2005, pp. 2008–2012.

[64] F. Zheng and T. Kaiser, "On the evaluation of channel capacity of multi-antenna UWB indoor wireless systems," in *ISSSTA2004, Sydney, Australia*, ser. International Symposium on Spread Spectrum Techniques and Applications, ISSSTA, 2004, pp. 525–529.

[65] L. C. Wang, W. C. Liu, and K. J. Shieh, "On the performance of using multiple transmit and receive antennas in pulse-based ultrawideband systems," *IEEE Transactions on Wireless Communications*, vol. 4, no. 6, pp. 2738–2750, Nov 2005.

[66] J. Keignart, C. bou Rjeily, C. Delaveaud, and N. Daniele, "UWB simo channel measurements and simulations," *IEEE Transactions on Microwave Theory and Techniques*, vol. 54, no. 4, pp. 1812–1819, Apr 2006.

[67] T. Kaiser. John Wiley & Sons, Inc., 2006, no. 9, ch. MIMO and UWB, pp. 205–225.

[68] G. J. Foschini and M. J. Gans, "On limits of wireless communications in a fading environment when using multiple antennas," *Wireless Personal Communications*, vol. 6, no. 3, pp. 311–335, 1998.

[69] E. Telatar, "Capacity of multi-antenna gaussian channels," *European Transactions on Telecommunications*, vol. 10, no. 6, pp. 585–595, Nov 1999.

[70] D. Gesbert, M. Shafi, D. S. Shiu, P. J. Smith, and A. Naguib, "From theory to practice: An overview of MIMO space-time coded wireless systems," *IEEE Journal on Selected Areas in Communications*, vol. 21, no. 3, pp. 281–302, Apr 2003.

[71] M. A. Jensen and J. W. Wallace, "A review of antennas and propagation for MIMO wireless communications," *IEEE Transactions on Antennas and Propagation*, vol. 52, no. 11, pp. 2810–2824, Nov 2004.

[72] W. A. T. Kotterman, G. F. Pedersen, and K. Olesen, "Capacity of the mobile MIMO channel for a small wireless handset and user influence," in *Personal, Indoor and Mobile Radio Communications, 2002.PIMRC 2002.13th IEEE International Symposium on*, vol. 4, Sep 2002, pp. 1937–1941.

[73] W. A. T. Kotterman, G. F. Pedersen, K. Olesen, and P. C. Eggers, "Correlation properties for radio channels from multiple base stations to two antennas on a small handheld terminal," in *Vehicular Technology Conference, 2002.Proceedings.VTC 2002-Fall.2002 IEEE 56th*, vol. 1, Sep 2002, pp. 462–466.

[74] K. Ogawa, H. Iwai, A. Yamamoto, and J. Takada, "Channel capacity of a handset MIMO antenna influenced by the effects of 3D angular spectrum, polarization, and operator," in *Antennas and Propagation Society International Symposium 2006, IEEE*, Jul 2006, pp. 153–156.

[75] K. Ogawa, S. Amari, and A. Yamamoto, "An analysis of the channel capacity of handset MIMO antennas under received power imbalance condition," *IEICE Tran.*, vol. J91-B, no. 9, Sep 2008, (to be published).

[76] A. J. Johansson, J. Karedal, F. Tufvesson, and A. F. Molisch, "MIMO channel measurements for personal area networks," in *Proceedings of VTC 2005 Spring Stockholm*, ser. IEEE Vehicular Technology Conference (VTC), vol. 61, May 2005, pp. 171–176.

[77] D. Neirynck, C. Williams, A. Nix, and M. Beach, "Exploiting multiple-input multiple-output in the personal sphere," *IET Microwaves, Antennas and Propagation*, vol. 1, no. 6, pp. 1170–1176, Dec 2007.

[78] H. Agus, J. Nielsen, and R. J. Davies, "Correlation analysis for indoor UWB channel," in *Wireless 2005*, Calgary, AB, Canada,, Jul 2005.

[79] C. Prettie, D. Cheung, L. Rusch, and M. Ho, "Spatial correlation of UWB signals in a home environment," in *Ultra Wideband Systems and Technologies, 2002.Digest of Papers.2002 IEEE Conference on*, ser. IEEE Conference on Ultra Wideband Systems and Technologies, 2004, pp. 65–69.

[80] W. Q. Malik, M. C. Mtumbuka, D. J. Edwards, and C. J. Stevens, "Performance analysis of ultra-wideband spatial MIMO communications systems," in *Proc.14th IST Mobile Comm.Summit.*, ser. IST Mobile Comm.Summit., Jun 2005.

[81] ——, "Increasing MIMO capacity in ultra-wideband communications through orthogonal polarizations," in *IEEE Workshop on Signal Processing Advances in Wireless Communications, SPAWC*, ser. IEEE Workshop on Signal Processing Advances in Wireless Communications, SPAWC, vol. 2005, 2005, pp. 575–579.

[82] W. Q. Malik, "Spatial correlation in ultrawideband channels," *IEEE Transactions on Wireless Communications*, vol. 7, no. 2, pp. 604–610, Feb 2008.

[83] X. Hong, C. X. Wang, B. Allen, and W. Q. Malik, "Correlation-based double-directional stochastic channel model for multiple-antenna ultra-wideband systems," *Iet Microwaves Antennas & Propagation*, vol. 1, no. 6, pp. 1182–1191, Dec 2007.

[84] L. M. Aubert, B. Uguen, and F. T. Talom, "Deterministic simulation of MIMO-UWB transmission channel," *Comptes Rendus Physique*, vol. 7, no. 7, pp. 751–761, Sep 2006.

[Paper A] Y. Wang, B. B. Ivan, J. Ø. Nielsen, I. Z. Kovacs and G. F. Pedersen, "Characterization of the Indoor Multi-Antenna Body-to-Body Radio Channel", *IEEE Transactions on Antennas and Propagation Special Issue on Body-Centric Wireless Communications*. (submitted, Jan 2008)

[Paper B] Y. Wang, J. Ø. Nielsen, I. Z. Kovacs and G. F. Pedersen, "MIMO Channel Modeling for Body-to-Body Communications", *IEEE Transactions on Wireless Communications*. (to be submitted, Aug 2008)

[Paper C] Y. Wang, I. Z. Kovacs and G. F. Pedersen, "Characterization and Modeling of UWB WBAN Channel in Indoor Environments", *IEEE Transactions on Antennas and Propagation*. (to be submitted, Aug 2008)

[Paper D] Y. Wang, I. Z. Kovacs, G. F. Pedersen, and K. Olesen, "Spatial Correlation of PAN UWB-MIMO Channel Including User Dynamics", *in EURO-COST 2100*, Duisburg, Sep 2007

Part II

Papers

Paper A

Characterization of the Indoor Multi-Antenna Body-to-Body Radio Channel

Yu Wang, Ivan B. Bonev, Jesper Ø. Nielsen, István Z. Kovács, and Gert F. Pedersen

The paper is submitted to
IEEE Transactions on Antennas and Propagation Special Issue on Body-Centric Wireless Communications, Jan 2008

The layout has been revised.

Abstract

In this paper, we investigate the wideband body-to-body radio channel with multiple antennas at both ends based on a time-domain radio channel measurement campaign. Four single-element transmitters and 8 quad-element receivers were mounted on three test persons. Both directional and omni-directional antennas have been investigated. A comparison between electromagnetic antenna simulations and the measurements shows that the multipath environment reduces the body losses effectively. Channel characterizations in terms of path-loss, body shadowing, small scale fading, and spatial correlation have been derived. Small path-loss exponents (< 2.0) are observed in the investigated environments. Considerable power loss due to body blockage makes the body shadowing a prominent factor in the short range body-to-body communications. Distributed antenna selection diversity is presented to mitigate the body shadowing. A 5 dB diversity gain in the average received power at both the mean and 10% outage levels has been identified based on the measurements with two distributed antennas mounted on both the transmitter and receiver person and without channel state information feedback to the transmitter.

1 Introduction

Body-centric wireless communication systems (BWCSs) are key components of future wireless communication systems, e.g. fourth generation (4G). A BWCS connects various devices around human bodies, such as body sensors, body monitors and wearable electronic devices. With respect to communication range, the BWCS are categorized as "off-body", e.g. links between a person and a local access point (AP) or between two persons, and "on-body" systems, e.g. connections between devices mounted/worn on the same person [1–4]. This paper deals with the off-body radio channel between two human bodies in particular.

In recent years off-body communications between wearable devices or systems have been investigated in the scope of wireless personal area networks (WPAN). Body-to-body radio channels differ from the body-to-AP channels in antenna heights and types, communication range, device types and the device on-body locations which are not limited to belts or pockets. Knowledge on the body-to-body radio channel is limited in the open literature, e.g. [5–7]. User proximity induced shadowing has been identified as a critical issue for this type of channels. The current paper gives a detailed insight into how body shadowing changes when devices are located on different parts of the human bodies.

Among the applications, which involve body-to-body communications, "smart clothes" [8] using E-textiles have been used in emergency services and firefighters [9], medical monitoring [10], militaries [11], sports as well as entertainment industries [12]. Recent

advances in small and wearable antennas for body area network (BAN) make it possible to embed antennas easily into the smart clothes, e.g. [13–15]. Therefore multiple antennas may be distributed to various positions all over the body. The BWCS can benefit from the distributed antennas which can effectively mitigate the body shadowing, enhance coverage and increase capacity by multiple-antenna techniques, e.g. antenna diversity and multiple-input multiple-output (MIMO) transmission. In [16], a diversity gain up to 9.6 dB with maximum ratio combining was reported by using two antenna elements on a smart jacket in a body-to-AP scenario at 868 MHz. A distributed body-worn transceiver system with multiple electro-textile antennas were proposed in [15] to achieve diversity gains when connecting with an AP. A vest with body-worn antennas for military use is reported in [11] which equips a pair of antenna arrays that surround the body of the wearer in order to mitigate the effects of shadowing. However to the authors' knowledge no comprehensive investigations have been done for the body-to-body channels with distributed on-body antennas. In this paper we give a systematic study of such channels based on empirical works.

The paper is organized as follows. Section II gives a description of a body-to-body channel measurement campaign. The electromagnetic simulations of the antennas used in the experiments are presented in Section III. In Section IV, characterizations of the measured channels are summarized and comparisons between the simulations and the measurements are provided. Diversity studies of the multiple-antenna body-to-body channel are given in Section V. Finally we conclude the paper in Section VI.

2 Measurement Campaign

The measurement campaign was performed in indoor environments with a 5.5 GHz carrier frequency and a -3dB bandwidth of about 100 MHz. A time domain correlation based MIMO channel sounder was used for the experiments. Four transmitters (Tx) simultaneously sent a pseudo noise (PN) sequence with different delays to realize temporal isolation of the transmit devices. On the receiver (Rx) side 8 channels were measured in parallel. By using switches, the number of receiver channels was expanded to 32. The full 4×32 (Tx $\times$ Rx) MIMO channel sampling rate was 60 Hz, which gives a maximum allowed relative speed between the Tx and the Rx of 1.6 m/s at 5.5 GHz. The duration of each measurement was 10 seconds during which 600 full MIMO channel snapshots were measured. The length of each channel impulse response (CIR) was 640 ns which is sufficient for the investigated indoor environments. Additional information about the sounder is available in [17].

Three types of antennas were used as shown in Fig. 1, one for the transmitters (Tx) and two for the receivers (Rx-A and Rx-B). Detailed descriptions are given in Section 3.

The Tx, Rx-A and Rx-B devices were placed on three test persons respectively.

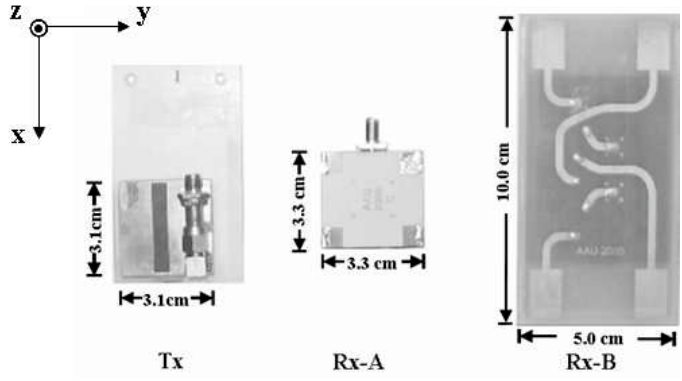

Figure 1: From left to right, the directional stacked patch antenna (Tx), the patch PIFA antenna (Rx-A) and the monopole antenna (Rx-B)

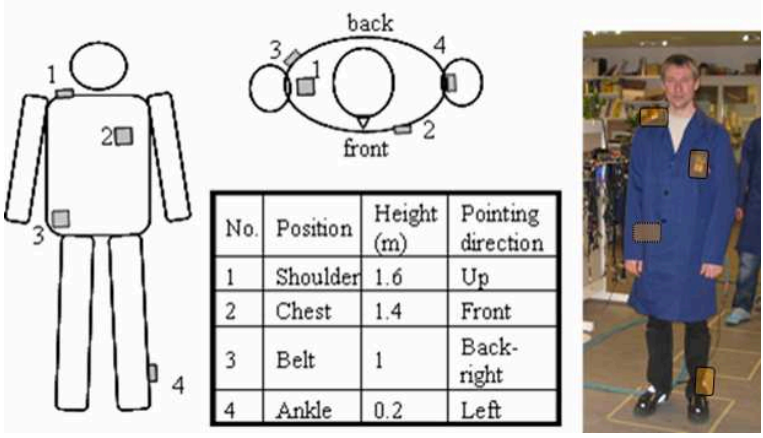

No.	Position	Height (m)	Pointing direction
1	Shoulder	1.6	Up
2	Chest	1.4	Front
3	Belt	1	Back-right
4	Ankle	0.2	Left

Figure 2: Device on-body positions and descriptions and an illustration of a test person standing in a 50 $\times$ 50 square area; the same setup was adopted for both the Tx test person and the two Rx test persons;

Four identical devices of each type were used simultaneously during the experiments. We included a variety of heights and orientations for the choices of device positions: shoulder (sh), chest (ch), belt (bl) and ankle (an) as shown in Fig. 2.

The experiments were performed in two indoor environments: a laboratory and a corridor. The laboratory is a large room containing furniture and equipment. Sketches of the environments are shown in Fig. 3. During the experiments, no people were moving in the area except the test persons.

Two scenarios called spot and route were defined for these investigations. In the spot scenario, the three test persons stood in three predefined 50×50 cm square areas respectively. They were moving randomly within the squares with arms waving slightly but not turning around. The size of the square ensures the channel stationarity of each measurement. In each square, the Tx test person was always oriented to the north and the Rx test persons had four orientations (north, east, south and west) measured in order to capture the body shadowing as depicted in Fig. 3.

The positions #1 to #7 (Fig. 3) were used to make in-line measurements. The Tx was placed in position #1 and the Rx-A and Rx-B in position #2 to #7. One extra measurement with Tx and Rx in position #7 and #6 respectively was done to obtain a large Tx-Rx separation (8 m). Similar in-line measurements were performed in the corridor. positions from #9 to #11 were arranged to be obstructed channels with a wooden shelf and a metal shelf between the Tx and Rx-A/Rx-B in the laboratory. Measurements at position #8 are not included in this study. Free space channels were also measured and used as references during which the devices were arranged horizontally with 10 cm separation and at 1 m height from the ground.

In the route scenario, the Tx test person and the Rx test persons walked towards each other along predefined routes with pedestrian speeds (0.8 m/s). Two routes in the laboratory and one in the corridor were measured.

3 Antenna Characterization

The Tx antennas are Directional Stacked Patch (DSP) antennas which consist of a slot in a ground plane fed by two symmetrical microstrip lines and a reflecting element in the bottom of the sandwich construction to ensure the directional properties [13]. The Rx-A antenna arrays consist of four Planar Inverted F-Antennas (PIFAs) which can be located rather close to each other and provide a certain front-to-back ratio for the hemisphere pointing away from the body. In the third antenna setup, the Rx-B antenna arrays are equipped with four monopole antennas which are very simple to integrate into any textile or product requiring very thin geometry but at the cost of no front-to-back ratio.

The antenna characteristics with user proximity were evaluated by simulations. The

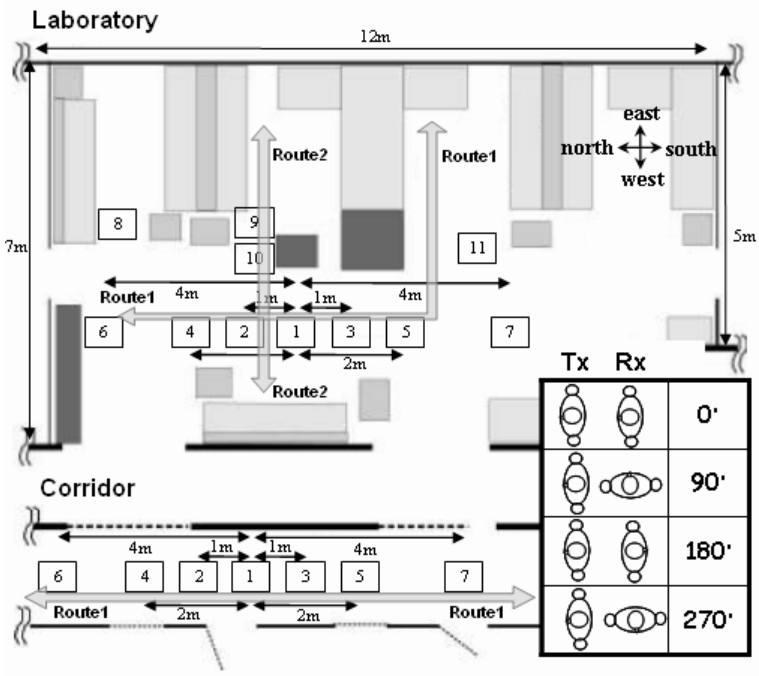

Figure 3: The layout of laboratory and corridor environments with measurement positions #1 to #11 marked with squares and route 1 and 2 marked with thick gray lines; to the right, an illustration of relative orientations of the three test persons

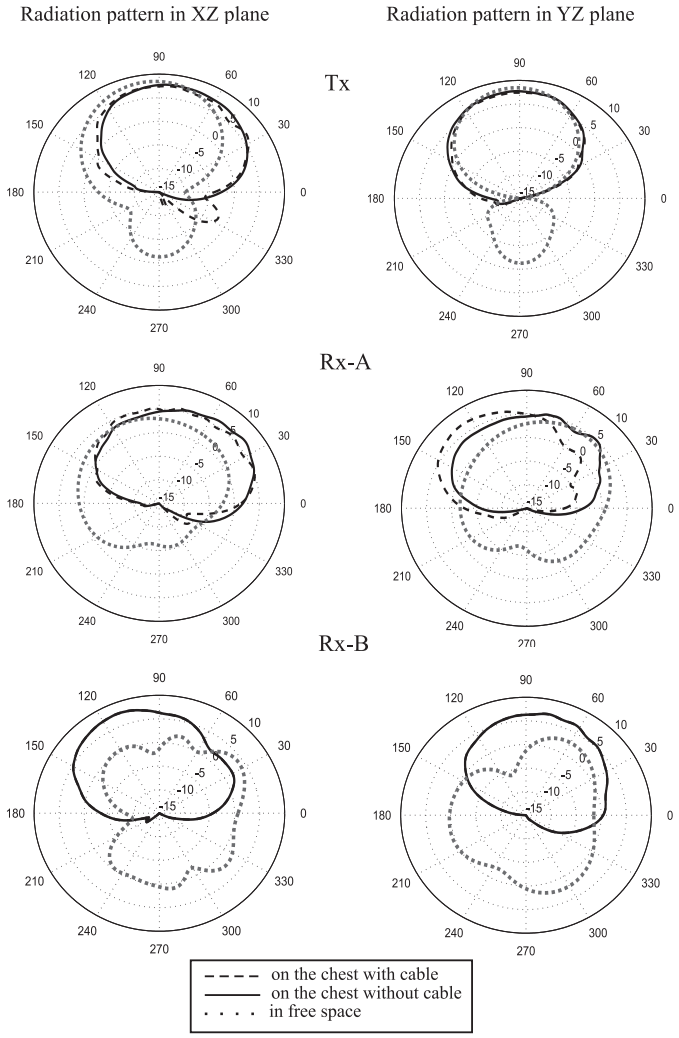

Figure 4: Simulated radiation patterns of the antennas in free space and on the chest (left) the XZ plane, (right) the YZ plane; top: Tx DSP antenna, middle: Rx-A PIFA antenna, bottom: Rx-B monopole antenna

numerical human body model developed in the Visible Human Project [18] is used with only muscle tissue (homogeneous version). The numerical investigation is based on the Finite Difference Time Domain (FDTD) method where all the antennas are modeled and simulated in the cases with and without the conductive cable and for all the measured positions on the body. The FDTD simulations are using uniform cubic grid of 1.5mm and for the termination of the simulation space the Perfect Matched Layer absorbing boundaries are used [19].

For all three types of the used antennas, the return loss is always less than 1 dB and the mutual coupling is less than -20 dB over the measured frequency band.

When the antennas are mounted on the body some of the power is absorbed, strongly dependent on the antenna type (directive or omni-directional) and the distance to the body. Table 1 summarizes the simulation results of the antenna efficiency. The advantage of using the directional antenna is evident.

The effective radiation patterns, which are defined as the radiation pattern of the antennas mounted on the human body, are simulated for all three types of antennas and four on-body positions. The results on the chest together with the free space patterns are shown in Fig. 4. The device is always oriented in the XY plane with the negative Z direction towards the body as shown in Fig. 1. It is clear from Fig. 4 and Table 1 that the body both absorbs and reflects some of the radiated power resulting in a directive radiation away from the body [3]. Compared to free space the effective radiation depends to a minor degree on where the device is located. When the antenna radiation patterns of the chest position are compared with the other locations, the maximum root mean square (RMS) difference is 4.7 dB with the shoulder position due to reflections from the head. In the other cases, the RMS difference is less than 3 dB.

Previous studies showed that the cable influence may be a problem for radio measurements with electrically small antennas [20]. At 5.5 GHz for the test devices as shown in Fig. 1 the cables may not have a significant influence. This is confirmed by comparing the simulated impedance reflection and the radiation pattern in case of no cable and with a cable of 400 mm long. The difference in impedance is less than 0.1 dB for all cases across the measured frequency band. The largest RMS difference in radiation patterns is approximately 2 dB. It happens to the Rx-A antenna and is shown in Fig. 4.

4 Channel Characterization

4.1 Channel representation and normalization

The analysis in this section is based on the spot measurements. It has been shown in the Section 3 that the Rx-A and Rx-B have similar on-body radiation patterns but different on-body radiation efficiency (See Table 1). In order to combine the measurements

Table 1: Antenna efficiency in dB due to power loss by absorption in the body. Distance to the body is 3 mm except for the last column (10 mm)

Position	Tx	Rx-A	Rx-B	Rx-B (10 mm)
Shoulder	-3.8	-2.0	-5.7	-2.3
Chest	-1.3	-2.0	-3.7	-1.7
Belt	-2.9	-2.1	-4.3	-2.0
Ankle	-1.5	-2.0	-2.7	-1.3

from two types of the receivers the change in the received power due to the efficiency difference has been compensated in the post-processing.

The measured MIMO channel is expressed as a 4×4×4 matrix $\mathbf{H}(\mathbf{m}, \mathbf{n})$, whose elements $h_{i,j,k}(m, n)$ are complex channel coefficients between the i-th Tx device and the k-th Rx antenna of the j-th Rx device at time $m \cdot \Delta t$ and delay $n \cdot \Delta\tau$ where $\Delta t = 16.7$ ms is the channel sampling interval and $\Delta\tau = 2.5$ ns is the length of the delay bin. A diagram of the measured channel is shown in Fig. 5 in which I, J and K are the total number of the Tx devices, Rx devices and antenna elements on each Rx device respectively. In the rest of the paper we refer the antennas at the same Rx device as 'co-located antennas', and as 'distributed antennas' otherwise.

The measured channel coefficients include path-loss, shadowing, fading and antenna gains. They are normalized by the corresponding measured in-line free space received power at the same Tx-Rx separation with the Tx antennas pointing to the Rx antennas. By doing so the normalized channel power will reflect the body loss compared to the free space channel power, and all the power variation due to body shadowing has been preserved.

The average wideband received power in each spot measurement was calculated as

$$\bar{P}_{i,j,k} = \sum_{n=0}^{N-1} \sum_{m=0}^{M-1} |h_{i,j,k}(m, n)|^2 \tag{1}$$

where M and N are the total number of delay bins and time samples of each measurement, respectively.

An alternative representation of the measured MIMO channel, $\mathbf{G}(\mathbf{l}, \mathbf{n})$, in the frequency domain is obtained by applying the discrete Fourier transform (DFT) in the delay domain to $\mathbf{H}(\mathbf{m}, \mathbf{n})$. Totally 64 subbands with 1.56 MHz bandwidth are located within the measured frequency band and used in the analysis.

4.2 Losses in received power due to body blockage

The simulated on-body antenna radiation patterns are used to obtain the body blockage loss when only one direct ray exists. By comparing the results with the measurement in

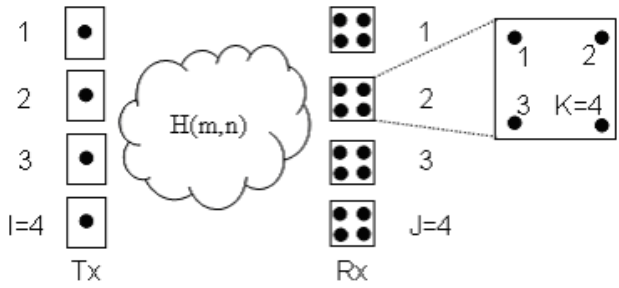

Figure 5: Diagram of the measured MIMO channel with $I = 4$ Tx devices each with single antenna elements and $J = 4$ Rx devices each with $K = 4$ antenna elements

the multipath environments, we can get an insight into how much of the received signal is coming from reflections, scattering and diffractions.

Simulated antenna gains in different scenarios are obtained according to the corresponding simulated 3-D patterns, locations of the antennas and orientations of the test persons. The simulated and measured received power loss of the chest-to-chest channel at 1 m distance due to body lockage is presented in Fig. 6. The A and B columns represent the Rx-A and Rx-B respectively, and the number indicates the relative orientations of the Rx and Tx as shown in Fig. 3. For each scenario the orientation A-180 which has no body shadowing is used as a reference.

The maximum power losses with the direct link only and in the multipath environments are 44 dB and 20 dB respectively. Both are much higher than the previously reported results in the body-to-AP scenarios [21, 22]. This new result suggests more severe body blockage loss which is highly environment dependent in the body-to-body channel since both communication ends are subject to the body shadowing. It has been found that the degree of power loss usually depends on size and richness of the scattering environments. For the measured channels the power loss in the laboratory is slightly (up to 3 dB) higher than in the corridor. This result is consistent with [21], but in [21] the difference between the environments is as high as 10 dB.

4.3 Path-loss

The path-loss is analyzed in this section based on the in-line channel measurements (positions #1 to # 7 in Fig. 3). Fig. 7 shows a scatter plot of the relative received power as a function of distance for the in-line scenario in the laboratory. The average received power at each Tx-Rx distance is marked out in the figure together with free space received power as a reference. Since the antenna radiation patterns become more directional when they are mounted on-body as shown in Section 3, some off-body channels have higher power than the free space channels.

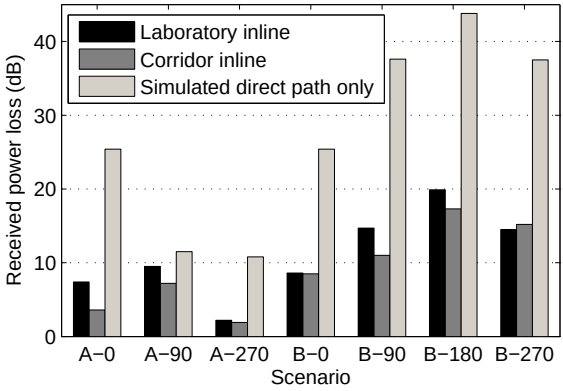

Figure 6: Power loss of the simulated channels with direct path only and the measured channels due to body blockage for the chest-to-chest link. For each scenario the orientation A-180 which has no body shadowing is used as a reference (for the orientations, see Fig. 3)

With the assumption of the classical model, the path-loss [dB] at a distance d [m] is expressed as

$$PL(d) = PL(d_0) + 10n \log_{10}\left(\frac{d}{d_0}\right) + X \tag{2}$$

where $PL(d0)$ is the path-loss in dB at $d0 = 1$ m, n is the path-loss exponent and X is a random variable representing shadowing. Linear fits with minimum squared error for both the free space and on-body measurements in the laboratory are shown in Fig. 7. For both of the environments, the free space and on-body channel path-loss exponent n is 1.1. For different combinations of the Tx/Rx device on-body positions the n is in the range of 1 to 2.3. In the literature an indoor short range handset to handset channel measurement showed an exponent well below 1 [7], and it was addressed that the body shadowing makes the exponent sensitive to the insufficient sample size. For our study the small exponent measured in the laboratory and the free space condition can not be explained by either the insufficient samples or the well-known waveguide effects. Therefore an independent power measurement with the same antenna set-up and radio environments was performed, and similar weak power-distance dependence is observed. When antennas with higher gain are used instead, the power drops faster with the distance. Therefore the small path-loss exponent is associated with the scattering environments and subject to further investigations.

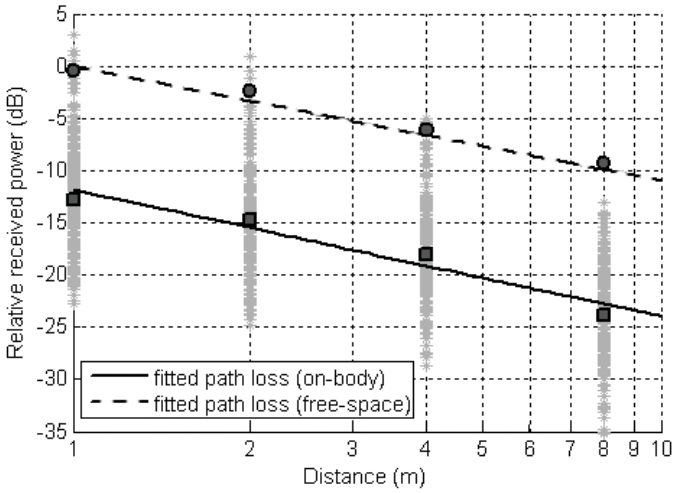

Figure 7: Scatter plot and fitted path-loss curve of the received power versus distance for the in-line scenario in the laboratory. Dark squares: average received power at each distance; dark rounds: average received power in the free space condition

4.4 Body shadowing statistics

The distribution of the body shadowing X in (2) is analyzed by the Kolmogorov-Smirnov (K-S) test. The Log-normal distribution with a zero mean and a standard deviation (σ_X) of 4.8 dB is proven to be the best fit compared with Weibull, Exponential, Laplace, Normal and Rayleigh distributions. Therefore, in (2) the X is modeled as a log-normal distributed random variable.

Fig. 8 gives the average relative received power and σ_X in dB in the different investigated scenarios. When the Tx and Rx are located at the same height on the bodies, the received power for the belt-belt scenario is 3-4 dB lower than the other scenarios partly due to the arm blockage. The channel with relatively higher average gain usually fluctuates more. In the obstructed condition, at least 10 dB extra power loss is observed. And the shoulder-to-shoulder channel has at least 2 dB higher received power than the others. One possible reason is that the antennas pointing upwards collect more energy from multipaths. For the ankle-shoulder channel the heights of the Tx and Rx are considerably different, and 3 to 7 dB lower received power is observed in the in-line measurements.

The difference in the average received power among the antennas results in branch power imbalance (BPI). The maximum BPI is usually less than 5 dB for the in-line scenario and less than 10 dB for the obstructed scenario as shown in Fig. 8. In practice the on-body positions with low average received power need to be avoided as suggested

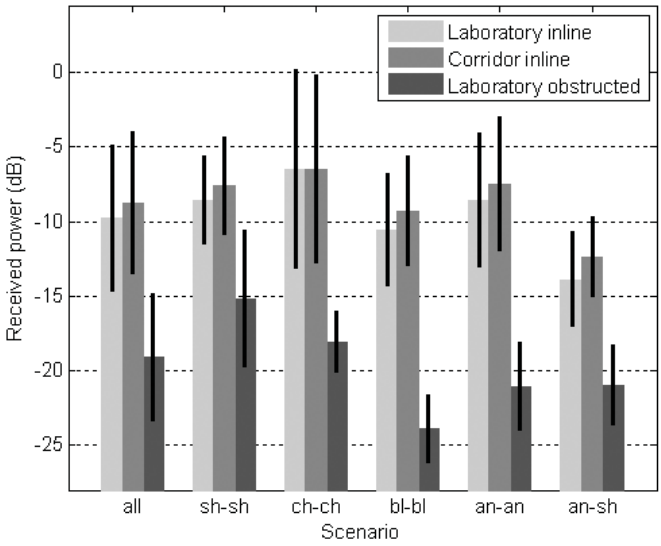

Figure 8: Average received power in different scenarios; $\pm\sigma_X$ from the average received power is indicated by dark thin bars

earlier in this section.

The correlation coefficients of the shadowing $\rho(\bar{P}_{i1,j1,k1}, \bar{P}_{i2,j2,k2})$ at the Rx side between the antennas are calculated. Selected results are shown in Fig. 9 where the Rx correlation respect to the Tx shoulder and Tx chest positions is plotted in the upper-right and lower-left part of the figure, respectively. The x and y-axis represent the Rx antenna on-body positions with the numbers in the brackets representing the k-th Rx antenna element as shown in Fig. 5. The value of correlation is always higher than 0.6 for the co-located antennas. For the distributed antennas the shadowing correlation ranges from 0.1 to 0.9 for the antennas allocated on the same side of the body and -0.7 to 0.4 for the antennas on different sides of the body. The dependence of the Rx shadowing correlation on the Tx on-body positions is evident with lower values respect to the Tx shoulder position.

4.5 Coherence bandwidth

The definition of the coherence bandwidth B_c is based on the correlation coefficients ($\rho_{\Delta l}$) between two subbands separated by Δl subbands (1.56 MHz) in the frequency domain. The channel is assumed to be frequency domain wide sense stationary (WSS).

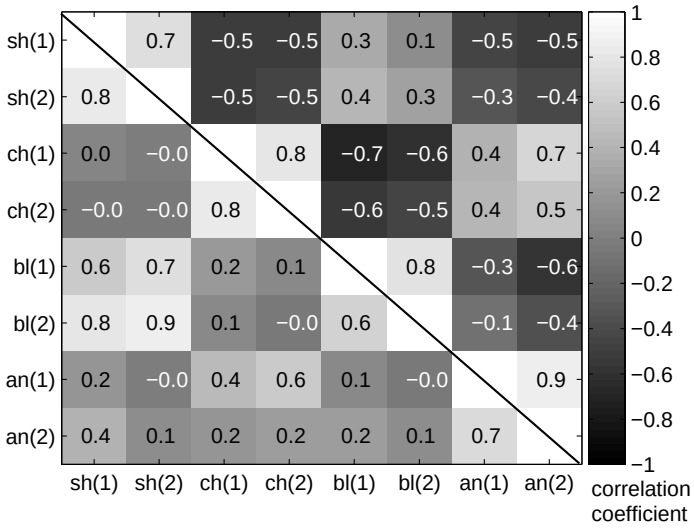

Figure 9: Rx shadowing correlation coefficients with respect to the Tx shoulder (upper-right part) and chest (lower-left part) positions; the x and y-axis represent the Rx antenna on-body positions with the numbers in the brackets representing the k-th antenna element at the Rx devices as shown in Fig. 5

The coherence bandwidth is

$$B_{cY} = \underset{\Delta l}{\arg}(\rho_{\Delta l} = Y) \tag{3}$$

The average $B_{c0.9}$ and $B_{c0.5}$ are 6.6 MHz and 28.2 MHz in the laboratory and 7.4 MHz and 30.0 MHz in the corridor respectively. The standard deviations of the $B_{c0.9}$ and $B_{c0.5}$ are less than 3 MHz. Various antenna combinations show similar results. The bandwidth for each subband (1.56 MHz) is well below the coherence bandwidth and therefore treated as a flat fading channel.

4.6 Fading statistics

The fading statistics and correlation were analyzed using subband channels in $\mathbf{G}(\mathbf{l}, \mathbf{n})$ based on the spot measurements. According to the K-S test, the measured data matches best to Rayleigh or Rician distribution. The K-factor of the Rician distribution is estimated by the moment method proposed in [23]. Generally the results show small K-factors in most cases. Higher K-factors can only be observed when the Tx and Rx are directly pointing to each other without any blockage, e.g. the chest to chest channel, and 99% of measured channels have the K-factor less than 5 dB. Both, the high possibility of body blockage and the rich radio scattering in the environments, contribute to

this result. In addition the effectively directional radiation patterns caused by the body rarely point to each other directly and therefore the reflected paths are relatively strong compared with the direct path.

When two devices have direct link between each other, the fading correlation between the co-located antennas is in a range of [0.3 0.7]. In all the other conditions and for all the other link pairs, the fading correlation is usually below 0.2.

5 Distributed Antenna Diversity for the body-to-body communication

In the previous section, we have shown considerable body shadowing (σ_X=4.8 dB) in the body-to-body channel. Since the duration of deep shadowing is usually in the order of seconds or even longer, time and frequency domain techniques such as channel coding and time or frequency diversity can not work for mitigation of the body shadowing. Distributed antenna diversity, which employs distributed antennas on different on-body positions, on the other hand, is promising to combat the shadowing due to the low shadowing correlation between the distributed antennas (see Fig. 9).

Furthermore, both forward link and backward link channels usually experience the same shadowing no matter they are separated in the frequency domain or the time domain. This property provides a unique opportunity of implementing Tx diversity requiring no channel state information feedback since the shadowing information estimated from the backward link can be used in the forward link directly.

5.1 Distributed antenna selection diversity of the spot measurements

Different from the traditional antenna diversity mainly used to mitigate small scale fading, we define a distributed antenna selection diversity using long-term average received power for the selection. The distributed antenna pair selected within a duration T is

$$[i', j']_{N'} = \arg\max_{[i,j]} \left(\sum_{n=0}^{N'-1} \sum_{m=0}^{M-1} |h_{i,j}(m,n)|^2 \right) \tag{4}$$

where N' is the number of channel samples within the duration $T(T = N' * \Delta t)$ In other words, the selected channel has the largest average received power within T seconds.

From Fig. 8 we can conclude that if we use only one antenna for transmission the shoulder-to-shoulder channel has the highest outage power among the investigated channels. Therefore the shoulder-to-shoulder channel is used as a reference to calculate the gain of the selection diversity. A mean diversity gain (γ_{mean}) and a 10% outage

Table 2: A summary of the 4-branch Rx/Tx selection diversity gain in dB for the spot measurements in the laboratory and corridor environments

Position	$\bar{P}_{mean}$		γ_{mean}		$\bar{P}_{outage}$		$\gamma_{10\%}$	
	Lab	Cor	Lab	Cor	Lab	Cor	Lab	Cor
([sh] reference)	-9	-7	-	-	-15	-13	-	-
[sh, ch]	-5	-4	4	3	-10	-10	5	3
[sh, be]	-8	-5	1	2	-13	-11	2	2
[sh, an]	-7	-5	2	2	-11	-10	4	3
[ch, be]	-4	-2	5	5	-10	-8	5	5
[ch, an]	-6	-5	3	2	-13	-12	2	1
[be, an]	-7	-6	2	1	-12	-11	3	2

diversity gain ($\gamma_{10\%}$) are defined as the increase of the average received power in the corresponding level.

T is set as the whole measurement time of 10 seconds. Table 2 summarizes the results of 4-branch Tx/Rx combined selection diversity in different scenarios. The Rx/Tx position column shows where the antennas were placed on both the Rx and the Tx test persons, and the first antenna at each Rx device, i.e. $k = 1$, is always used. The mean and 10% outage of the averaged received power, $\bar{P}_{mean}$ and $\bar{P}_{outage}$, are also shown in the table.

The diversity gain depends on the antenna on-body positions. As highlighted in the table the chest and belt positions obtained the highest gain which is 5 dB in both the γ_{mean} and $\gamma_{10\%}$ and in both the laboratory and corridor environments.

5.2 Distributed antenna selection diversity of the route measurements

With the route measurements the proposed selection diversity is evaluated in dynamic scenarios. From the findings above the optimal positions for the 4-branch Tx/Rx diversity are the chest and belt (see Table 2 row 5). Therefore we focus on these two positions in this section.

First the channel is normalized to remove the distance dependent path-loss. The normalization is done by time intervals. The duration of each segment is set as 0.5 second corresponding to $\tilde{N} = 30$ channel samples. With the walking speed of approximately 0.8 m/s, the distance of each segment is about 40 cm. Within each segment the measured channel is normalized as

$$\frac{1}{\tilde{N}} \sum_{n=0}^{\tilde{N}-1} \sum_{m=0}^{M-1} \| \mathbf{H}(\mathbf{m}, \mathbf{n}) \|_F^2 = I \cdot J \cdot K \tag{5}$$

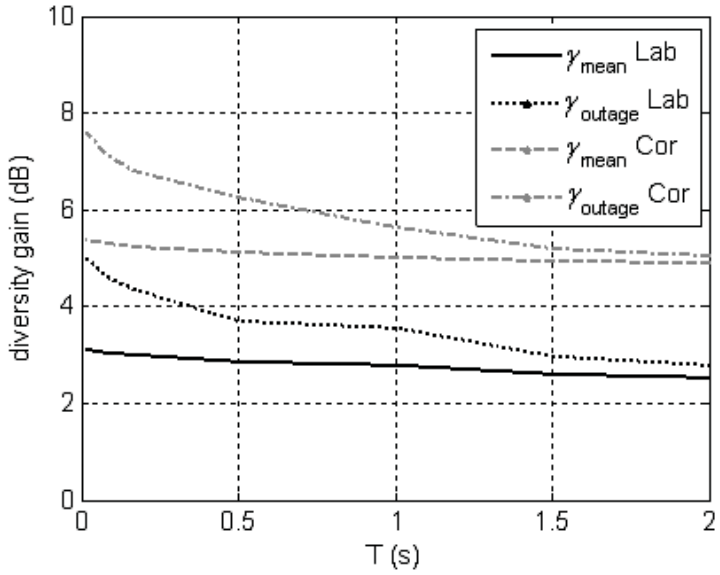

Figure 10: Mean and 10% outage distributed antenna diversity gains calculated based on the route measurements in both the laboratory and corridor. The diversity gain is shown with respect to the averaging interval T

where $\| \bullet \|_F$ is the Frobenius norm.

Fig. 10 shows the γ_{mean} and $\gamma_{10\%}$ with the different T. The shoulder-to-shoulder channel is used as the reference when the diversity gain is calculated. In the investigated scenario, the γ_{mean} is almost flat for $T \leq 2$ s, and the $\gamma_{10\%}$ increase about 2 dB when the T decreases to the channel sampling interval (16.7 ms) since parts of the small scale fading effects are included when the average is only taken in the frequency domain. In the corridor both the γ_{mean} and $\gamma_{10\%}$ are 3 dB higher than in the laboratory. As shown in Fig. 3, parts of the route 1 in the laboratory are in the obstructed condition where the reference, shoulder-to-shoulder channel, has at least 2 dB higher received power than others as stated in Section 4.4. This explains the lower diversity gain in the laboratory environment.

6 Conclusion

Based on wideband radio channel measurements with realistic devices and scenarios, we have investigated several indoor body-to-body radio channels with multiple-antennas at both the transmit and receive end. Our investigations include three types of antennas and two environments. All types of the antennas show similar directional

radiation patterns when put on human bodies according to simulations. And similar channel characterizations are observe with the two different environments. It implies that the results in this paper may be extended to other antenna types and similar radio environments.

The comparison between the channels with direct path only obtained by antenna simulations and the propagation measurements shows that the multipath environment reduces the power loss due to the body shadowing effectively. The maximum power losses with the direct link only and in the multipath environments are 44 dB and 20 dB respectively. The measured path-loss exponent is less than 2.0, and the log-normal distributed shadowing has a standard deviation of 4.8 dB. It makes the body shadowing a prominent factor in short range body-to-body communications.

Due to the low shadowing correlation between the distributed antennas, a distributed antenna selection diversity scheme is presented to mitigate the body shadowing. The proposed scheme utilizes both the Rx and Tx diversity and do not require channel state information feedback. The shoulder-to-shoulder channel is used as a reference when the diversity gain is computed. When two distributed antennas are employed on both of the Tx and Rx side, the chest and belt positions obtained the highest gain. The mean selection diversity gain is 5 dB for the in-line measurements, and 3 dB and 5 dB for the route measurements in the laboratory and corridor respectively.

References

[1] P. S. Hall and Y. Hao, "Antennas and propagation for body centric communications," in *European Space Agency, (Special Publication) ESA SP*, vol. 626 SP, Oct 2006.

[2] Y. I. Nechayev, P. S. Hall, C. C. Constantinou, Y. Hao, A. Alomainy, R. Dubrovka, and C. G. Parini, "On-body path gain variations with changing body posture and antenna position," in *Antennas and Propagation Society International Symposium, 2005 IEEE*, vol. 1B, Dec 2005, pp. 731–734.

[3] A. Fort, J. Ryckaert, C. Desset, P. De Doncker, P. Wambacq, and L. Van Biesen, "Ultra-wideband channel model for communication around the human body," *IEEE Journal on Selected Areas in Communications*, vol. 24, no. 4, pp. 927–933, Apr 2006.

[4] P. S. Hall and Y. Hao, *Antennas and propagation for body-centric wireless communications*. Artech House, INC., 2006.

[5] I. Z. Kovacs, Y. Wang, P. C. Eggers, and K. Olesen, "UWB radio channel model for short-range mobile-to-mobile communication scenarios," in *Wireless Personal Multimedia Communications (WPMC) Symposia 2005*, Sep 2005, pp. 2008–2012.

[6] J. Karedal, A. J. Johansson, F. Tufvesson, and A. F. Molisch, "Characterization of MIMO channels for handheld devices in personal area networks at 5 GHz," in *14th European Signal Processing Conference (EUSIPCO 2006)*, Sep 2006.

[7] ——, “Shadowing effects in MIMO channels for personal area networks,” in *Proceedings of VTC 2006 Fall*, Sep 2006, pp. 1–5.

[8] Z. W. Tang and A. S. Mohan, “An investigation of MIMO performance in the indoor ricean environment,” *Wireless Personal Communications*, vol. 39, no. 1, pp. 99–113, Oct 2006.

[9] L. Jones, N. Deo, and B. Lockyer, “Wireless physiological sensor system for ambulatory use,” in *Wearable and Implantable Body Sensor Networks, 2006.BSN 2006.International Workshop on*, Apr 2006.

[10] J. Edimison, D. Lehn, M. Jones, and T. Martin, “E-textile based automatic activity diary for medical annotation and analysis,” in *Wearable and Implantable Body Sensor Networks, 2006.BSN 2006.International Workshop on*, Apr 2006, pp. 4–7.

[11] E. C. Kohls, A. Abler, P. Siemsen, J. Hughes, R. Perez, and D. Widdoes, “A multi-band body-worn antenna vest,” in *Antennas and Propagation Society International Symposium, 2004.IEEE*, vol. 1, 2004, pp. 447–450.

[12] F. Lorussi, W. Rocchia, E. P. Scilingo, A. Tognetti, and D. De Rossi, “Wearable, redundant fabric-based sensor arrays for reconstruction of body segment posture,” *IEEE Sensors Journal*, vol. 4, no. 6, pp. 807–818, Dec 2004.

[13] M. Klemm, I. Z. Kovacs, G. F. Pedersen, and G. Troster, “Novel small-size directional antenna for UWB wban/wPAN applications,” *IEEE Transactions on Antennas and Propagation*, vol. 53, no. 12, pp. 3884–3896, Dec 2005.

[14] P. Salonen, Y. Rahmat-Samii, and M. Kivikoski, “Wearable antennas in the vicinity of human body,” in *Antennas and Propagation Society International Symposium, 2004.IEEE*, vol. 1, 2004, pp. 467–470.

[15] Y. Ouyang and W. Chappell, “Distributed body-worn transceiver system with the use of electro-textile antennas,” in *Microwave Symposium, 2007.IEEE/MTT-S International*, Jun 2007, pp. 1229–1232.

[16] S. L. Cotton and W. G. Scanlon, “Spatial diversity and correlation for off-body communications in indoor environments at 868 MHz,” in *Vehicular Technology Conference, 2007.VTC2007-Spring.IEEE 65th*, 2007, pp. 372–376.

[17] J. Ø. Nielsen, J. B. Andersen, P. C. Eggers, G. F. Pedersen, K. Olesen, E. H. Sørensen, and H. Suda, “Measurements of indoor 16x32 wideband MIMO channels at 5.8 GHz,” in *Proceedings of the 2004 International Symposium on Spread Spectrum Techniques and Applications (ISSSTA 2004)*, 2004, pp. 864–868.

[18] M. Ackerman, “The visible human project,” in *Proceeding of the IEEE*, vol. 86, Mar 1998, pp. 504–511.

[19] A. Taflove, *Computational Electrodynamics, The Finite-Difference Time-Domain Method*. Artech House Publishers, 1995.

[20] W. A. T. Kotterman, G. F. Pedersen, K. Olesen, and P. C. Eggers, “Cable-less measurement set-up for wireless handheld terminals,” in *Personal, Indoor and Mobile Radio Communications, 2001 PIMRC 12th IEEE International Symposium on*, vol. 1, Sep 2001, pp. B112–B116.

[21] K. I. Ziri-Castro, W. G. Scanlon, and N. E. Evans, "Indoor radio channel characterization and modeling for a 5.2-GHz body worn receiver," *IEEE Antennas and Wireless Propagation Letters*, vol. 3, no. 1, pp. 219–222, 2004.

[22] T. B. Welch, R. L. Musselman, B. A. Emessiene, P. D. Gift, D. K. Choudhury, D. N. Cassadine, and S. M. Yano, "The effects of the human body on UWB signal propagation in an indoor environment," *IEEE Journal on Selected Areas in Communications*, vol. 20, no. 9, pp. 1778–1782, Dec 2002.

[23] L. J. Greenstein, D. G. Michelson, and V. Erceg, "Moment-method estimation of the ricean k-factor," *IEEE Communications Letters*, vol. 3, no. 6, pp. 175–176, Jun 1999.

Paper B

MIMO Channel Modeling for Body-to-Body Communications

Yu Wang, Jesper Ø. Nielsen, István Z. Kovács, and Gert F. Pedersen

The paper will be submitted to
IEEE Transactions on Wireless Communications , Aug 2008

The layout has been revised.

Abstract

In this paper, we propose a novel correlation based stochastic model with correlated shadowing (CBSM-CS) for body-to-body multiple-input multiple-output (MIMO) radio channels. The model introduces a shadowing matrix consisting of correlated Lognormal distributed entries to represent unbalanced and correlated body shadowing. A Rayleigh-Lognormal (RLN) distributed CBSM-CS channel model is derived based on an indoor measurement campaign, and the modeling accuracy in terms of channel capacity is verified by a different set of experiments.

We analyze the influence of the modeling parameters, i.e. shadowing standard deviation, shadowing correlation and branch power imbalance (BPI), on the MIMO channel capacity by both numerical and experimental studies. The shadowing standard deviation determines the distribution of the channel power in dB, and consequently it is dominant to the channel capacity. Antenna diversity gains for body shadowing mitigation can be achieved when the shadowing correlation between the antennas is low. Therefore the shadowing correlation affects the outage capacity significantly. The relationship between the RLN and Lognormal statistics is derived in order to extract the modeling parameters from the measured shadowed fading channels. Finally a group of modeling parameters is suggested based on the measurement results.

1 Introduction

Body-centric wireless communication systems (BWCSs) are key components of future wireless communication systems. A BWCS connects various devices around human bodies, such as body sensors, body monitors and wearable electronic devices. The BWCS is categorized as "off-body" and "on-body" systems [1]. The on-body BWCS refers to connections between devices mounted/worn on the same person. This paper deals with the off-body radio channel between two human bodies in particular.

In recent years, off-body radio communications between wearable devices or systems have been investigated and user proximity induced shadowing has been identified as a critical issue for this type of channels, e.g. [2–4]. The body shadowing usually changes during a fraction of a second or several seconds. Consequently the changes in channel power due to the body shadowing and small-scale fading are hard to be separated especially when people change their relative orientations frequently. Therefore joint modeling of the shadowing and fading becomes a necessity in the body-to-body communications.

Recent advances in "smart clothes" [5] and wearable antennas which can be easily embedded into clothes, e.g. [6, 7], provide a unique opportunity to mitigate body shadowing by distributing antennas to various body positions. The smart clothes have found their applications in emergency and rescue services, medical monitoring, military ap-

plications, sports as well as entertainment industries [3]. To investigate the performance of such multi-antenna systems a multiple-input multiple-output (MIMO) channel model which takes the body shadowing into consideration is required.

Compound shadowed fading distributions have been studied [8] and used in diversity performance evaluations [9] and cellular system coverage analysis [10]. Effects of environment shadowing on bit error rate [11] and outage capacity [12] of MIMO systems have been investigated for wireless personal area networks (WPANs) and cellular systems, respectively. Studies of the MIMO channel in the off-body BCWS have been focused on fading correlation [13, 14], body shadowing statistics [4] and capacity enhancements [15]. However to the authors' knowledge no works in the open literature investigate and model the body-to-body MIMO channel with distributed on-body antennas. In this paper we propose a correlation based stochastic model with correlated shadowing (CBSM-CS) based on our previous work presented in [3], analyze channel capacity by numerical studies and verify the model with a new measurement campaign.

The paper is organized as follows. Section II presents the CBSM-CS model. Numerical analysis of modeling parameters is given in Section III. Section IV provides a description of a body-to-body channel measurement campaign. Measured channel capacity is summarized and used to verify the proposed channel in Section V. Finally we conclude the paper in Section VI.

2 Body-to-Body MIMO Channel Model

The body shadowing and small-scale fading in the body-to-body channel need to be modeled jointly since they often change simultaneously. Several shadowed fading channel statistics have been proposed by compounding independent shadowing and fading distributions, e.g. Rayleigh-Lognormal (RLN) [8] and Nakagami-m Lognormal [10]. Similar strategies can be extended to MIMO channels,

$$\mathbf{H} = [\mathbf{X}]^{1/2} \cdot \mathbf{G} \tag{1}$$

where $\mathbf{G}$ and $\mathbf{X}$ are the $N_T \times N_R$ fading and power shadowing matrices respectively, N_T and N_R are the number of transmitter (Tx) and receiver (Rx) antennas respectively, $([\bullet]^n)$ denotes entry wise exponentiation with an exponent n and $(\cdot)$ represents the entry wise product.

According to our previous experiments based body-to-body channel study in [3], entries of $\mathbf{G}$ are identical independent distributed (iid) complex Gaussian random variables (RVs) with zero means and unit variances. The body shadowing was determined as Lognormal distributed. Therefore (1) can be expressed as,

$$\mathbf{H} = 10^{\mathbf{X}_{\mathrm{dB}}/20} \cdot \mathbf{G} \tag{2}$$

$\mathbf{X}_{\mathrm{dB}}$ in (2) is modeled as

$$\mathbf{X}_{\mathrm{dB}} = \mathbf{\Sigma}_{\mathrm{X,dB}} \cdot \left(\mathbf{R}_{\mathrm{X,dB}}^{1/2}\mathbf{G}_{\mathrm{X,dB}}\right) + \mathbf{M}_{\mathrm{X,dB}} \tag{3}$$

where $\mathbf{M}_{\mathrm{X,dB}}$ and $\mathbf{\Sigma}_{\mathrm{X,dB}}$ are mean and standard deviation matrices of the body shadowing respectively, $\mathbf{G}_{\mathrm{X,dB}}$ contains standard normal distributed RVs, $\mathbf{R}_{\mathrm{X,dB}}$ is a shadowing correlation coefficient matrix, $(\bullet)^{1/2}$ is defined such as $\mathbf{R}^{1/2}(\mathbf{R}^{1/2})^H = \mathbf{R}$ and $(\bullet)^H$ stands for the complex conjugate transpose. Since the correlated shadowing is introduced in (2) and in principle $\mathbf{G}$ can be obtained from any available CBSM, the proposed model is called CBSM with correlated shadowing (CBSM-CS).

The relationship between the $\mathbf{X}$ and $\mathbf{X}_{\mathrm{dB}}$ means and variances is derived based on [16],

$$\mathbf{M}_{\mathrm{X}} = e^{\left(\lambda\mathbf{M}_{\mathrm{X,dB}} + \frac{\lambda^2}{2}[\mathbf{\Sigma}_{\mathrm{X,dB}}]^2\right)} \tag{4}$$

$$[\mathbf{\Sigma}_{\mathrm{X}}]^2 = [\mathbf{M}_{\mathrm{X}}]^2 \cdot \left(e^{\lambda^2[\mathbf{\Sigma}_{\mathrm{X,dB}}]^2} - 1\right) \tag{5}$$

where $\lambda = \ln 10/10$.

2.1 Normalized CBSM-CS

Since the fading and shadowing are independent from each other, to simplify the analysis the normalized RLN distributed channel is expressed as the product of a normalized Rayleigh and a normalized Lognormal RV,

$$\mathbf{H}^{\mathrm{norm}} = [\mathbf{K}_{\mathrm{X}} \cdot \mathbf{X}]^{1/2} \cdot K_G\mathbf{G} \tag{6}$$

where $K_G = 1/\sqrt{2}$ and $\mathbf{K}_{\mathrm{X}} = [\mathbf{M}_{\mathrm{X}}]^{-1}$. For the normalized channel,

$$E\left[\| \mathbf{H}^{\mathrm{norm}} \|_F^2\right] = N_T \cdot N_R \tag{7}$$

where $E[\bullet]$ is the expectation taken over channel realizations and $\| \bullet \|_F$ represents the Frobenius norm.

The average channel power difference among the entries in $\mathbf{H}^{\mathrm{norm}}$ is due to the branch power imbalance (BPI). A matrix $\mathbf{P}_{\mathrm{BPI,dB}}$ is defined to represent the BPI in dB in the channel model explicitly. To preserve the normalized channel power,

$$\mathbf{M}_{\mathrm{X,dB}}^{\mathrm{norm}} = -\frac{\lambda}{2}\left[\mathbf{\Sigma}_{\mathrm{X,dB}}^{\mathrm{norm}}\right]^2 + \mathbf{P}_{\mathrm{BPI,dB}} \tag{8}$$

$$\| 10^{\mathbf{P}_{\mathrm{BPI,dB}}/10} \|_F^2 = N_T \cdot N_R \tag{9}$$

The channel model after the normalization is presented as follows. The superscript

'$norm$' is omitted for conciseness.

$$\mathbf{H} = 10^{\mathbf{X}_{\mathrm{dB}}/20} \cdot \sqrt{\frac{1}{2}}\mathbf{G} \tag{10}$$

$$\mathbf{X}_{\mathrm{dB}} = \mathbf{\Sigma}_{\mathrm{X,dB}} \cdot \left(\mathbf{R}_{\mathrm{X,dB}}^{1/2}\mathbf{G}_{\mathrm{X,dB}}\right) - \frac{\lambda}{2}\left[\mathbf{\Sigma}_{\mathrm{X,dB}}\right]^2 + \mathbf{P}_{\mathrm{BPI,dB}} \tag{11}$$

2.2 Structure of $\mathbf{R}_{\mathrm{X,dB}}$

To identify the structure of $\mathbf{R}_{\mathrm{X,dB}}$ two assumptions are made: independent shadowing between the Tx side and the Rx side and equal entries in $\mathbf{\Sigma}_{\mathrm{X,dB}}$. The first assumption is straightforward since the behaviors of the people in the BWCS are usually not coordinated. The second assumption is justified by the measurement results presented in Section 5.1. After a few steps derivation based on the correlation coefficient definition, the entries of $\mathbf{R}_{\mathrm{X,dB}}$ can be expressed as the average of Tx and Rx shadowing correlation coefficients,

$$\psi_{i1j1,i1j2} = \left(\psi_{i1i2} + \psi_{j1j2}\right)/2 \tag{12}$$

where ψ_{i1i2} and ψ_{j1j2} are the shadowing correlation coefficients between the Tx antennas $i1$ and $i2$ and Rx antennas $j1$ and $j2$, respectively. When $i1 = i2$ or $j1 = j2$, $\psi = 1$. It should be noticed that $\mathbf{R}_{\mathrm{X,dB}}$ usually does not have a Kronecker structure which is considered as the case for small-scale fading correlation in MIMO systems [17].

For analysis in the next section, $\mathbf{R}_{\mathrm{Bulk}}$, $\mathbf{R}_{\mathrm{Indp}}$ and $\mathbf{R}_{\mathrm{Nega}}$, are defined to represent strongly positive correlated, independent and negatively correlated shadowing respectively. For $i1{\neq}i2$ and $j1{\neq}j2$, $\psi_{i1i2}^{Bulk}{=}\psi_{j1j2}^{Bulk}{=}0.9$, $\psi_{i1i2}^{Indp}{=}\psi_{j1j2}^{Indp}{=}0$ and $\psi_{i1i2}^{Nega}{=}\psi_{j1j2}^{Nega}{=}-0.7$.

The relationship in (12) and the correlation values set above are verified by the measured channel statistics presented in Section 5.1.

3 Numerical Analysis of Modeling Parameters and Channel Capacity

The MIMO capacity with the assumptions of no channel knowledge at the Tx and perfect channel knowledge at the Rx is expressed as [18]

$$C = \log_2 \det\left(\mathbf{I}_{\mathrm{N_R}} + \frac{\rho}{N_T}\mathbf{H}\mathbf{H}^H\right) \tag{13}$$

where $\mathbf{I}_{\mathrm{a}}$ is an identity channel matrix with size a and ρ is the average signal to noise ratio (SNR) at the Rx.

The composite RLN distribution is specified by a Suzuki probability density function (PDF) which is not expressed in a closed form [19]. Although an explicit expression was derived in [20] and several simpler alternative PDFs were suggested, e.g. in [9], analytical studies of the MIMO channel capacity in the eigenspace are still difficult. Therefore we evaluate the capacity by numerical simulations in this section and by experimental studies in Section 5.

Different channel conditions have been simulated with a 2×2 MIMO setup and a 20 dB SNR (ρ). Cumulative density functions (CDFs) of some simulated channel capacity are shown in Fig. 1.

3.1 Effects of $\mathbf{\Sigma}_{\mathrm{X,dB}}$ on Channel Capacity

Equal values are set to all the entries ($\sigma_{X,dB}$) in $\mathbf{\Sigma}_{\mathrm{X,dB}}$ for the simulations. Three values of $\sigma_{X,dB}$, 0, 5 and 10 dB, are simulated to represent the Rayleigh channel, typical indoor body shadowing [3, 4] and severe shadowing conditions respectively. Fig. 1 shows the shadowing depth represented by $\sigma_{X,dB}$ plays a dominant role to the channel capacity. In the $\mathbf{R}_{\mathrm{Indp}}$ condition the typical and severe shadowing degrade the ergodic capacity by 1.2 and 4.5 bit/s/Hz respectively compared with the Rayleigh channel, and the degradation of the 1% outage capacity is 1.9 and 5.6 bit/s/Hz respectively.

The channel capacity approximately linearly depends on SNR in dB when the SNR is higher than 10 dB. Fig. 2 shows the probability density functions (PDF) of the Rayleigh and the RLN channel power in dB. The average channel power is normalized to one for all the channels. As shown in the figure both mean and outage channel power in dB decrease when $\sigma_{X,dB}$ increases. Therefore the capacity of the Rayleigh channel, which is a special case of the RLN channel when $\sigma_{X,dB} = 0$, is an upper bound of the RLN channel capacity as shown in Fig. 1.

3.2 Effects of $\mathbf{R}_{\mathrm{X,dB}}$ on Channel Capacity

The independent and negative shadowing correlation in $\mathbf{R}_{\mathrm{Indp}}$ and $\mathbf{R}_{\mathrm{Nega}}$ provide antenna diversity gains to mitigate the body shadowing. Therefore, as shown in Fig. 1, the outage capacity is improved significantly in the $\mathbf{R}_{\mathrm{Indp}}$ and $\mathbf{R}_{\mathrm{Nega}}$ conditions compared with the $\mathbf{R}_{\mathrm{Bulk}}$ channel. The improvement is about 1.8 bit/s/Hz with the typical shadowing. On the other hand the improvement in the ergodic capacity is always less than 1 bit/s/Hz in all the simulated cases. The ergodic capacity in the $\mathbf{R}_{\mathrm{Nega}}$ condition is slight lower than in the $\mathbf{R}_{\mathrm{Indp}}$ channel and the 1% outage capacity shows an opposite trend. Overall the influences of the shadowing correlation on capacity increase with $\sigma_{X,dB}$.

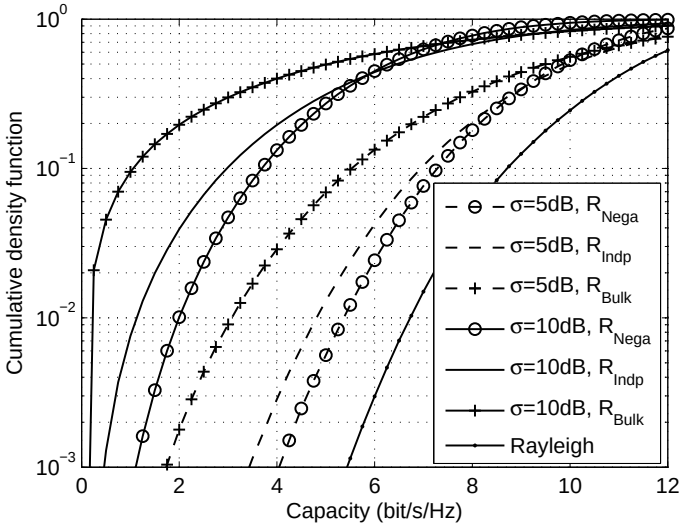

Figure 1: CDF of the simulated 2×2 MIMO channel capacity with the different shadowing correlation conditions and shadowing standard deviation (SNR = 20 dB, BPI = 0 dB)

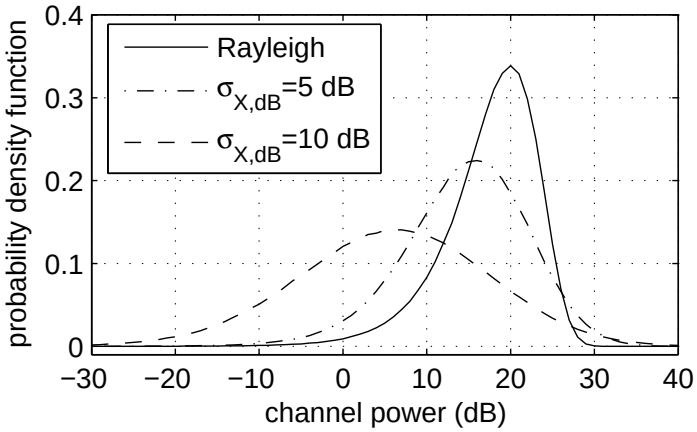

Figure 2: Probability density functions of channel power in dB with the different shadowing standard deviations

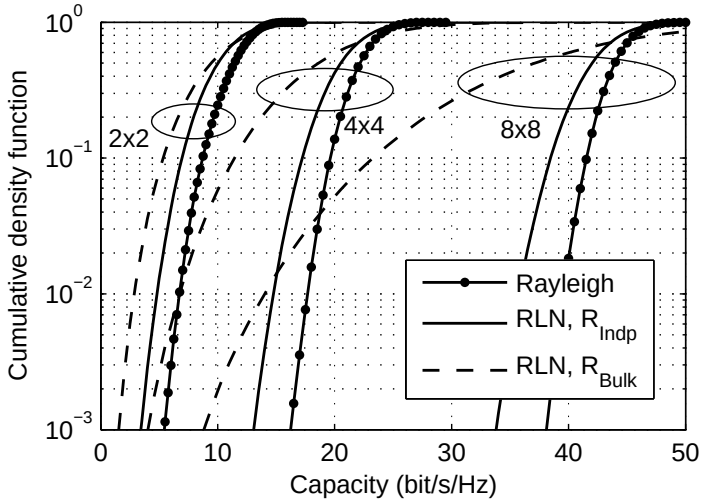

Figure 3: CDF of the simulated MIMO channel capacity in the typical shadowing with the different MIMO sizes and shadowing correlation conditions (SNR = 20 dB)

3.3 Effects of BPI on Channel Capacity

The BPI is represented by setting the average channel power ratio between the two Rx antennas to different values, i.e. 0, 5 and 10 dB. The BPI shows the most significant effects on the channel capacity in the Rayleigh channel. When BPI=10 dB the ergodic and 1% outage capacity decrease by 1.3 and 0.3 bit/s/Hz compared with the balanced channels (BPI=0 dB). In other simulated conditions the BPI degrades the channel capacity by less than 1 bit/s/Hz.

3.4 MIMO Size and Channel Capacity

For a MIMO system working in the high SNR and uncorrelated fading condition, the channel capacity decreases $N{=}\min(N_T, N_R)$ bit/s/Hz with 3 dB SNR reduction. As analyzed in Section 3.1 it is the different distribution of channel power in dB that degrades the capacity of the RLN channel. Therefore the absolute capacity loss of the RLN channel is expected to increase with the MIMO size. This is confirmed by simulations in the typical shadowing condition and the results are demonstrated in Fig. 3. Due to the diversity gain the outage capacity degradation of the $\mathbf{R}_{\mathrm{Indp}}$ channel is much less sensitive to the MIMO size than in the $\mathbf{R}_{\mathrm{Bulk}}$ condition. The measurement results in Section 5.2 confirm this conclusion as well. Therefore it implies that keeping low shadowing correlation becomes more essential with larger MIMO arrays.

Table 1: Channel ergodic capacity in bit/s/Hz with the different MIMO configurations

Configuration	Rayleigh	$\sigma = 5$ dB		$\sigma = 10$ dB	
		CH1	CH2	CH1	CH2
2x2	11.3	9.8	9.7	6.4	5.8
2x2(4x4) PS	13.5	13.4	12.0	11.6	8.1
2x2(4x4) IS	14.4	14.3	12.8	11.9	8.5
4x4	22.1	19.3	19.0	12.6	11.4

3.5 Body-to-Body MIMO Systems with Antenna Selection

It is well known that for the Rayleigh fading MIMO channel hybrid antenna selection/MIMO (H-S/MIMO) schemes are good tradeoffs between MIMO gains and system complexity since additional antenna elements are usually inexpensive compared to the radio frequency (RF) elements [21]. This strategy is especially attractive in the body-to-body channel case with the distributed antennas.

Considering a system with four antennas placed at two body positions, such a system may benefit from the higher SNR and MIMO transmission at the same time by selecting the two less shadowed antennas. We use CH1 to represent this channel setup. The performance of a 2×2 channel selected from a 4×4 channel is evaluated with the CH1 setup. Another channel condition with four antennas co-located at the same body position (CH2) is also simulated for comparison. The same antenna setup are applied to both the Tx and Rx sides. An ideal selection (IS) and a power based selection algorithms (PS) are considered. In the IS the capacity of all possible antenna selection combinations is compared, and the 2×2 channel associated with the maximum capacity is selected. This method provides an upper bound of the H-S/MIMO capacity. The PS selects the antennas with the highest power. The simulated ergodic capacity results are summarized in Table 1.

The PS performs almost as good as the IS for the H-S/MIMO scheme. The H-S/MIMO capacity in the typical shadowing condition is close to the Rayleigh channel capacity. In the severe shadowing condition the 2×2 H-S/MIMO capacity is approaching the 4×4 channel capacity. It is evident that the H-S/MIMO is more efficient in the body-to-body channel especially with distributed antennas (CH1) and in the severe shadowing condition.

4 Measurement Setup and Data Processing

A body-to-body measurement campaign was performed in two indoor environments with a 5.5 GHz carrier frequency and a -3 dB bandwidth of about 100 MHz. A correlation based MIMO channel sounder was used for the experiments. Four Tx antennas

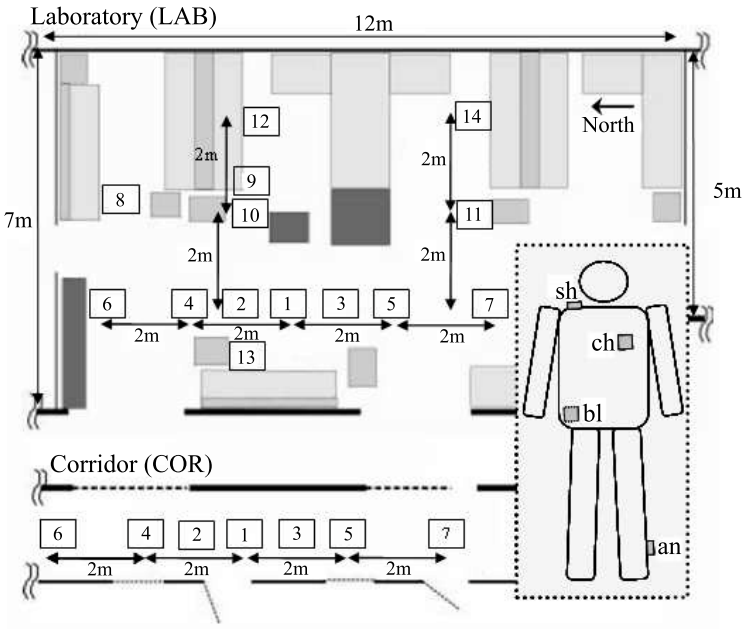

Figure 4: The layout of the laboratory and corridor environments with measurement spots #1 to #14 marked with squares; to the right: an illustration of the device on-body positions

and 32 Rx antennas were measured simultaneously. The full 4×32 MIMO channel sampling rate was 60 Hz, which gives a maximum allowed relative speed between the Tx and the Rx of 1.6 m/s at 5.5 GHz. The length of each channel impulse response (CIR) was 640 ns which is sufficient for the investigated indoor environments. Additional information about the sounder is available in [22].

4.1 Measurement Devices, Environments and Scenarios

Three types of devices and antennas were used in the measurements. The Tx was emulating small size devices with a directional stacked patch antenna (DSP) [6]. Two types of receivers, Rx-A and Rx-B, were equipped with four antennas on each device. In the Rx-A four Planar Inverted F-Antennas (PIFAs) are located rather close to each other and provide a certain front-to-back ratio. The Rx-B antennas are four monopole-like antennas which are very simple to integrate into many textiles or products.

The Tx, Rx-A and Rx-B devices were placed on three test persons respectively. In order to obtain channel characteristics between different body positions, four identical devices of each type were used simultaneously during the experiments. We included a variety of heights and orientations for the choices of device positions: shoulder (sh),

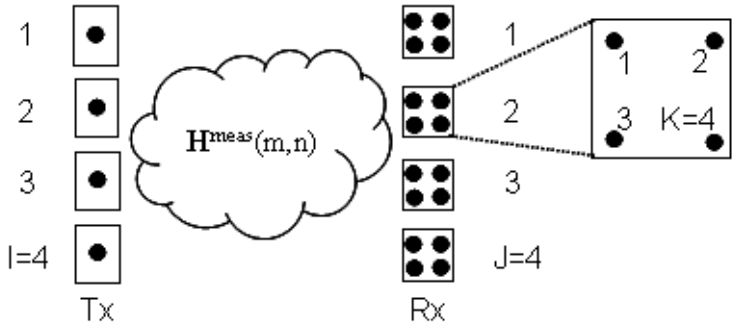

Figure 5: Diagram of the measured MIMO channel with $I = 4$ Tx devices with single antenna elements and $J = 4$ Rx devices each with $K = 4$ antenna elements

chest (ch), belt (bl) and ankle (an). The experiments were performed in two indoor environments: a laboratory (LAB) and a corridor (COR). During the experiments, no people were moving in the area except the test persons. An illustration of the device positions and sketches of the laboratory and the corridor are shown in Fig. 4. More detailed information about the measurement devices and the environments can be found in [3].

The measurements were performed with the users located at fixed positions as shown in Fig. 4. Different from the experiments performed in [3] during the measurements the three test persons moved randomly within three predefined 50×50 cm square areas, respectively. The size of the square ensures the channel stationarity of each measurement. All three test persons continuously turned around within the squares in a random manner for 90 seconds. Spots $\#1$ to $\#14$ in the LAB and $\#1$ to $\#7$ in the COR were used to make measurements. The Tx-Rx distance was fixed to 2 meters and all spots separated by 2 meters were measured. Measurements at spot $\#8$ $\#9$ and $\#13$ in the LAB are not included in this study.

4.2 Measured Channel Representation and Data Processing

The measurements from the two types of the Rx are combined and the size of each full measured MIMO channel is 4×16. The measured MIMO channel is transferred into the frequency domain by applying the discrete Fourier transform (DFT). Totally 64 subbands with 1.56 MHz bandwidth are located within the measured frequency band and used in the analysis. The frequency-domain MIMO channel is expressed as a $4\times4\times4$ matrix $\mathbf{H}^{\mathrm{meas}}(m,n)$, whose entries $h^{meas}_{i,j,k}(m,n)$ are complex channel coefficients between the i-th Tx device and the k-th Rx antenna of the j-th Rx device at a time index m and a frequency index n. A diagram of the measured channel is shown in Fig. 5

in which I, J and K are the total number of the Tx devices, Rx devices and antenna elements on each Rx device, respectively. We refer to the antennas at the same device as 'co-located antennas', and as 'distributed antennas' otherwise.

The measured channel coefficients include path-loss, body shadowing, small-scale fading and antenna pattern gains. The average channel power of the entire MIMO channel matrix is normalized to the number of links which is $4\times16{=}64$ for the system setup. By this 'global' normalization, the relative power difference among measured on-body positions and the channel power fluctuation due to both fading and body shadowing are preserved.

To map the RLN statistics of the measured channel to the modeling parameters in (11), a series of relations are derived and presented in Appendix 6.

5 Measured Channel Capacity and Model Verification

The channel statistics and capacity presented in this section are based on the LAB measurement. Similar results are obtained in the COR as well. All the measurements are used for the model verification.

5.1 Measured Channel Statistics

For antennas mounted on various parts of the bodies the shadowing statistics can be different [3]. This is confirmed by $\mathbf{M}_{\mathrm{X,dB}}$ and $\mathbf{\Sigma}_{\mathrm{X,dB}}$ associated with the different on-body positions as shown in Fig. 6. The maximum BPI is 7.2 dB and $\sigma_{X,dB}$ ranges from 4.0 to 6.2 dB. These results are basically consistent with the ones obtained in [3] while slight differences are observed due to the different measurement scenarios.

$\mathbf{R}_{\mathrm{X,dB}}$ of two 2×2 channel configurations are illustrated in Fig. 7. One of them is formed by the chest and belt Tx antennas and the distributed Rx antennas at the same positions, and the other consists of the same Tx antennas and two co-located Rx antennas at the chest. If we set the correlation between the co-located antennas to 0.9 and between the distributed antennas to -0.7 as presented in [3], the value of each entry in $\mathbf{R}_{\mathrm{X,dB}}$ can be calculated by (12). The results are very close to the measured values given in Fig. 7 which proves the analysis in Section 2.2. The shadowing correlation with respect to the other antenna positions can be found in [3].

5.2 Measured Channel Capacity

To analyze the channel capacity with different MIMO sizes and antenna on-body positions, channel subsets are defined by selecting parts of the entire measured channel matrix. Each channel subset forms an individual MIMO channel with a certain array size and antenna position combinations.

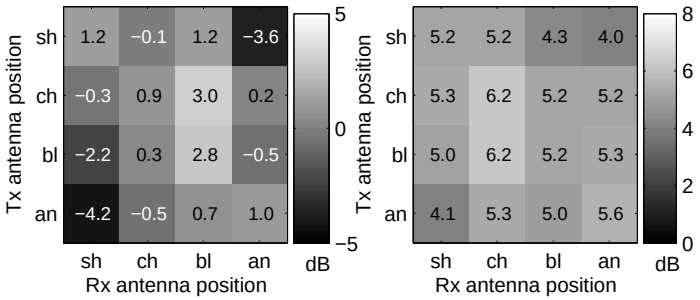

Figure 6: Mean ($\mathbf{M}_{\mathrm{X,dB}}$, left) and standard deviation ($\mathbf{\Sigma}_{\mathrm{X,dB}}$, right) of the body shadowing in dB respect to the different Tx and Rx antenna positions

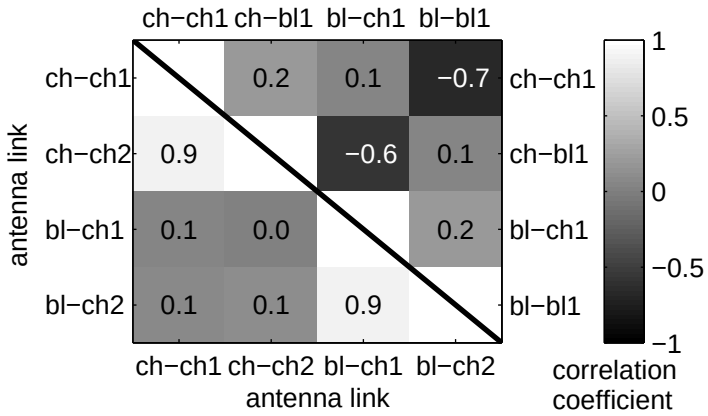

Figure 7: Shadowing correlation coefficients ($\mathbf{R}_{\mathrm{X,dB}}$) with the distributed (upper-right part) and co-located (lower-left part) Rx antennas; the x and y-axis represent the antenna on-body positions (Tx-Rx, see Fig. 4) with the numbers representing the k-th antenna element at the Rx devices (see Fig. 5)

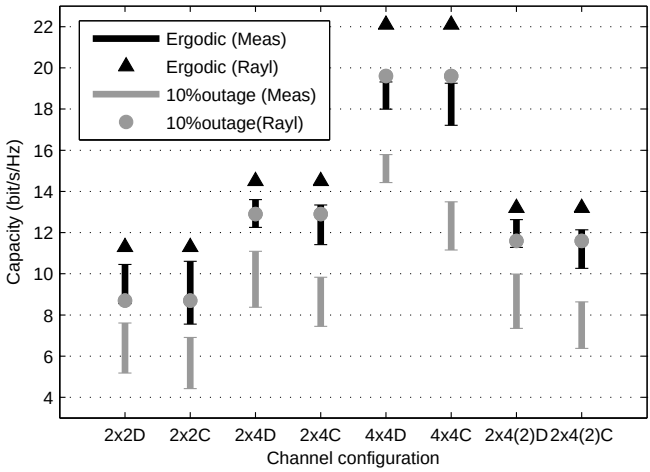

Figure 8: Channel capacity of the measured channels with various MIMO configurations (SNR = 20 dB). Each vertical line represents the range of the capacity obtained from all the possible channel subsets given the corresponding MIMO configuration.

Fig. 8 shows the ergodic and 10% outage capacity for different MIMO configurations. In the x-axis $N_T \times N_R$ is the size of the MIMO channel, and 'D' and 'C' stand for the distributed and co-located Rx antennas respectively. The last two items represent the H-S/MIMO with the IS algorithm (see Sec. 3.5) where the number in the bracket, L_R, is the number of selected Rx antennas. Each vertical line represents the range of the measured capacity obtained from all the channel subsets which satisfy the corresponding MIMO configurations.

It is evident that the capacity of the MIMO channel with the same number of antennas varies significantly. The Rayleigh channel always overestimates the body-to-body channel capacity. Table 2 summarizes the capacity of the 2×2 channel subsets which have the maximum and minimum ergodic capacity. By examining the shadowing statistics in Fig. 6, we find that when $\sigma_{X,dB}$ is similar the capacity difference is mainly due to the average channel power. The difference between the distributed and co-located Rx antennas is noticeable but limited due to the diversity gain provided by the distributed Tx antennas. The shadowing statistics shown in Fig. 6 and in [3] can be used as references for practice antenna position selection in order to achieve higher channel capacity.

The outage capacity degradation with the distributed Rx antennas is much less sensitive to the MIMO size than with the co-located Rx antennas. This result is consistent with the conclusion in Section 3.4.

Table 2: Capacity of the channel subsets associated with the maximum and minimum ergodic capacity and the corresponding MIMO configurations

MIMO	positions		capacity (bit/s/Hz)	
configuration	Tx	Rx	ergodic	10% outage
2x2D (max)	ChBl	ChBl	10.5	7.6
2x2D (min)	ShCh	ChAn	9.0	5.2
2x2C (max)	ChBl	Bl	10.6	6.9
2x2C (min)	BlAn	Sh	7.6	4.4

5.3 Model verification

The capacity of the measured and modeled channels is compared in terms of the capacity to verify the proposed CBSM-CS model. In this section the channel power of each measured channel subset is normalized individually. Due to the measurement setup the channel with co-located antennas at both the Tx and Rx sides are not verified.

Fig. 9 illustrates the CDFs of the measured and modeled 2×2 and 4×4 channel capacity. The antenna position configurations in Fig.7 are selected for the 2×2 channels. The 4×4D channel includes the $1st$ antenna of all four Rx devices and the 4×4C channel contains all four co-located Rx antennas at the belt position. The averaged model errors in ergodic and 1% outage capacity are shown in Fig. 10. The model error is calculated as the absolute difference between the measured and modeled capacity at the corresponding levels.

When the shadowing statistics extracted from the measurements are assigned as the modeling parameters, the model exhibits excellent accuracy. The measured and modeled capacity CDF curves are very close to each other as shown in Fig. 9. Overall the model error is always less than 0.5 bit/s/Hz (or less than 5% of the capacity of each MIMO configuration) for all the MIMO configurations, in both of the environments and at both the ergodic and 1% outage level.

To facilitate the use of the proposed model, a group of simplified parameters (SP) is suggested and evaluated with the measurements. For the SP model the balanced channel (BPI=0 dB) with $\sigma_{X,dB} = 5$ dB is assumed. The correlation coefficient is set to 0.9 for the co-located antennas and zero for the distributed antennas. Then $R_{\mathrm{X,dB}}$ is calculated according to (12). Fig. 9 shows the model error increases up to 15% and 30% of the channel capacity at the ergodic and outage levels respectively. The errors for the configurations with the distributed Rx antennas are higher since the shadowing of several on-body positions is actually positively correlated [3]. Therefore the SP model tends to overestimate the channel capacity in these cases. Even though the SP is a reasonable simplification of the proposed CBSM-CS model and is much more accurate than the Rayleigh channel model.

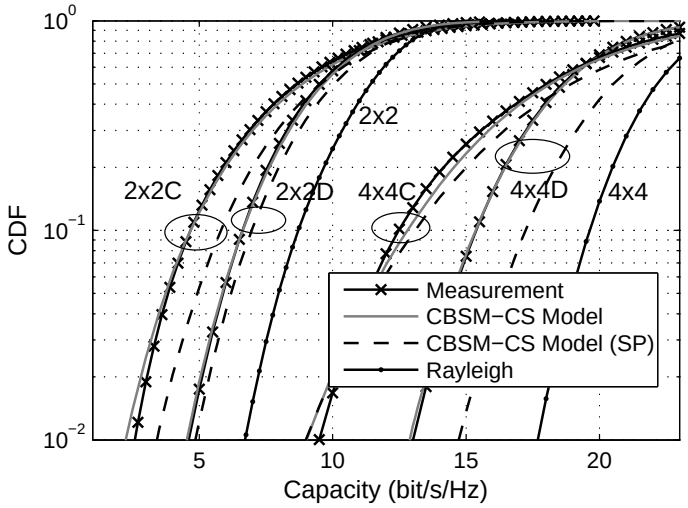

Figure 9: CDFs of the measured and modeled 2×2 channel capacity with the distributed and co-located Rx antennas

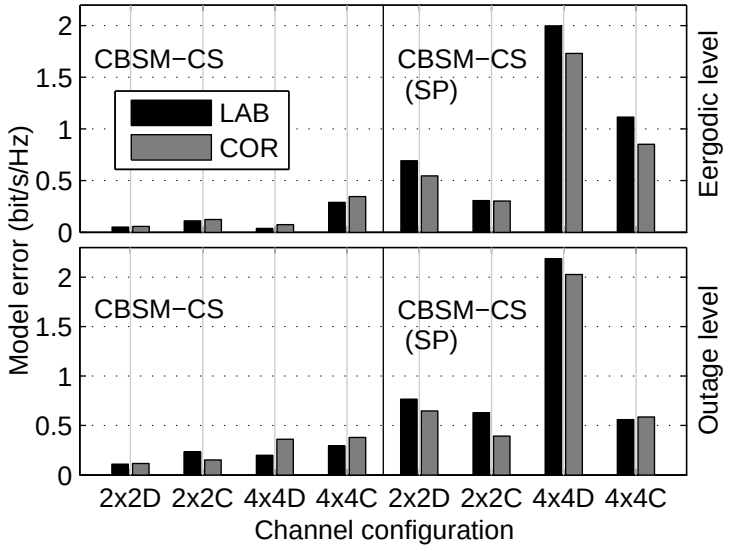

Figure 10: Average model error for the different MIMO configurations in the LAB and COR

6 Conclusion

In this paper, we propose a correlation based stochastic model with correlated shadowing (CBSM-CS) for body-to-body multiple-input multiple-output (MIMO) radio channels. The model introduces a shadowing matrix consisting of correlated Lognormal distributed entries to represent unbalanced and correlated body shadowing. A Rayleigh-Lognormal (RLN) distributed CBSM-CS channel model is derived based on an indoor measurement campaign, and the modeling accuracy in terms of channel capacity is verified by a different set of experiments with less than 5% relative model errors. A group of typical modeling parameters is also suggested to facilitate the implementation of the model.

The maximum measured BPI is 7.2 dB and the shadowing standard deviation ranges from 4.0 to 6.2 dB. The impacts of the modeling parameters, i.e. shadowing standard deviation ($\sigma_{X,dB}$), shadowing correlation and branch power imbalance (BPI), on the MIMO channel capacity are analyzed by both numerical and experimental studies. Since both mean and outage channel power in dB decrease when $\sigma_{X,dB}$ increases, $\sigma_{X,dB}$ is dominant to the ergodic capacity. The capacity of the Rayleigh channel ($\sigma_{X,dB} = 0$) is an upper bound of the body-to-body channel capacity. Antenna diversity gains for body shadowing mitigation can be achieved when the shadowing correlation between the antennas is low. Therefore the shadowing correlation affects the outage capacity significantly. The 2×2 channel simulations at 20 dB SNR reveal a 1.2 bit/s/Hz ergodic capacity degradation when $\sigma_{X,dB} = 5$ dB compared with the Rayleigh fading channel. The high (> 0.9) shadowing correlation scenario yields another 1.8 bit/s/Hz capacity drop at 1% outage level compared with the independent shadowing. This difference increases rapidly with the MIMO size and it implies that keeping low shadowing correlation becomes more essential with larger MIMO arrays. The effects of the BPI on the capacity are limited and decrease as $\sigma_{X,dB}$ increases. In practice the difference in the average channel power associated with the different antenna positions also need to be taken into account for the antenna position selection. Hybrid antenna selection/MIMO (H-S/MIMO) schemes are proved efficient in the shadowed fading MIMO channels especially with distributed antennas and in the severe shadowing condition with $\sigma_{X,dB} = 10$.

[Mapping RLN Statistics to Lognormal Statistics in dB] In the following derivations, $\mathbf{H}$, $\mathbf{R}$ and $[\mathbf{X}]^{1/2}$ represent normalized RLN, Rayleigh and Lognormal random matrices respectively. The mean and standard deviation of the normalized Rayleigh RV, m_{R} and σ_{R}, are known values. The target is to obtain $\mathbf{\Sigma}_{\mathrm{X,dB}}$, $\mathbf{P}_{\mathrm{X,dB}}$ and $\mathbf{R}_{\mathrm{X,dB}}$ in (11) given the statistics of $\mathbf{H}$.

According to (4) and (5),

$$\left[\mathbf{\Sigma}_{\mathrm{X,dB}}\right]^2 = \frac{1}{\lambda^2}\ln\left(\left[\frac{\mathbf{\Sigma}_{\mathrm{X}}}{\mathbf{M}_{\mathrm{X}}}\right]^2 + 1\right) \tag{14}$$

$$\mathbf{M}_{\mathrm{X,dB}} = -\frac{\lambda}{2}\left[\mathbf{\Sigma}_{\mathrm{X,dB}}\right]^2 + \frac{1}{\lambda}\ln\left(\mathbf{M}_{\mathrm{X}}\right) \tag{15}$$

According to (14) and the definition of variance,

$$\left[\mathbf{\Sigma}_{\mathrm{X,dB}}\right]^2 = 4\left[\mathbf{\Sigma}_{[\mathrm{X}]^{1/2},\mathrm{dB}}\right]^2 = \frac{4}{\lambda^2}\ln\left(\frac{\left[\mathbf{\Sigma}_{\mathrm{H}}\right]^2 + \left[m_{\mathrm{R}}\right]^2}{\left[\mathbf{M}_{\mathrm{H}}\right]^2 + \left[\sigma_{\mathrm{R}}\right]^2}\right) \tag{16}$$

Compare (15) and (8)

$$\mathbf{P}_{\mathrm{BPI,dB}} = \frac{1}{\lambda}\ln\left(\mathbf{M}_{\mathrm{X}}\right) = \frac{\lambda}{2}\left[\mathbf{\Sigma}_{\mathrm{X,dB}}\right]^2 \cdot \ln\left(\frac{\mathbf{M}_{\mathrm{H}}}{m_{\mathrm{R}}}\right) \tag{17}$$

According to the definition of correlation coefficient,

$$\mathbf{R}_{[\mathrm{X}]^{1/2}} = \mathbf{R}_{\mathrm{H}} \cdot \frac{\mathrm{vec}\left(\mathbf{\Sigma}_{\mathrm{H}}\right)\mathrm{vec}^H\left(\mathbf{\Sigma}_{\mathrm{H}}\right)}{m_{\mathrm{R}}\mathrm{vec}\left(\mathbf{\Sigma}_{[\mathrm{X}]^{1/2}}\right)\mathrm{vec}^H\left(\mathbf{\Sigma}_{[\mathrm{X}]^{1/2}}\right)} \tag{18}$$

where $\mathrm{vec}\left(\bullet\right)$ represents vectorization and according to (5)

$$\left[\mathbf{\Sigma}_{[\mathrm{X}]^{1/2}}\right]^2 = \left[\frac{\mathbf{M}_{\mathrm{H}}}{m_R}\right]^2 \cdot \left(e^{\frac{\lambda^2}{4}\left[\mathbf{\Sigma}_{\mathrm{X,dB}}\right]^2} - 1\right) \tag{19}$$

And as presented in [11]

$$\begin{aligned}\mathbf{R}_{\mathrm{X,dB}} &= \mathbf{R}_{[\mathrm{X}]^{1/2},\mathrm{dB}} \\ &= \frac{\ln\left\{\left(e^{\frac{\lambda^2}{4}\left[\mathrm{vec}\left(\mathbf{\Sigma}_{\mathrm{X,dB}}\right)\mathrm{vec}^H\left(\mathbf{\Sigma}_{\mathrm{X,dB}}\right)\right]^2} - 1\right)\cdot\mathbf{R}_{[\mathrm{X}]^{1/2}} + 1\right\}}{\lambda\left[\mathrm{vec}\left(\mathbf{\Sigma}_{\mathrm{X,dB}}\right)\mathrm{vec}^H\left(\mathbf{\Sigma}_{\mathrm{X,dB}}\right)\right]^2}\end{aligned} \tag{20}$$

References

[1] P. S. Hall and Y. Hao, "Antennas and propagation for body centric communications," in *European Space Agency, (Special Publication) ESA SP*, vol. 626 SP, Oct 2006.

[2] I. Z. Kovacs, Y. Wang, P. C. Eggers, and K. Olesen, "UWB radio channel model for short-range mobile-to-mobile communication scenarios," in *Wireless Personal Multimedia Communications (WPMC) Symposia 2005*, Sep 2005, pp. 2008–2012.

[3] Y. Wang, B. B. Ivan, I. Z. Kovacs, J. Ø. Nielsen, and G. F. Pedersen, "Characterization of the indoor multi-antenna body-to-body radio channel," *IEEE Transaction on Antenna and Propagation Special issue on Body-Centric Wireless Communications*, Dec 2008, (submitted).

[4] J. Karedal, A. J. Johansson, F. Tufvesson, and A. F. Molisch, "Shadowing effects in MIMO channels for personal area networks," in *Proceedings of VTC 2006 Fall*, Sep 2006, pp. 1–5.

[5] Z. W. Tang and A. S. Mohan, "An investigation of MIMO performance in the indoor ricean environment," *Wireless Personal Communications*, vol. 39, no. 1, pp. 99–113, Oct 2006.

[6] M. Klemm, I. Z. Kovacs, G. F. Pedersen, and G. Troster, "Novel small-size directional antenna for UWB wban/wPAN applications," *IEEE Transactions on Antennas and Propagation*, vol. 53, no. 12, pp. 3884–3896, Dec 2005.

[7] P. Salonen, Y. Rahmat-Samii, and M. Kivikoski, "Wearable antennas in the vicinity of human body," in *Antennas and Propagation Society International Symposium, 2004.IEEE*, vol. 1, 2004, pp. 467–470.

[8] G. L. Steuber, *Principles of mobile communication*. Springer, 2004, vol. 2nd.

[9] P. M. Shankar, "Performance analysis of diversity combining algorithms in shadowed fading channels," *Wireless Personal Communications*, vol. 37, no. 1-2, pp. 61–72, Apr 2006.

[10] J. C. Lin, W. C. Kao, Y. T. Su, and T. H. Lee, "Outage and coverage considerations for microcellular mobile radio systems in a shadowed-rician/shadowed-nakagami environment," *IEEE Transactions on Vehicular Technology*, vol. 48, no. 1, pp. 66–75, Jan 1999.

[11] Z. Lin, X. M. Peng, K. B. Png, and F. Chin, "Kronecker modelling for correlated shadowing in UWB MIMO channels," in *Wireless Communications and Networking Conference, 2007.WCNC 2007.IEEE*, Mar 2007, pp. 1583–1587.

[12] W. Roh and A. Paulraj, "MIMO channel capacity for the distributed antenna systems," in *Vehicular Technology Conference, 2002.Proceedings.VTC 2002-Fall.2002 IEEE 56th*, vol. 56, 2002, pp. 706–709.

[13] W. A. T. Kotterman, G. F. Pedersen, and K. Olesen, "Capacity of the mobile MIMO channel for a small wireless handset and user influence," in *Personal, Indoor and Mobile Radio Communications, 2002.PIMRC 2002.13th IEEE International Symposium on*, vol. 4, Sep 2002, pp. 1937–1941.

[14] J. Karedal, A. J. Johansson, F. Tufvesson, and A. F. Molisch, "Characterization of MIMO channels for handheld devices in personal area networks at 5 GHz," in *14th European Signal Processing Conference (EUSIPCO 2006)*, Sep 2006.

[15] D. Neirynck, C. Williams, A. Nix, and M. Beach, "Exploiting multiple-input multiple-output in the personal sphere," *IET Microwaves, Antennas and Propagation*, vol. 1, no. 6, pp. 1170–1176, Dec 2007.

[16] R. Vaughan and J. B. Andersen, *Channels, Propagation and Antennas for Mobile Communications*. Institution of Electrical Engineers, 2003.

[17] J. P. Kermoal, L. Schumacher, K. I. Pedersen, P. E. Mogensen, and F. Frederiksen, "A stochastic MIMO radio channel model with experimental validation," *IEEE Journal on Selected Areas in Communications*, vol. 20, no. 6, pp. 1211–1226, Aug 2002.

[18] G. J. Foschini, G. D. Golden, R. A. Valenzuela, and P. W. Wolniansky, "Simplified processing for high spectral efficiency wireless communication employing multi-element arrays," *IEEE Journal on Selected Areas in Communications*, vol. 17, no. 11, pp. 1841–1852, Nov 1999.

[19] H. Suzuki, "Statistical-model for urban radio propagation," *IEEE Transactions on Communications*, vol. 25, no. 7, pp. 673–680, 1977.

[20] S. Kotz and S. Nadarajah, "An explicit expression for the rayleigh-log normal probability density function," *Ultrasound in Medicine and Biology*, vol. 33, no. 3, pp. 487–487, Mar 2007.

[21] A. F. Molisch and M. Z. Win, "MIMO systems with antenna selection," *IEEE Microwave Magazine*, vol. 5, no. 1, pp. 46–56, Mar 2004.

[22] J. Ø. Nielsen, J. B. Andersen, P. C. Eggers, G. F. Pedersen, K. Olesen, E. H. Sørensen, and H. Suda, "Measurements of indoor 16x32 wideband MIMO channels at 5.8 GHz," in *Proceedings of the 2004 International Symposium on Spread Spectrum Techniques and Applications (ISSSTA 2004)*, 2004, pp. 864–868.

Paper C

Characterization and Modeling of UWB WBAN Channel in Indoor Environments

Yu Wang, István Z. Kovács, and Gert F. Pedersen

The paper will be submitted to
IEEE Transactions on Antennas and Propagations, Aug 2008

The layout has been revised.

Abstract

Ultra-wideband (UWB) is a promising technology for wireless body area networks (WBANs) which are essential parts of future wireless communication systems. In this paper we characterize and model the UWB WBAN channel based on experiments performed in two typical indoor environments. Totally 15 *antenna on-body positions are investigated. According to the measurements the channel wideband power is Lognormal distributed and the power varies up to* 20 *dB among the antenna positions. The channel rms delay spread ranges from* 5 *to* 20 *ns.*

The WBAN channel is featured by the radio propagation around human bodies, i.e. direct link, body diffraction and body reflection. To separate the around body propagation from the environment propagation the first cluster (FC) is detected and separated from the remaining clusters (RC) of the measured channel impulse responses (CIRs). The amplitude of the FC shows different distributions when the antenna is mounted on different parts of the body. The statistics of the power ratio and arrival time intervals between the FC and the RC also depends on the antenna on-body positions. The cluster decay factor of the RC is linearly related to the FC/RC power ratio in dB.

Based on the knowledge above we propose a UWB WBAN channel model which extends existing indoor UWB models for the WBAN applications. The model uses a joint approach to generate and combine the around body and the environment propagation in the delay domain. Modeling procedures are presented in order to implement the channel for system evaluations.

1 Introduction

An essential component of next generation wireless communication systems is a body-centric wireless communication system (BWCS). The BWCS connects various devices around human bodies, such as body sensors, body monitors and wearable electronic devices. According to the range of the communication the BWCS can be categorized as "off-body" and "on-body" systems [1]. The on-body BWCS has found applications in health monitoring, wearable PCs and entertainment systems. A radio network consisting of the on-body devices is called a wireless body area network (WBAN). In a typical WBAN scenario a number of sensors, e.g. health monitors and motion detectors, are distributed to a variety of on-body positions, and connect with a central device such as a personal digital assistant (PDA) for further processing and communications with other systems.

Ultra-wideband (UWB) is a promising technology for short range radio communications. Given the low power consumption and low complexity properties the UWB is a competent candidate for the WBAN applications. To gain the full potential advantages provided by the UWB comprehensive channel knowledge is required.

The UWB channel in indoor environments have been extensively studied in recent years [2, 3]. Compared with other radio channels the WBAN channel is featured by the short range direct link, body diffraction and body reflection. The penetration through the body is negligible [4]. The term of the 'around body' propagation is used in this study to represent the radio propagation close to human bodies. An extensive summary of narrowband on-body channel propagation was given by [5]. The investigation of the UWB WBAN channel is complicated by the large bandwidth or correspondingly the fine resolution in the delay domain. Finite-difference time-domain (FDTD) was usually used as a channel simulation method [4, 6]. A simpler ray theories based approach also provided reliable solutions [6]. Most experimental investigations for the WBAN channel were performed in anechoic chambers and focused on the around body propagation. Body diffraction was found as the dominant propagation mechanism between the ears of the human head [4]. Path-loss models along torsos were derived in [7–9]. Distance dependent exponential power decay with decay factors between 2.7 and 4.4 was reported. The distribution of the body diffraction components was summarized in [10, 11] and Lognormal was found as a good fit for the small-scale fading statistics. Some WBAN channel parameters, e.g. delay spread, were proved sensitive to the antenna positions, body gestures and antenna types [8].

When the on-body BWCS system works in real life the reflection, diffraction and scattering from the multipath environments will also be included in the radio channel. However few experimental studies have been conducted for the UWB WBAN channel in real scenarios. The measurement results on channel path loss [12], wideband power variation [13], path arrival times [14] and delay spread [12, 13] had been presented. In reference [7] the body diffraction and surrounding environments are modeled separately when the antennas were placed on the torso. In this paper we propose a UWB WBAN channel model which uses a joint approach to take both the around body and the environment propagation into consideration. The study is based on measurements performed in two typical indoor environments with dynamic users and a large collection of device on-body positions.

The paper is organized as follows. Section II gives a description of the measurement setup. The channel characteristics including wideband power, delay spread and the first cluster properties are presented in Section III. In Section IV we propose and verify a UWB WBAN model based on the measured channel investigations. Finally the paper is concluded in Section V.

2 Measurement Setup

The radio channel measurements were performed with a time domain UWB sliding correlator channel sounder. The measurement bandwidth was 2.5 GHz centered at 4.5

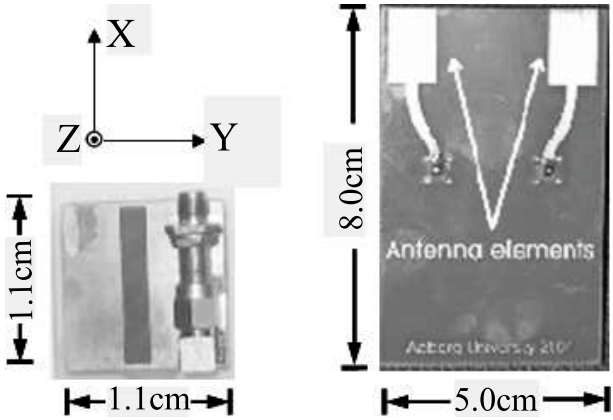

Figure 1: Left: a body-worn (Tx) device with a UWB directional stacked patch antenna; right: a belt-mounted (Rx) device with two omni-directional planar printed monopole UWB antennas

GHz. The effective delay resolution was 0.4 ns. The measurement set-up allowed the full separation of the $2 \times 4 = 8$ simultaneously measured radio links. The radio channel sampling rate was 39 Hz, which accommodates the expected channel change rate at normal walking speed of 1 m/s at the upper frequency of 5.75 GHz. A RF on fiber optic link instead of conductive cable connections was used to minimize the effects of the measurement cables on the antenna radiation characteristics [13]. The instantaneous dynamic range is 15-30 dB. A more detailed description of the measurement equipment can be found in [15].

2.1 Measurement Devices, Environments and Scenarios

To investigate the channel between a body sensor and a centralized device, e.g. a handset or a PDA, two types of devices were selected. Pictures of the devices are shown in Fig. 1. The transmitters (Tx) were small size devices with a directional stacked patch antenna on each of them [16]. Radiation patterns of the Tx antenna at the center frequency (4.5 GHz) are plotted in Fig. 2. The receiver (Rx) was a PDA like device equipped with two custom designed omni-directional planar printed monopole UWB antennas. Since the patterns of small antennas become directional when placed on the body regardless of their radiation patterns in free space [4, 17], the directional antenna used in our measurements cover general small antennas mounted close to the body.

Both the Tx and Rx antennas were placed on the same test person. The Rx was mounted on the front-right side of the waist, and the Tx was mounted at totally 15 different on-body positions. An illustration of the device positions is shown in Fig. 3. The selected Tx positions covered a variety of antenna heights, orientations and relative

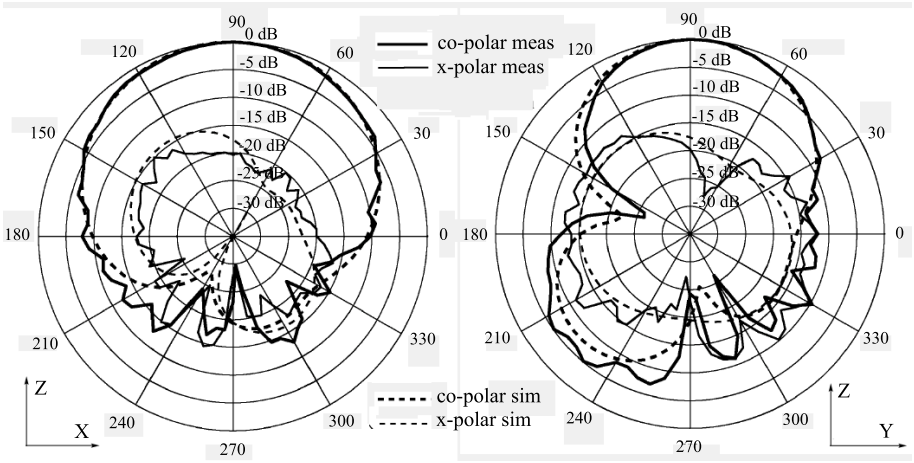

Figure 2: Measured and simulated radiation patterns of the Tx antenna at 4.5 GHz, left: XZ plane; right: YZ plane (the coordinate is shown in Fig. 1)

distances to the Rx.

The experiments were performed in two indoor environments: a laboratory (LAB) and a corridor (COR). Two routes in the LAB and one route in the COR were used. Each test person walked along the routes back and forth six times to have all the Tx positions tested. Totally four persons were measured for each route. No people were moving in the area except the test persons. Fig. 4 shows a sketch of the environments and a picture of a test person with the Tx placed at the upper torso.

2.2 Data Processing

The measured channel impulse responses (CIRs) were compensated for all measurement system influences except the antennas. Each measurement route was split up into consecutive time segments corresponding to 10 sampled CIRs each. An average power delay profile (PDP) was calculated for each data segment. Channel wideband power statistics and delay domain parameters were extracted based on these PDPs. The signal rays in the delay domain have been estimated using a CLEAN algorithm applied to the amplitude data of each individual CIR instead of the average PDP. The identified rays were used to characterize the around body propagation. Detailed descriptions of the channel data processing can be found in [3, 15].

The distribution fitting in this paper is analyzed by the Kolmogorov-Smirnov (K-S) test. Lognormal, Weibull, Exponential, Laplace, Normal and Rayleigh distributions are considered as candidates. The distribution is accepted as a fit when the p-value is larger than 0.01. Among all the fitted distributions the one with the largest p-value is

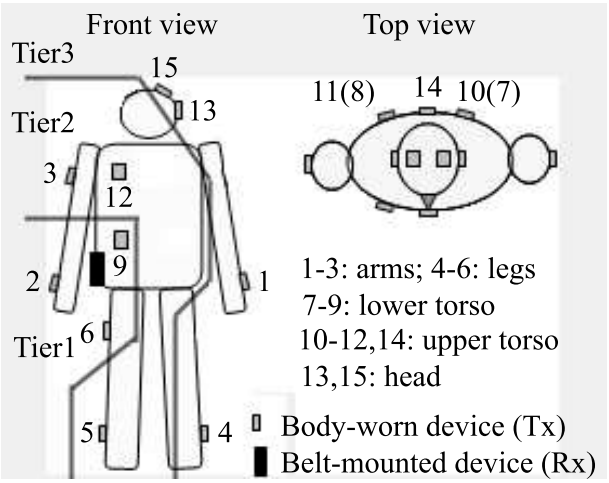

Figure 3: An illustration of the Tx and Rx on-body positions and the channel classification according to the relative Tx/Rx positions

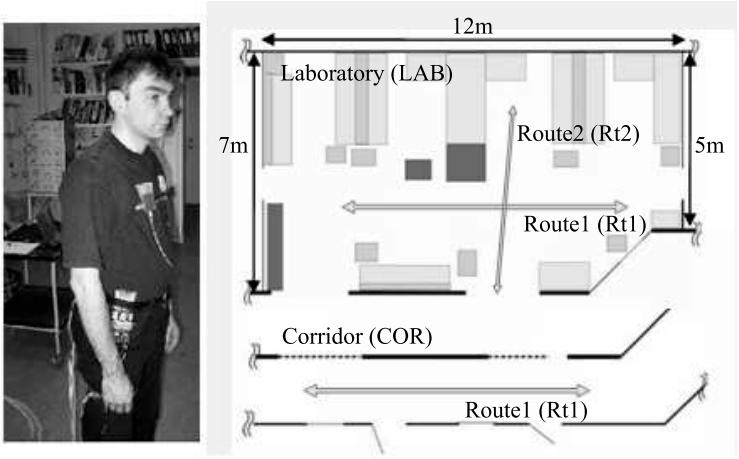

Figure 4: Left: a test person with the Tx at the upper torso and the Rx mounted on the front-right waist; right: a layout of the laboratory (LAB) and corridor (COR) environments

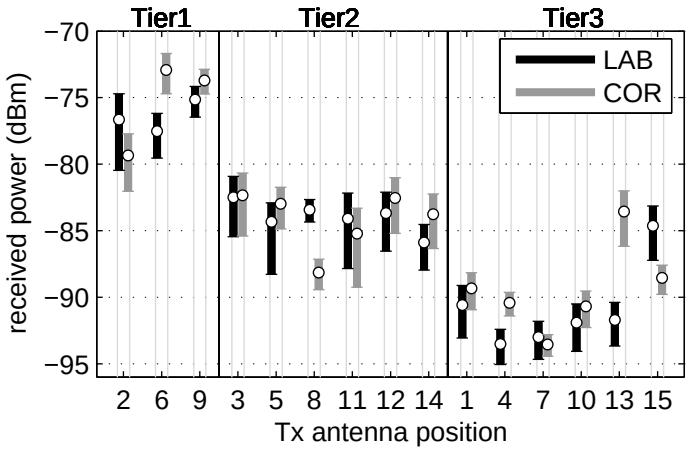

Figure 5: Channel wideband power respect to the different Tx antenna positions; round dot: mean wideband power, vertical bar: $\pm\sigma_P^{dB}$ around the mean power calculated in dB

considered as the best fit.

3 Channel Characterization

To generalize the results, the Tx positions are classified into three categories according to their relative positions to the Rx as illustrated in Fig. 3. The propagation situations are different among the three types of the channels. The Tier1 channel propagation is dominant by the short range direct link between the Tx and the Rx. The Tx in the Tier3 channels are located at the opposite body side with respect to the Rx. The reflection from the environment is the primary propagation mode in this condition. Other positions are categorized into Tier2. Both the body diffraction and the environment propagation contribute to the channel of these positions.

3.1 Channel Wideband Power

The channel wideband power is calculated by integrating the power of the average PDP in the delay domain. The Lognormal distribution fits all the measurements and is the best fit for 80% of the measured Tx positions. Fig. 5 shows the mean wideband power expressed in dB (m_P) by round dots, and the power standard deviation (σ_P^{dB}) around the mean taken in dB by vertical bars. It should be noticed that m_P is larger than the dB mean.

Table 1: Classifications of the on-body transmitter positions and channel parameters in the LAB

Type	m_P (dBm)	σ_P^{dB} (dBm)	rms delay (ns)	W90 (ns)
Tier1	-76.3	2.3	7.5	9.4
Tier2	-84.0	2.4	15.2	31.5
Tier3	-92.0	1.8	17.0	47.1

Antenna Position Dependence

The mean wideband power of each channel type measured in the LAB is shown in Table 1. Similar results are obtained in the COR. The Tier2 and Tier3 have approximately 8 and 16 dB more attenuation in the channel wideband power than the Tier1 channel. On the other hand all the channel types have the similar σ_P^{dB}. In the walking condition the most power fluctuation happens at the arm and ankle on the same side of the Rx, i.e. at position 2, 3, and 5 σ_P^{dB} is approximately 2.7 dB.

The difference in m_P between the two environments is less than 4 dB with the exception of the position 13 (right side head). The higher power at the position 13 in the COR could be explained by the strong reflections from the ceiling and side walls due to the shorter distance between the test persons and the walls. The reflections are not blocked by the human body because of the higher antenna height.

Branch Power Imbalance

The branch power imbalance (BPI) between the two Rx antennas is less than 3 dB for most of the measured channels. The Tx positions which have direct line-of-sight (LOS) link to the Rx, e.g. position 2, 3, 5, 6 and 9, show higher BPI in several measurements. The different antenna gains in the LOS direction is the most possible reason for the imbalanced power. Since the BPI was not observed in all the measurements for a certain Tx position, the small changes in the device positions among the measurements may cause significant variations of the antenna gain in a certain direction. The directional radiation pattern of the body-mounted antennas is also attributed to the BPI. Similar phenomenon was reported in [18]. The correlation of wideband power at the two Rx antennas is uniformly distributed in the range of $[0.2,\ 0.8]$.

3.2 Channel Delay Spread

Two parameters, root mean square (rms) delay spread and 90% energy delay window (W90), are used to characterize the channel delay spread. Fig. 6 and Table 1 demonstrate the results. Overall the delay spread is slightly smaller in the COR due to the smaller space compared with the LAB. The variation of the Tier2 channel spread is larger than

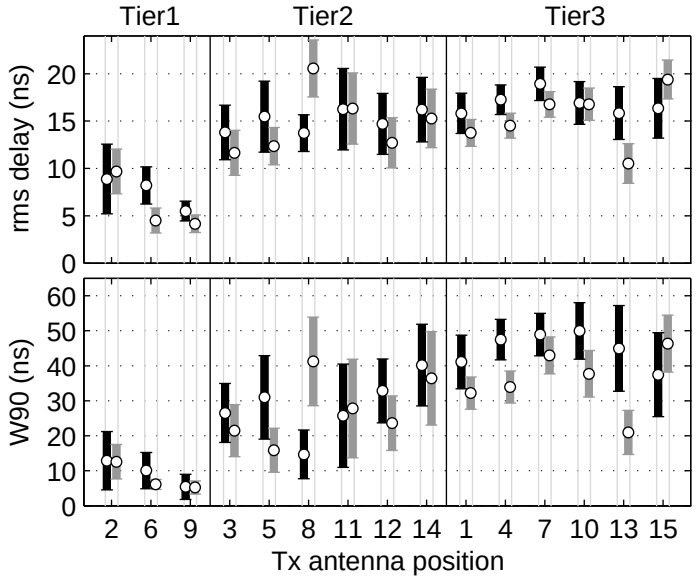

Figure 6: The rms delay spread and 90% energy delay window of the measured channel respect to the different Tx antenna positions; square dot: mean rms delay spread, vertical bar: standard deviation around the mean value; Dark bar: LAB, light bar: COR

the others. Since neither the body diffraction nor the environment multipaths is always dominant in the Tier2 channel, they may exhibit more influences by turns and result in the larger channel variation.

3.3 First Cluster Characterization

It is well known that the indoor UWB channel usually consists of a number of clusters [2, 3, 7, 10]. In most of the WBAN channels the first cluster (FC) arriving at the Rx is composed of the rays from the around body propagation which usually does not depend on the environment. Therefore the FC and the remaining clusters (RC) of the CIR can be modeled separately [10]. To model the whole CIR the power ratio and arrival time intervals between the FC and the RC are also required. The FC/RC join characteristics are summarized in this section. The analysis is based on the individual CIRs after the CLEAN algorithm was applied to the measured data.

FC Detection and Separation

Due to the system dynamic range limitations the power of the FC in some measured channels is not high enough to be detected. To avoid fall detections the absolute propa-

gation delay of the first ray in the measured CIR is compared with the wave propagation time along the direct or body diffraction path which is calculated based on the relative Tx/Rx positions. Due to the body movements a detection window is defined to accommodate the variation in the path length. The duration of the window is set as 2 ns corresponding to a distance of 60 cm. If the absolute propagation delay of the measured first ray falls out of the detection window, the FC of the channel is considered as not being detected.

The separation of the FC and the RC depends on the duration of the FC and the distance between the test persons and the closest scatterer which is 50 cm in the measurements. With this distance the FC arrives at the Rx usually more than 2 ns earlier than the RC. As presented in [10], the FC power decays approximately 10 dB/ns. Accordingly the power of the FC is 20 dB below the peak at the delay of 2 ns. Therefore the first cluster after 2 ns delay is considered as the start of the RC to minimize the FC/RC overlapping. The ground reflection for the position 4 and 5 can not be separated from the detected FC due to their short distances to the floor. Since the ground reflection is usually also environment independent, they are considered as part of the FC for these two positions.

Totally 90% of the measured channels have the FC detected and separated from the RC. The following analysis is based on these measured channels.

FC and RC Power Ratio

The power ratio between the FC and RC expressed in dB (K_P^{dB}) reflects the propagation mechanism. Large K_P^{dB} corresponds to direct link or body diffraction dominant scenarios, and small K_P^{dB} indicates that most channel power comes from the environment propagation. Fig. 7 illustrates K_P^{dB} with respect to the different antenna positions. The mean ($m_{K_P^{dB}}$) and standard deviation ($\sigma_{K_P^{dB}}$) of K_P^{dB} are presented in Table 2. When compared with the results presented in [7] we find similar K_P^{dB} of the Tier1 channel, and smaller K_P^{dB} for the Tier3 channel.

By the K-S test the Normal distribution is the best fits for $K_P^{dB} > 0$.

The negative correlation between K_P^{dB} and the channel delay spread is obvious as shown in Figure 7 and Figure 6. The correlation coefficient is -0.7 in both the LAB and COR. However when the two environments are compared the COR has the smaller K_P^{dB} and less rms delay at the same time. Therefore the K_P^{dB} and the physical environments both contribute to the channel delay spread.

FC and RC Arrival Interval

The interval between the FC and the RC depends on the difference between the length of the direct or body diffraction path and the distance from the test persons to the closest scatterer. It is shown in Fig. 8 that the FC/RC arrival interval (Δ_τ) is both antenna

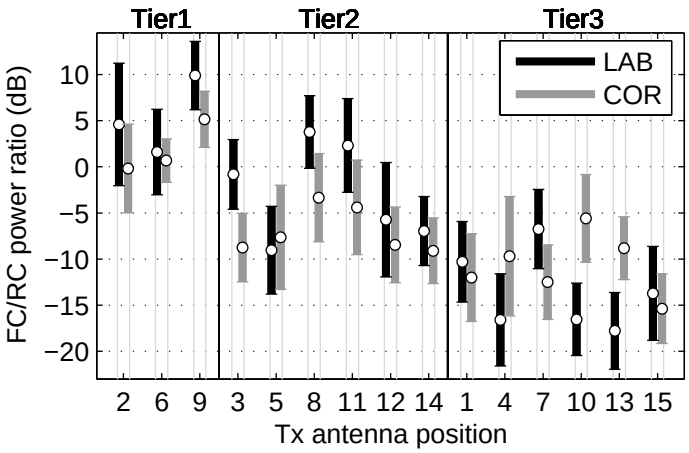

Figure 7: Power ratio expressed in dB (K_P^{dB}) between the first cluster (FC) and the remaining clusters (RC) of the CIR respect to the different Tx antenna positions

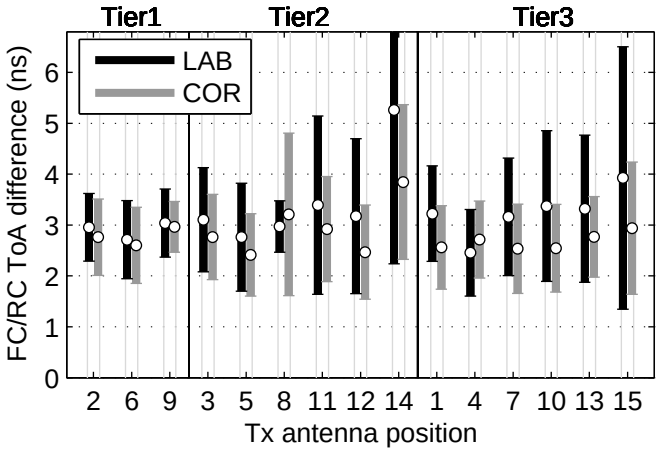

Figure 8: Arrival intervals(Δ_τ) between the first cluster (FC) and the remaining clusters (RC) of the CIR respect to the different Tx antenna positions

Table 2: First cluster (FC) characteristics with respect to the different channel types in the LAB and the COR

Type		m_{Δ_τ} (ns)	σ_{Δ_τ} (ns)	$m_{K_P^{dB}}$ (dB)	$\sigma_{K_P^{dB}}$ (dB)
Tier1	LAB	2.9	0.7	5.5	6.2
	COR	2.8	0.7	1.9	4.3
Tier2	LAB	3.4	1.8	-3.7	7.6
	COR	2.9	1.2	-7.7	5.7
Tier3	LAB	3.1	1.2	-13.5	6.1
	COR	2.6	1.8	-9.7	5.4

position and environment dependent. The mean (m_{Δ_τ}) and standard deviation (σ_{Δ_τ}) of Δ_τ are presented in Table 2.

The mean and variance of Δ_τ are both smaller in the COR which is a constrained space with simple structures. The largest Δ_τ observed in the LAB and COR is 14 ns and 12 ns at the Tx position 14 and 12 respectively. Both positions are at the back of the torso.

None of the statistics considered by the K-S test fits Δ_τ for a majority of the Tx positions.

Characterization of Rays in FC

Totally 86% of the FC contains two rays. Therefor we model the FC as a two-ray cluster.

The power of the body diffraction has been found in previous studies to be Lognormal [10, 19] or Weibull [19] distributed. We observe different ray amplitude distributions for the different channel types based on the K-S test. For the first ray in the FC, Normal, Weibull and Lognormal distributions are identified as the best fits for the Tier1 to Tier3 channels respectively. The distribution parameters are summarized in Table 3.

The second ray in the FC follows the same distribution as the first ray. The mean power ratio in dB (R_P^{dB}) and arrival interval (δ) between the first and the second ray are summarized in Table 3. The power decay of the FC is between 5 dB/ns and 10 dB/ns depending on the Tx positions. The correlation coefficient between the two rays in the FC is 0.7 in the LAB and 0.6 in the COR. Similar high correlation was presented in [7].

Overall the ray statistics are only slightly different in the two environments. It is as expected since the around body propagation should be independent with the environment propagation.

3.4 Body Propagation and Environment Propagation

The human body in the WBAN not only acts as a medium of the around body propagation but also shadows the signal coming from the environment. For the Tier1 channel

Table 3: Ray characteristics in the FC with respect to the different channel types in the LAB and the COR

Type		δ (ns)	R_P^{dB} (dB)	Best fit distribution parameter
Tier1	LAB	1.3	11.3	Normal: $\mu = 0.4, \sigma = 0.9$
	COR	1.2	12.6	Normal: $\mu = 0.3, \sigma = 1.0$
Tier2	LAB	1.4	8.7	Weibull: $\alpha = 2.6, \beta = 1.0$
	COR	1.5	9.7	Weibull: $\alpha = 2.6, \beta = 1.0$
Tier3	LAB	1.7	6.0	Lognormal: $\mu = -0.4, \sigma = 2.2$
	COR	1.6	6.8	Lognormal: $\mu = -0.7$,$\sigma = 2.4$

the earlier environment reflections will not be blocked by the body and the later ones arriving from the other side of the body will be shadowed. The situation is the opposite for the Tier3 channel. Therefore it implies that the decay factor (Γ_{RC}) of the RC increases with K_P^{dB}. To calculate Γ_{RC} the FC is removed from the measured average PDP. Since it has been found that indoor channels exhibit dual-slope PDPs with a breaking point at 25 ns [3], we evaluate the cluster decay factor of the two decay regions separately. Only the decay factor of the first delay region depends on K_P^{dB} since the arrival directions of the later environment multipaths become random. Fig. 9 shows a scatter plot of Γ_{RC} as a function of K_P^{dB} for all the Tx positions. Linear fits with the minimum squared error are also plotted in the same figure. The data of the position 12 is considered as outlier and excluded from the fitting process. The linear dependence between Γ_{RC} and K_P^{dB} in the LAB and the COR is expressed in (1) and (2) below respectively.

$$\Gamma_{RC,LAB} = 0.025 \cdot K_P^{dB} - 0.40 \tag{1}$$

$$\Gamma_{RC,COR} = 0.077 \cdot K_P^{dB} - 1.13 \tag{2}$$

The slope of the fitting curve in the COR is steeper. It indicates the higher body influences in the more constrained environments. Γ_{RC} is as small as 0.02 dB/ns when the RC is dominant. Similar small values were observed in [20]. Γ_{RC} increases linearly with K_P^{dB}. In the COR when the power of the FC increases to the same as the RC, the RC power drops 1.2 dB/ns.

Other environment channel parameters, e.g. cluster arrival rate, do not change significantly respect to the channel types [10].

4 Channel Model and Verification

Based on the investigations in the previous sections we propose a UWB WBAN channel model which extends existing indoor UWB models for the WBAN applications. The model uses a joint approach to take both the around body and the environment propa-

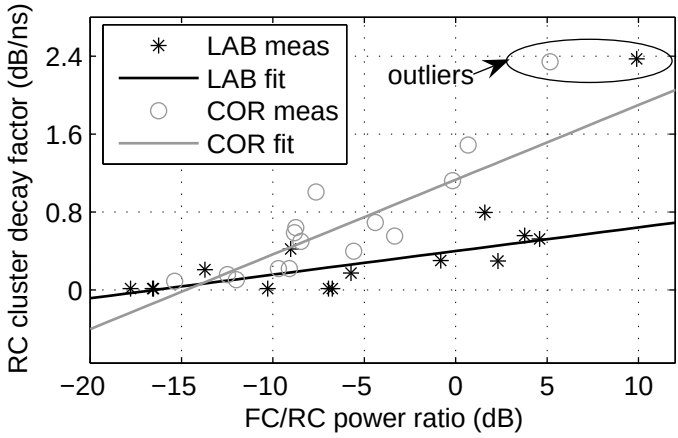

Figure 9: Scatter plot and linear fitting of the RC cluster decay factor (Γ_{RC}) as a function of the FC/RC power ratio (K_P^{dB})

gation into consideration. The CIR is modeled in three steps. First the FC is generated using correlated Normal, Weibull or Lognormal random variable (RVs) according to the channel types as presented in Table 3. The power and delay of the second ray respect to the first ray is set according to R_P^{dB} and δ in Table 3. In the second step the RC is generated based on available indoor UWB channel models. The cluster decay factor needs to be adjusted based on (1) or (2). In the last step the FC and the RC are combined together in the delay domain. The power ratio in dB between the two parts is modeled as a Normal RV. Since their arrival interval does not follow any considered distributions it is also modeled as a Normal RV as an approximation. The mean and standard deviation of the two RVs (m_{Δ_τ}, σ_{Δ_τ}, $m_{K_P^{dB}}$ and $\sigma_{K_P^{dB}}$) can be found in Table 2. The large-scale power variation is represented by a Lognormal RV as suggested in Table 1.

We simulate the UWB WBAN channel based on the suggested procedures. An indoor mobile-to-mobile UWB model presented in [20] is selected as the environment propagation model. The body proximity and similar antenna heights considered in the mobile-to-mobile model make it superior to other models. Furthermore the mobile-to-mobile model was based on a set of measurements performed in the same environment (LAB) which facilitates the channel verification. Totally 1000 channel realizations are generated for each channel type. The model is verified by the rms delay spread. The cumulative density functions (CDFs) of the delay spreads are shown in Fig. 10. The simulated and measured CDF curves are very close to each other. Therefore the proposed model can extend the indoor channel model for the WBAN applications accurately.

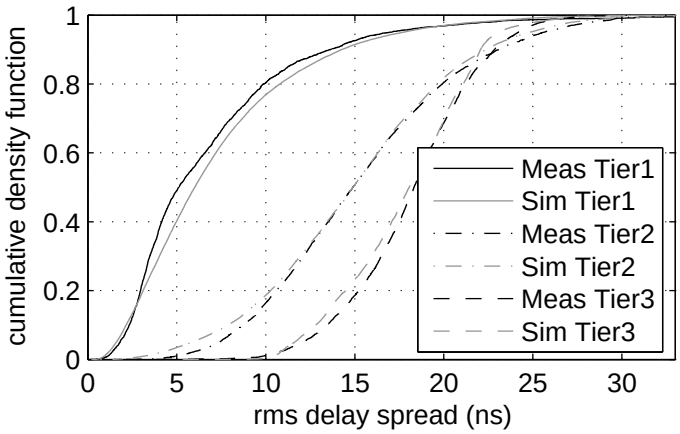

Figure 10: CDF of the simulated and measured rms delay spread for the different channel types

5 Conclusion

In this paper, we characterize and model the UWB WBAN channel in real multipath environments. The study is based on experiments performed in a laboratory and a corridor with dynamic testing persons. The Rx was placed on the waist and totally 15 Tx on-body positions were evaluated. A WBAN channel classification according to relative Tx/Rx positions is presented. Channel parameter analysis is carried out for each Tx position and channel type.

The channel wideband power is Lognormal distributed. The Tier2 and Tier3 channel have approximately 8 and 16 dB more attenuation in the wideband power compared with the Tier1 channel. Channel rms delay spread ranges from 5 to 20 ns among the different antenna positions. To separate the around body propagation from the environment propagation the first cluster (FC) is detected and separated from the remaining clusters (RC) of the measured channel impulse responses (CIRs). Power ratio and arrival time interval between the FC and the RC are characterized. Rays in the FC are modeled as Normal, Weibull or Lognormal distributed depending on the channel types. The RC decay factors is found linearly dependent on the FC/RC power ratio in dB.

Based on the above knowledge a UWB WBAN channel model which extends existing indoor UWB models for the WBAN applications is proposed. The model uses a joint approach to generate and combine the around body and environment propagation in the delay domain. Modeling procedures are presented in order to implement the channel for system evaluations. The modeling parameters extracted are specific to our measurement campaign. However, the methodology can easily be reproduced and the model is general. More experiments in different environments and with different

antenna types are encouraged by the authors to extend and verify the proposed model.

References

[1] P. S. Hall and Y. Hao, "Antennas and propagation for body centric communications," in *European Space Agency, (Special Publication) ESA SP*, vol. 626 SP, Oct 2006.

[2] A. F. Molisch, "Ultrawideband propagation channels - theory, measurement, and modeling," *IEEE Transactions on Vehicular Technology*, vol. 54, no. 5, pp. 1528–1545, Sep 2005.

[3] I. Z. Kovacs, H. T. Nguyen, P. C. Eggers, and K. Olesen, "Enhanced UWB radio channel model for short-range communication scenarios including user dynamics," in *IST Mobile & Wireless Communications Summit*, ser. IST Mobile & Wireless Communications Summit, 2005.

[4] T. Zasowski, G. Meyer, F. Althaus, and A. Wittneben, "UWB signal propagation at the human head," *IEEE Transactions on Microwave Theory and Techniques*, vol. 54, no. 4, pp. 1836–1845, Apr 2006.

[5] P. S. Hall and Y. Hao, *Antennas and propagation for body-centric wireless communications*. Artech House, INC., 2006.

[6] Y. Zhao, Y. Hao, A. Alomainy, and C. Parini, "UWB on-body radio channel modeling using ray theory and subband fdtd method," *IEEE Transactions on Microwave Theory and Techniques*, vol. 54, no. 4, pp. 1827–1835, Apr 2006.

[7] A. Fort, J. Ryckaert, C. Desset, P. De Doncker, P. Wambacq, and L. Van Biesen, "Ultra-wideband channel model for communication around the human body," *IEEE Journal on Selected Areas in Communications*, vol. 24, no. 4, pp. 927–933, Apr 2006.

[8] A. Alomainy, Y. Hao, X. Hu, C. G. Parini, and P. S. Hall, "UWB on-body radio propagation and system modelling for wireless body-centric networks," *IEE Proceedings-Communications*, vol. 153, no. 1, pp. 107–114, Feb 2006.

[9] H. Ghannoum, C. Roblin, and X. Begaud, "Investigation and modeling of the UWB on-body propagation channel," *Wireless Personal Communications (Article in Press)*, pp. 1–12, 2008.

[10] A. Fort, C. Desset, P. De Doncker, P. Wambacq, and L. Van Biesen, "An ultra-wideband body area propagation channel model - from statistics to implementation," *IEEE Transactions on Microwave Theory and Techniques*, vol. 54, no. 4, pp. 1820–1826, Apr 2006.

[11] K. T. Pak, H. C. Yong, C. O. Ling, M. K. Haldar, and L. Bin, "Small-scale transmission statistics of UWB signals for body area communications," in *Proceedings of VTC 2006 Fall*, Sep 2006, pp. 1–5.

[12] Y. P. Zhang, L. Bin, and C. Qi, "Characterization of on-human-body UWB radio propagation channel," *Microwave and Optical Technology Letters*, vol. 49, no. 6, pp. 1365–1371, Jun 2007.

[13] I. Z. Kovacs, G. F. Pedersen, P. C. Eggers, and K. Olesen, "Ultra wideband radio propagation in body area network scenarios," in *Proc.IEEE Eighth International Symposium on Spread Spectrum Techniques and Applications*, Sep 2004, pp. 102–106.

[14] A. A. Goulianos and S. Stavrou, "UWB path arrival times in body area networks," *IEEE Antennas and Wireless Propagation Letters*, vol. 6, pp. 223–226, 2007.

[15] IST-2004-507102, "My personal Adaptive Global Net (MAGNET) deliverable 3.1.2b: PAN radio channel characterization (part 2)," Tech. Rep., Dec 2005. [Online]. Available: http://www.ist-magnet.org/public+deliverables/phase1wp3

[16] M. Klemm, I. Z. Kovacs, G. F. Pedersen, and G. Troster, "Novel small-size directional antenna for UWB wban/wPAN applications," *IEEE Transactions on Antennas and Propagation*, vol. 53, no. 12, pp. 3884–3896, Dec 2005.

[17] Y. Wang, B. B. Ivan, I. Z. Kovacs, J. Ø. Nielsen, and G. F. Pedersen, "Characterization of the indoor multi-antenna body-to-body radio channel," *IEEE Transaction on Antenna and Propagation Special issue on Body-Centric Wireless Communications*, Dec 2008, (submitted).

[18] D. Neirynck, C. Williams, A. Nix, and M. Beach, "Exploiting multiple-input multiple-output in the personal sphere," *IET Microwaves, Antennas and Propagation*, vol. 1, no. 6, pp. 1170–1176, Dec 2007.

[19] S. L. P. Tang and G. K. Stylios, "An overview of smart technologies for clothing design and engineering," *International Journal of Clothing Science and Technology*, vol. 18, no. 1-2, pp. 108–128, 2006.

[20] I. Z. Kovacs, Y. Wang, P. C. Eggers, and K. Olesen, "UWB radio channel model for short-range mobile-to-mobile communication scenarios," in *Wireless Personal Multimedia Communications (WPMC) Symposia 2005*, Sep 2005, pp. 2008–2012.

Paper D

Spatial Correlation of PAN UWB-MIMO Channel Including User Dynamics

Yu Wang, István Z. Kovács, Gert F. Pedersen and Kim Olesen

The paper has been reported in *COST 2100, Duisburg Germany*, Sep 2007

The layout has been revised.

Abstract

In this paper we present and analyze spatial correlation properties of indoor 4x2 MIMO UWB channels in personal area network (PAN) scenarios. The presented results are based on measurement of radio links between an access point like device and a hand held or belt mounted device with dynamic user. It is found the channel shows spatial correlated wideband power, and spatial uncorrelated complex channel coefficients at different frequencies and delays with respect to a correlation coefficient threshold of 0.7*. The Kronecker model is proved not suitable for the investigated scenarios. The MIMO UWB channel achieves an ergodic capacity close to i.i.d. Rayleigh channel capacity. However the outage capacity degrades due to the wideband power fluctuation / shadowing introduced by user's body.*

1 Introduction

The Ultra wide band (UWB) technology has been one of the most popular topics among the communications research community since the 1990's due to its potential on the high data rate and/or reliable transmission with low transmission power. The frequency selective nature of UWB channels makes the fading of wideband power much smaller than other communication systems. However, the rigid power constrains, regulated by regulator bodies e.g. FCC and ETSI, make the design of a UWB system a big challenge.

The combination of UWB and multi-input multi-output (MIMO) techniques is considered as a potential solution, to improve reliability and coverage, increase the data rate and reduce power consumption of UWB systems. Being aware of the strong limitations imposed on UWB communications by regulation bodies, the UWB-MIMO system was justified from different aspects including additional capacity enhancement [1, 2] and extra diversity and coding gains [3–5]. The performance of such systems was shown dependent upon spatial correlation properties between transmission links. The spatial correlation of UWB multiple antenna systems based on indoor channel measurements was investigated in [1, 6–8]. The spatial correlation was characterized either in the frequency domain [1, 6, 7] or the delay domain [8].

The UWB technology is considered as a candidate PHY solution for body-centric personal area network (PAN) communications which is characterized by short range and low power wireless links. In PAN environments a significant impact of the user proximity and user dynamics on the signal propagation was disclosed since transceivers are often body worn or hand held devices [9]. The spatial correlation properties of MIMO radio channels in such PAN scenarios are also expected to be time variant because of the user movements [9, 10].

In this paper, the spatial correlation of multi-antenna UWB channels was investigated in PAN scenarios based on experimental data in the lower UWB frequency band

Figure 1: Antenna setup for the measurement setup, left: handheld user device (UD); right: access point device (AP))

of 3-5 GHz with 4 receive antennas and 2 transmit antennas [9, 10]. Compared with previous studies our measurement was unique in the antenna configurations and the scenarios with dynamic users.

The spatial structure of the channel was unveiled and a Kronecker model was evaluated in the view of UWB MIMO channel modeling. The capacity of the measured UWB-MIMO channel was evaluated.

The paper is organized as follows. Section II describes the experimental work and the scenarios. Section III presents the data analysis and processing. In Section IV the MIMO spatial correlation analysis is presented. Finally, the paper is ended by a conclusion in Section V.

2 Measurement Setup And Environment

The radio channel measurements were conducted with a time domain UWB sliding correlator channel sounder. The measurement bandwidth was 2.5 GHz centered at 4.5 GHz. The effective delay resolution was 0.4 ns [10].

A linear array of four UWB planar monopoles was used at the access point (AP) (Fig. 1, right) and two cylindrical monopoles were used in user devices (UD) (Fig. 1 left). The antenna separation distance was $\lambda/2$ at both AP and UD, where $\lambda = 6.7$ cm is the wavelength at center frequency 4.5 GHz. A more detailed description of the measurement system can be found in [10].

Table 1 summarizes the main characteristics of the measurement environments and radio channels. In all scenarios the UD was carried by users at 1 m height from the room's floor and with $v \approx 1$m/s speed. Three typical environments, laboratory (LAB), conference room (CAN) and hallway (HAA) have been investigated with user routes, covering the most likely user movement patterns relative to the location of the AP. As an example, the layout of the conference room environment is shown in Fig. 2.

The main difference between the three environments is in the AP height, which leads

Table 1: Main Characteristics of the measurement environments and user routes [10]

Environment	Area Dimension W×L×H (m)	AP height (m)	AP-UD range (m)	RMS delay spread (ns)	Number of routes
LAB	8×14×2.3	2.3	2-7	13	3
CAN	15×17×2.3	2.3	2-7	25	5
HAA	12×17×11	6	6-17	35	6

to a different signal clustering in the channel impulse response (CIR). Furthermore, in the LAB environment the density of the scattering objects (furniture, equipment, etc.) was much higher compared to the CAN and HAA environments.

The number of routes measured in each environment is listed in Table 1. Approximately a number of 25 different measurements runs were taken in each scenario with different users and moving directions. The radio channel sampling rate was 40 Hz, i.e. every 0.025 s a MIMO snapshot containing $4 \times 2 = 8$ simultaneously measured radio links was recorded. The duration of each measurement route was either 12.5 s or 25 s depending on the length of the route. Therefore, in total more than $10,000$ MIMO channel snapshots were measured.

Unless otherwise stated, the statistical results shown in the following sections were based on measured data from all the environments.

3 Data Analysis and Processing

3.1 Stationarity of the measured channel

The wideband power is considered as stationary over the whole measurement route since the path loss effect is almost negligible compared with body shadowing for the measured scenarios.

The complex channel coefficients at different frequencies and delays are non-stationary due to the dynamics of the user. The non-stationarity was caused by the variation of the scatterers when user moved in the environment. The channel may be treated as stationary over a short interval. To identify the channel stationarity a quantified metric was applied to the measured channels in order to obtain stationary interval.

The metric is similar to the one proposed in [11]. First, the averaged power delay profile over all links was computed by,

$$PDP\left(t,\tau\right)=\frac{1}{L}\sum_{l=1}^{L}\left|h\left(t,\tau,l\right)\right|^{2} \tag{1}$$

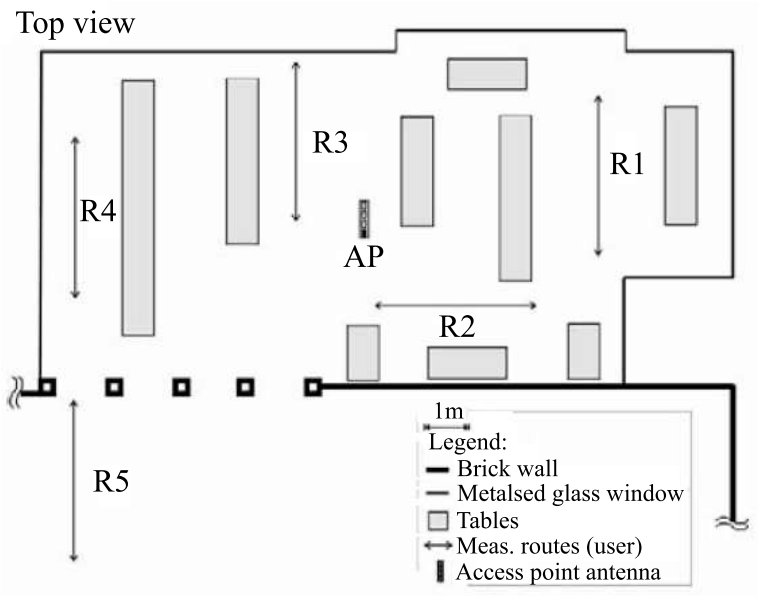

Figure 2: Layout of Conference Room (CAN) environment

where $h\left(t,\tau,l\right)$ is the complex channel coefficient at time t, delay τ and SISO link l and L is the total number of SISO links. Then the small scale fading was averaged out by performing sliding window time averaging with a window length of 10 channel samples which produces $\overline{PDP}\left(t',\tau\right)$. The time-domain PDP correlation metric used is defined as:

$$\rho_{\overline{PDP}}\left(\Delta t'\right)=\frac{\sum_{\tau}\overline{PDP}\left(t'_0,\tau\right)\overline{PDP}\left(t'_0+\Delta t',\tau\right)}{\max\left\{\sum_{\tau}\overline{PDP}\left(t'_0,\tau\right)^2\overline{PDP}\left(t'_0+\Delta t',\tau\right)^2\right\}} \tag{2}$$

and decreases when channel wideband power and/or structure of $\overline{PDP}$ varies significantly between the two time instances $\Delta t'$ apart. Therefore $\rho_{\overline{PDP}}\left(\Delta t'\right)$ is used as an indicator of channel stationarity, i.e. the interval during which $\rho_{\overline{PDP}}\left(\Delta t'\right)$ is greater than a predefined threshold $C_{th}=0.5$ is considered as stationary as recommended in [11].

Only blocks with more than 50 samples were used in this paper. And statistical results based on a large amount of measurement data were obtained to ensure the reliability of the analysis.

3.2 Spatial Correlation

The measured time-varying UWB-MIMO channels can be expressed either in time-delay domain as $\mathbf{H}(\mathrm{t}, \tau)$, or in time-frequency domain as $\mathbf{G}(\mathrm{t}, \mathrm{f})$. In this study the channels was investigated in both time-frequency and time-delay domains.

The presence of orthogonal MIMO links is a necessary condition to realize the linear increase in MIMO capacity [12]. The spatial correlation between the links is an important measure to identify the independence of the links. The correlation coefficient was calculated between each pair of the links. It is expressed as

$$\rho_{(m1n1,m2n2)} = \langle \beta_{m1n1}, \beta_{m2n2} \rangle \tag{3}$$

where $\langle \cdot \rangle$ is the correlation coefficient operation, and defined as,

$$\langle a, b \rangle = \frac{E\left[ab^*\right] - E\left[a\right] E\left[b^*\right]}{\sqrt{\left(E\left[|a|^2\right] - |E\left[a\right]|^2\right)\left(E\left[|b|^2\right] - |E\left[b\right]|^2\right)}} \tag{4}$$

where $(\cdot)^*$ is the complex conjugate and $E\left[\cdot\right]$ denotes the expectation.

By replacing β with $h\left(t, \tau\right)$, $g\left(t, f\right)$ and $p(t)$ in (3), the spatial correlation in the delay domain ρ_{delay}, frequency domain ρ_{freq} and wideband power ρ_{pow} is obtained respectively, where $h\left(t, \tau\right)$ and $g\left(t, f\right)$ are elements in $\mathbf{H}(\mathrm{t}, \tau)$ and $\mathbf{G}(\mathrm{t}, \mathrm{f})$, and

$$p(t) = \sum_r \left| h\left(t, \tau\right) \right|^2 \tag{5}$$

ρ_{delay} and ρ_{freq} are calculated within each stationary time block defined based on (12), and ρ is calculated over the whole measurement route.

In this work we use a threshold of 0.7 for the correlation coefficient to be considered as 'correlated'.

4 Results Analysis

4.1 Spatial correlation of wideband power (ρ_{pow})

Due to the large bandwidth of the investigated channel, there is no fading in the wideband power. The spatial correlation of the wideband power is mainly introduced by body shadowing. Therefore the wideband power at the receiver is correlated since the receiver antennas usually see the same shadowing. On the contrary the transmitter which is belt-mounted or hand-held by the users can undertake different shadowing, hence lower spatial correlation.

This is proved by Fig. 3 (left) which plots the mean spatial correlation of wideband power. The upper left and lower right corners of the figure correspond to the spatial

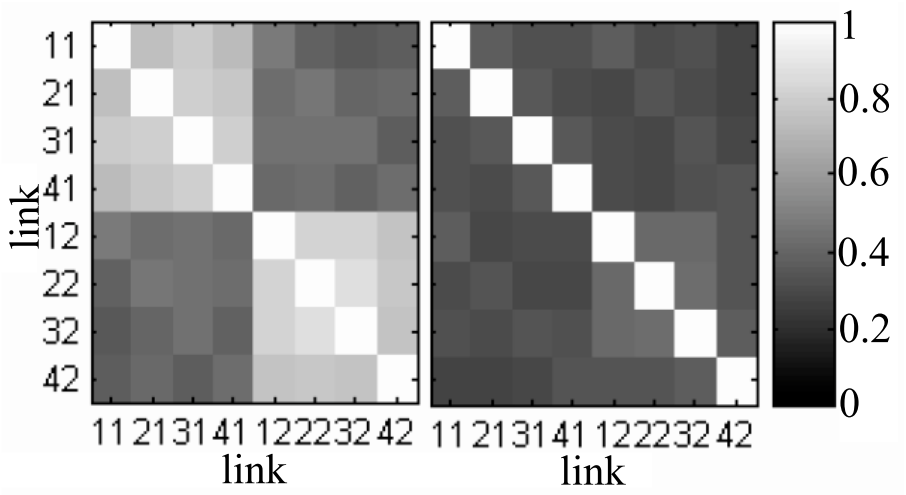

Figure 3: Mean spatial correlation of different link-pairs; left: ρ_{pow}, right: ρ_{freq}; Link 41 indicates the link between receive antenna 4 and transmit antenna 1

correlation at the receiver refer to the two transmitter antennas respectively. They are significantly higher than the correlation between other links as expected.

4.2 Spatial correlation of complex channel coefficients at different delays (ρ_{delay})

The mean and 10% CDF spatial correlation at different delays is illustrated in Fig. 4. The 10% CDF refers to the value which is higher than 90% of data. The mean spatial correlation is approximately 0.5 in the first delay bin, and decays to about 0.3 in 20 ns. Similar results were reported in [8]. The 10% CDF correlation is only significant, i.e. above 0.7, for the first 5 ns delay spread, in general corresponding to the most significant direct signal paths. A correlation of 0.6 was observed between spatial correlation and channel gains at different delays. It implies a smaller angular spread for the clusters containing more power, e.g. the direct or main reflection clusters.

4.3 Spatial correlation of complex channel coefficients at different frequency (ρ_{freq})

The spatial correlation does not show differences in the mean and 10% CDF values at different frequencies within the whole frequency band. Both mean (Fig. 3 right) and 10% CDF correlation are below 0.6, which implies the potential of spatial diversity.

To identify the variation of the spatial correlation respect to frequency separations,

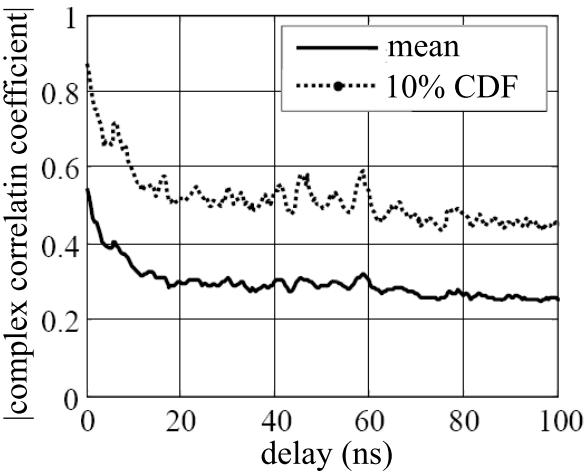

Figure 4: Mean and 10% CDF spatial correlation at different delays

a metric called correlation matrix distance (CMD) was used. The CMD was originally proposed in [13] to describe the non-stationarity of MIMO channels. Here we define the modified CMD as

$$CMD\left(f_1, f_1\right) = 1 - \frac{\left|tr\left\{R\left(f_1\right) R\left(f_2\right)\right\}\right|}{\left\|R\left(f_1\right)\right\|_F \left\|R\left(f_2\right)\right\|_F} \tag{6}$$

where $\|\cdot\|_F$ represents Frobenius norm.

The CMD becomes zero for identical correlation matrices and unity for maximally differed matrices. When the CMD is greater than 0.2 [13], the channel matrix undertakes a significant change. Fig. 5 shows the CMD varies faster, and reaches 0.2 with a 5, 40 and 100 MHz frequency separation in the HAA, LAB and CAN environment respectively.

4.4 Spatial correlation at transmitter and receiver

The receiver and transmitter correlation measures analyzed here represent spatial correlations between two radio links sharing the same transmit and receive antenna respectively. The correlation between other link pairs is referred as 'others'.

The difference of ρ_{pow} at the transmitter and receiver sides has been discussed in Section 4.1. For the ρ_{delay} and ρ_{freq}, the transmitter and receiver correlations are normally different due to antenna configurations, richness of local scatterers, user movements, etc. Table 2 shows mean and 10% CDF spatial correlation at transmitter and receiver.

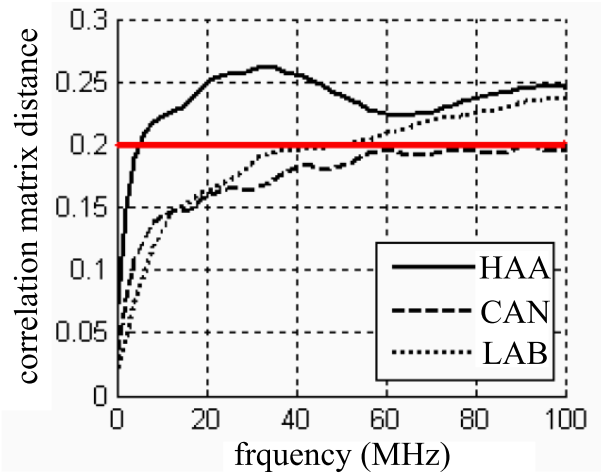

Figure 5: Mean correlation matrix distance with respect to frequency separations in different environments

In our measurement system, the antenna elements separation was the same at transmitter and the receiver with 0.5λ. The receiver antenna array was always fixed on the ceiling, therefore it yield a higher spatial correlation. However, the difference is not significant, and both at the transmitter and the receiver the channel is spatially uncorrelated due to the rich scatters in all the investigated environments. Furthermore, at the transmitter side the antenna near field effects due to the user proximity may result in different radiation patterns for transmitter antenna elements which decrease the correlation.

4.5 Spatial correlation with different Rx antenna spacing

The receive correlation is further analyzed in terms of antenna elements separation in this section. Table III shows the mean and 10% CDF receiver spatial correlation with different antenna spacing. The results show that the antenna spacing ranging from $\lambda/2$ to $3\lambda/2$ has little effect on the ρ_{delay} and ρ_{freq} . And they are always uncorrelated with all antenna separations.

The effects of the antenna separation are more considerable for the ρ_{pow} . However, the channel is always spatially correlated for the wideband power. Therefore, from a system perspective the deployment of a selection diversity scheme at the access point like device based on wideband power measurements requires an antenna elements spacing of at least $3\lambda/2$.

Table 2: Mean and 10% CDF spatial correlation at receiver (Rx) and transmitter (Tx)

	ρ_{delay}		ρ_{freq}		ρ_{pow}	
	mean	10%	mean	10%	mean	10%
Rx	0.35	0.63	0.38	0.65	0.84	0.95
Tx	0.30	0.53	0.34	0.60	0.57	0.84
Others	0.27	0.49	0.30	0.56	0.51	0.80

Table 3: Mean and 10% CDF receiver spatial correlation with different antenna spacing

	ρ_{delay}		ρ_{freq}		ρ_{pow}	
	mean	10%	mean	10%	mean	10%
0.5λ	0.35	0.63	0.38	0.65	0.83	0.95
λ	0.32	0.58	0.34	0.60	0.80	0.93
1.5λ	0.31	0.55	0.33	0.58	0.75	0.93

4.6 Spatial structure of the measured channel

In PAN environments the transmitter and receiver are usually located in the same cluster of scatterers due to the short range of transmission. Therefore we expect that the spatial correlation at the receiver side is not completely independent from the spatial correlation at the transmitter side. This is contrary to one assumption of a well known Kronecker model for MIMO channels, which was proved to be valid for both outdoor [14] and indoor [15] MIMO channel modeling with certain antenna configurations. In the Kronecker model the channel covariance matrix is estimated as

$$\rho^{[Kron]}_{(m1n1,m2n2)} = \overline{\rho}^{[Kron]}_{(Rx,m1m2)} \overline{\rho}^{[Kron]}_{(Rx,n1n2)} \tag{7}$$

where

$$\overline{\rho}^{[Kron]}_{(Rx,m1m2)} = E\left[\langle \beta_{m1n}, \beta_{m2n} \rangle\right], n \in [1,2] \tag{8}$$

$$\overline{\rho}^{[Kron]}_{(Rx,n1n2)} = E\left[\langle \beta_{mn1}, \beta_{mn2} \rangle\right], m \in [1,2,3,4] \tag{9}$$

And the model error is defined as,

$$\Psi = \frac{\|R - R_{Kron}\|_F}{\|R\|_F} \tag{10}$$

where R and R_{Kron} are channel correlation matrix whose elements are $\rho_{(m1n1,m2n2)}$ and $\rho^{[Kron]}_{(m1n1,m2n2)}$ respectively.

For th ρ_{delay} and ρ_{freq}, the model error is unreliable since they are calculated with limited number of samples. From Table 2 it is clear that the mean correlation of link pairs without common antennas is much larger than the product of the mean receiver and

Table 4: Model Error

Model error	LAB		CAN		HAA	
of ρ_{pow}	4×2	2×2	4×2	2×2	4×2	2×2
mean (%)	9.8	6.9	16.9	10.2	13.3	6.1
standard deviation (%)	3.9	4.1	9.2	6.0	10.2	3.5
% of routes with $\Psi < 4\%$	0	25	0	12.5	8.3	33.3

transmitter correlation, which violates the Kronecker model assumption specified in (7). It is shown in the previous sections that for the ρ_{delay} and ρ_{freq}, all link-pairs exhibited similar cross correlation. With respect to an ideal spatially white case whose channel matrix is an i.i.d. random matrix [16], the investigated channel is called quasi spatially white. It is characterized by non-zero correlation due to the insufficient richness of the scattering to provide fully decorrelate links and small difference in the correlation of different link pairs.

For the ρ_{pow} as explained in the Section 4.1 the correlation is caused by body shadowing instead of local scatterers. Interestingly, the Kronecker model shows fitness for some of the measurement routes. It's because the effect of body shadowing at the transmitter and receiver can be separated. Table IV summarizes the model error of ρ_{pow} in the different environments with 4×2 or 2×2 antenna configuration. Since the number of samples (520) to calculate the ρ_{pow} is still not sufficient to achieve accurate correlation, a model error less than 4% is considered as a good fit. For the 2×2 antenna configuration, overall the Kronecker model is suitable for $1/4$ of the measurement routes.

4.7 Capacity

To calculate channel capacity, the UWB-MIMO channel first normalized to ensure that

$$E_{t,f}\left[\left\|\mathbf{G}_{\mathrm{norm}}\left(t,f\right)\right\|_F^2\right] = N_{Tx}N_{Rx} \tag{11}$$

This normalization retains the relative power fluctuations for each measurement route.

With the assumption of no channel state information (CSI) at the transmitter and perfect CSI at the receiver, the sub-band and wideband capacity in [bit/s/Hz] are defined as,

$$C_{SB}\left(t,f\right) = \log_2\left[\det\left(\mathbf{I}_{\mathrm{N_{Rx}}} + \frac{SNR}{N_{Tx}}\mathbf{G}_{\mathrm{norm}}\left(t,f\right)\mathbf{G}_{\mathrm{norm}}\left(t,f\right)^H\right)\right] \tag{12}$$

$$C_{WB}\left(t\right) = \frac{1}{B}\int_B C_{SB}\left(t,f\right)df \tag{13}$$

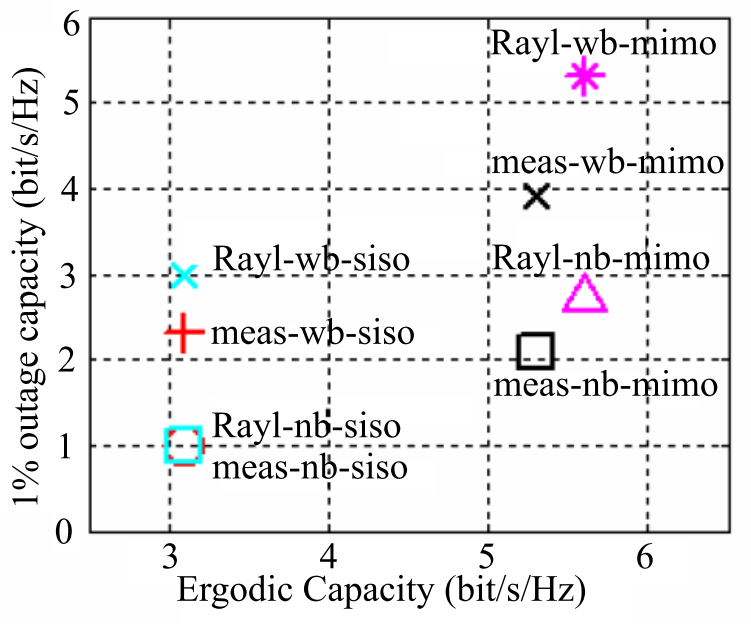

Figure 6: Ergodic and 1% outage capacity of the measured channels

where SNR is a receiver signal to noise ratio which is selected to be 10 dB, $\mathbf{I}$ is an identity matrix, $(\cdot)^H$ means complex conjugate transpose, $\det(\cdot)$ denotes the determinant and B is the bandwidth of measured channel which is 1 GHz in our study.

The ergodic and 1% outage capacity at 10 dB SNR is shown in Fig. 6. The increase of the MIMO ergodic capacity respect to the SISO channel and of the wideband outage capacity respect to the narrowband channel are both significant. The ergodic and 1% outage capacity for the MIMO UWB channel is 5.4 b/s/Hz and 4 b/s/Hz respectively. Compared to the i.i.d. Rayleigh channel capacity, the outage capacity drops approximately 25% mainly due to the signal shadowing introduced by users' body and movements.

The capacity with three different antenna configurations, 4×2 MIMO, 2×2 MIMO and 2×2 MIMO with 2 extra antennas on the receiver providing selection diversity, was evaluated. It is shown in Fig. 7 that by increasing the MIMO from 2×2 to 4×2 the ergodic capacity increases about 12% and adding two extra antennas on the receiver side providing selection diversity can improve the outage capacity by about 10%.

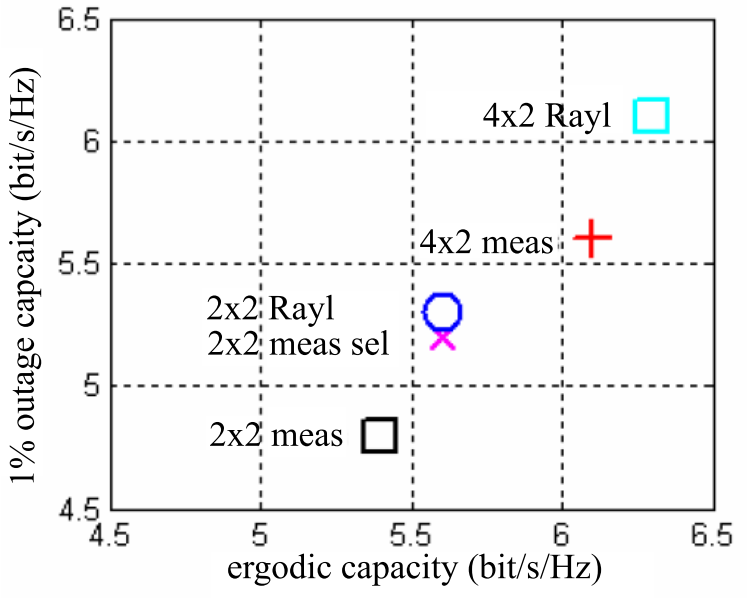

Figure 7: Ergodic and 1% outage capacity of the measured channels with different antenna configurations

5 Conclusion

In this paper we presented an analysis of the spatial correlation properties of indoor PAN UWB-MIMO channels based on the channel measurement of radio links between an access point like device and a dynamic user with hand held or belt mounted device It is found the channel shows spatial correlated wideband power, and spatial uncorrelated complex channel coefficients at different frequencies and delays with respect to a correlation coefficient threshold of 0.7. In both time-frequency and time-delay domain, the investigated PAN UWB-MIMO channel was found to be quasi spatially white since all link pairs showed similar correlation properties. The Kronecker model was proved not suitable for these PAN scenarios where the receiver and transmitter are located in the same cluster of main radio scatterers. A quarter of the measurement routes show fitness of the Kronecker model in the spatial correlation in the wideband power. It is because the effects of body shadowing, which introduces the correlation, can be separated at the transmitter and the receiver sides. Since the body shadowing usually is the same at all receiver antennas and different at transmitter antennas, the wideband power is spatially correlated at the receiver and uncorrelated at the transmitter. In the time-delay domain only the 10% CDF correlation of the first 5 ns is higher than 0.7 and the spatial correlation was found to be correlated with the channel gain at different delays. In the time-frequency domain the spatial correlation was disclosed to be independent

over frequency offsets ranging from 2 MHz to 30 MHz depending on the radio environment. This information is useful for frequency domain UWB MIMO channel modeling in similar PAN scenarios and further for the optimization of the frequency-domain link-adaptation and packet scheduling algorithms. The ergodic and 1% outage capacity of the measured channel were determined to be 5.4 b/s/Hz and 4 b/s/Hz at 10 dB SNR. And the 1% outage capacity drops approximately 25% mainly due to the signal shadowing introduced by users's body and movements.

Acknowledgment

This paper describes work partially undertaken in the context of the IST-FP6/2002/IST/1, 'My personal Adaptive Global Net' (IST-2004-507102 MAGNET www.ist-magnet.org), in WP3.1 'PAN Radio Channel Measurements and Models'.

References

[1] W. Q. Malik, M. C. Mtumbuka, D. J. Edwards, and C. J. Stevens, "Performance analysis of ultra-wideband spatial MIMO communications systems," in *Proc.14th IST Mobile Comm.Summit.*, ser. IST Mobile Comm.Summit., Jun 2005.

[2] F. Zheng and T. Kaiser, "On the evaluation of channel capacity of multi-antenna UWB indoor wireless systems," in *ISSSTA2004, Sydney, Australia*, ser. International Symposium on Spread Spectrum Techniques and Applications, ISSSTA, 2004, pp. 525–529.

[3] W. P. Siriwongpairat, M. Olfat, and K. J. R. Liu, "Performance analysis and comparison of time-hopping and direct-sequence UWB-MIMO systems," *Eurasip Journal on Applied Signal Processing*, vol. 2005, no. 3, pp. 328–345, Mar 2005.

[4] W. P. Siriwongpairat, W. F. Su, M. Olfat, and K. J. R. Liu, "Multiband-omm MIMO coding framework for UWB communication systems," *IEEE Transactions on Signal Processing*, vol. 54, no. 1, pp. 214–224, Jan 2006.

[5] A. Sibille, "Time-domain diversity in ultra-wideband MIMO communications," *Eurasip Journal on Applied Signal Processing*, vol. 2005, no. 3, pp. 316–327, Mar 2005.

[6] C. Prettie, D. Cheung, L. Rusch, and M. Ho, "Spatial correlation of UWB signals in a home environment," in *Ultra Wideband Systems and Technologies, 2002.Digest of Papers.2002 IEEE Conference on*, ser. IEEE Conference on Ultra Wideband Systems and Technologies, 2004, pp. 65–69.

[7] A. S. Y. Poon and M. Ho, "Indoor multiple-antenna channel characterization from 2 to 8 GHz," in *Communications, 2003.ICC '03.IEEE International Conference on*, ser. Communications, ICC IEEE International Conference on, vol. 5, 2003, pp. 3519–3523.

[8] J. Keignart, C. bou Rjeily, C. Delaveaud, and N. Daniele, "UWB simo channel measurements and simulations," *IEEE Transactions on Microwave Theory and Techniques*, vol. 54, no. 4, pp. 1812–1819, Apr 2006.

[9] I. Z. Kovacs, Y. Wang, P. C. Eggers, and K. Olesen, "UWB radio channel model for short-range mobile-to-mobile communication scenarios," in *Wireless Personal Multimedia Communications (WPMC) Symposia 2005*, Sep 2005, pp. 2008–2012.

[10] IST-2004-507102, "My personal Adaptive Global Net (MAGNET) deliverable 3.1.2b: PAN radio channel characterization (part 2)," Tech. Rep., Dec 2005. [Online]. Available: http://www.ist-magnet.org/public+deliverables/phase1wp3

[11] N. D. Skentos, A. G. Kanatas, P. I. Dallas, and P. Constantinou, "MIMO channel characterization for short range fixed wireless propagation environments," *Wireless Personal Communications*, vol. 36, no. 4, pp. 339–361, Mar 2006.

[12] G. J. Foschini and M. J. Gans, "On limits of wireless communications in a fading environment when using multiple antennas," *Wireless Personal Communications*, vol. 6, no. 3, pp. 311–335, 1998.

[13] M. Herdin and E. Bonek, "A MIMO correlation matrix based metric for characterizing non-stationarity," in *IST Mobile & Wireless Communications Summit*, ser. IST Mobile & Wireless Communications Summit, 2004.

[14] J. P. Kermoal, L. Schumacher, K. I. Pedersen, P. E. Mogensen, and F. Frederiksen, "A stochastic MIMO radio channel model with experimental validation," *IEEE Journal on Selected Areas in Communications*, vol. 20, no. 6, pp. 1211–1226, Aug 2002.

[15] K. Yu and B. Ottersten, "Models for MIMO propagation channels: a review," *Wireless Communications & Mobile Computing*, vol. 2, no. 7, pp. 653–666, Nov 2002.

[16] W. Weichselberger, M. Herdin, H. Ozcelik, and E. Bonek, "A stochastic MIMO channel model with joint correlation of both link ends," *IEEE Transactions on Wireless Communications*, vol. 5, no. 1, pp. 90–100, Jan 2006.